

ตัวรับรู้แก๊สเอทิลีนจากวัสดุเชิงประกอบพอลิเอทิลีน/ทินออกไซด์/มัลติวอลล์คาร์บอนนาโนทิวบ์
ที่สังเคราะห์เชิงไฟฟ้าเคมี

นายประสิทธิ์ พัฒนะนุวัฒน์

วิทยานิพนธ์นี้เป็นส่วนหนึ่งของการศึกษาตามหลักสูตรปริญญาวิทยาศาสตรมหาบัณฑิต
สาขาวิชาวัสดุศาสตร์ ภาควิชาวัสดุศาสตร์
คณะวิทยาศาสตร์ จุฬาลงกรณ์มหาวิทยาลัย
ปีการศึกษา 2554
ลิขสิทธิ์ของจุฬาลงกรณ์มหาวิทยาลัย

บทคัดย่อและแฟ้มข้อมูลฉบับเต็มของวิทยานิพนธ์ตั้งแต่ปีการศึกษา 2554 ที่ให้บริการในคลังปัญญาจุฬาฯ (CUIR)
เป็นแฟ้มข้อมูลของนิสิตเจ้าของวิทยานิพนธ์ที่ส่งผ่านทางบัณฑิตวิทยาลัย

The abstract and full text of theses from the academic year 2011 in Chulalongkorn University Intellectual Repository (CUIR)
are the thesis authors' files submitted through the Graduate School.

ETHYLENE GAS SENSOR FROM ELECTROCHEMICALLY SYNTHESIZED
POLYANILINE/ TIN OXIDE/ MULTIWALL CARBON NANOTUBE
COMPOSITES

MR. PRASIT PATTANANUWAT

A Dissertation Submitted in Partial Fulfillment of the Requirements
for the Degree of Doctor of Philosophy Program in Material Science

Department of Material Science

Faculty of Science

Chulalongkorn University

Academic Year 2011

Copyright of Chulalongkorn University

นายประสิทธิ์ พัฒนะภูวัฒน์ : ตัวรับรู้แก๊สเอทิลีนจากวัสดุเชิงประกอบพอลิแอนิไลน์/ทินออกไซด์/มัลติวอลล์คาร์บอนนาโนทิวบ์ที่สังเคราะห์เชิงไฟฟ้าเคมี (ETHYLENE GAS SENSOR FROM ELECTROCHEMICALLY SYNTHESIZED POLYANILINE/TIN OXIDE/MULTIWALL CARBON NANOTUBE COMPOSITES) อ. ที่ปรึกษาวิทยานิพนธ์: รศ.ดร. ดวงดาว อาจองค์, 161หน้า.

ตัวรับรู้แก๊สเอทิลีนถูกประดิษฐ์และพัฒนาขึ้นจากพอลิแอนิไลน์ โดยทำการศึกษาอิทธิพลของตัวแปรต่างๆที่มีผลต่อการรับรู้แก๊สเอทิลีน ได้แก่ ปริมาณการฝังตัวของพอลิแอนิไลน์ ชนิดกรดที่ใช้โคป 5 ชนิด (กรดไฮโดรคลอริก กรดซัลฟูริก กรดฟอสฟอริก กรดโทลูอินซัลโฟนิก และกรดโคเคซัล เบนโซซีน ซัลโฟนิก) ที่ความเข้มข้นของกรดในการโคปต่างๆกัน (0.1, 0.075, 0.05, 0.025 และ 0.01 โมล) ปริมาณของมัลติวอลล์คาร์บอนนาโนทิวบ์(ร้อยละ 0.2 0.4 และ 0.8โดยน้ำหนัก)และ ปริมาณของอนุภาคนาโนโลหะทินออกไซด์(ที่ระยะเวลาการฝังตัวต่างๆกัน (60, 90, 120 และ 150 วินาที)

ผลการทดลองพบว่า สภาวะที่เหมาะสมในการสังเคราะห์พอลิแอนิไลน์โดยวิธีการทางไฟฟ้าเคมี คือ การให้ศักย์ไฟฟ้าเคมีแบบสลับในช่วง -0.3-1.0 โวลต์ ด้วยอัตราเร็ว 10 มิลลิโวลต์/วินาที ที่จำนวนรอบ 10 รอบ พอลิแอนิไลน์ที่ได้มีโครงสร้างทางสัณฐานวิทยาแบบ โครงสร้างเส้นใยนาโน จากการศึกษาอิทธิพลของชนิดของกรด 5 ชนิดที่ใช้โคปพบว่า ลำดับความไวของกรดที่ใช้โคปที่มีต่อการตอบสนองแก๊สเอทิลีนคือ กรดซัลฟูริก>กรดฟอสฟอริก>กรดโทลูอินซัลโฟนิก>กรดโคเคซัล เบนซีน ซัลโฟนิก> กรดไฮโดรคลอริก หลังจากการเก็บตัวรับรู้พอลิแอนิไลน์โคป 3 เดือนพบว่า ตัวรับรู้ที่โคปด้วยกรดซัลฟูริก 0.1 โมล ให้ผลต่อการตอบสนองแก๊สเอทิลีนในระดับ 10 ส่วนในล้านส่วน โดยมีความไวในการตรวจวัดที่ร้อยละ 2.94 ภายใต้ระยะเวลาเก็บรักษา 3 เดือน การเติมมัลติวอลล์คาร์บอนนาโนทิวบ์ในตัวรับรู้พอลิแอนิไลน์ส่งผลช่วยเพิ่มเสถียรภาพทางความร้อนต่อตัวรับรู้พอลิแอนิไลน์ และที่การเติมมัลติวอลล์คาร์บอนนาโนทิวบ์ ปริมาณร้อยละ 0.2 เพิ่มความไวในการตรวจวัดแก๊สเอทิลีนระดับ 10 ส่วนในล้านส่วน จากร้อยละ 2.94 เป็น 4.39 ภายใต้ระยะเวลาเก็บรักษา 3 เดือน ตัวรับรู้เชิงประกอบของ พอลิแอนิไลน์,มัลติวอลล์คาร์บอนนาโนทิวบ์และอนุภาคนาโนโลหะทินออกไซด์ ถูกขึ้นรูปโดย ทำการฝังตัวของอนุภาคนาโนโลหะทินออกไซด์ด้วยวิธี อิเล็กโตรโพสิซีตและทำการฝังตัวของพอลิแอนิไลน์/มัลติวอลล์คาร์บอนนาโนทิวบ์ โดยให้ศักย์ไฟฟ้าคงที่ในสารละลายของ แอนิไลน์/มัลติวอลล์คาร์บอนนาโนทิวบ์ พบว่า ที่ระดับปริมาณการฝังตัวของอนุภาคนาโนโลหะทินออกไซด์ 60 วินาที ในพอลิแอนิไลน์/มัลติวอลล์คาร์บอนนาโนทิวบ์ให้ความไวในการตอบสนองต่อแก๊สเอทิลีนสูงสุดที่ระดับ 10 ส่วนในล้านส่วน

ภาควิชา วัสดุศาสตร์ลายมือชื่อนิสิต.....
สาขาวิชา วัสดุศาสตร์ลายมือชื่อ อ.ที่ปรึกษาวิทยานิพนธ์.....
ปีการศึกษา 2554

นายประสิทธิ์ พัฒนะภูวัฒน์ : ตัวรับรู้แก๊สเอทิลีนจากวัสดุเชิงประกอบพอลิแอนิไลน์/ทินออกไซด์/มัลติวอลล์คาร์บอนนาโนทิวบ์ที่สังเคราะห์เชิงไฟฟ้าเคมี (ETHYLENE GAS SENSOR FROM ELECTROCHEMICALLY SYNTHESIZED POLYANILINE/TIN OXIDE/MULTIWALL CARBON NANOTUBE COMPOSITES) อ. ที่ปรึกษาวิทยานิพนธ์: รศ.ดร. ดวงดาว ออาจงค์, 161หน้า.

ตัวรับรู้แก๊สเอทิลีนถูกประดิษฐ์และพัฒนาขึ้นจากพอลิแอนิไลน์ โดยทำการศึกษาอิทธิพลของตัวแปรต่างๆที่มีผลต่อการรับรู้แก๊สเอทิลีน ได้แก่ ปริมาณการฝังตัวของพอลิแอนิไลน์ ชนิดกรดที่ใช้โคป 5 ชนิด (กรดไฮโดรคลอริก กรดซัลฟูริก กรดฟอสฟอริก กรดโทลูอินซัลโฟนิก และกรดโคเดคซิล เบนโซซีน ซัลโฟนิก) ที่ความเข้มข้นของกรดในการโคปต่างๆกัน (0.1, 0.075, 0.05, 0.025 และ 0.01 โมล) ปริมาณของมัลติวอลล์คาร์บอนนาโนทิวบ์(ร้อยละ 0.2 0.4 และ 0.8โดยน้ำหนัก)และ ปริมาณของอนุภาคนาโนโลหะทินออกไซด์(ที่ระยะเวลาการฝังตัวต่างๆกัน (60, 90, 120 และ 150 วินาที)

ผลการทดลองพบว่า สภาวะที่เหมาะสมในการสังเคราะห์พอลิแอนิไลน์โดยวิธีการทางไฟฟ้าเคมี คือ การให้ศักย์ไฟฟ้าเคมีแบบสลับในช่วง -0.3-1.0 โวลต์ ด้วยอัตราเร็ว 10 มิลลิโวลต์/วินาที ที่จำนวนรอบ 10 รอบ พอลิแอนิไลน์ที่ได้มีโครงสร้างทางสัณฐานวิทยาแบบ โครงสร้างเส้นใยนาโน จากการศึกษาอิทธิพลของชนิดของกรด 5 ชนิดที่ใช้โคปพบว่า ลำดับความไวของกรดที่ใช้โคปที่มีต่อการตอบสนองแก๊สเอทิลีนคือ กรดซัลฟูริก>กรดฟอสฟอริก>กรดโทลูอินซัลโฟนิก>กรดโคเดคซิล เบนซีน ซัลโฟนิก> กรดไฮโดรคลอริก หลังจากการเก็บตัวรับรู้พอลิแอนิไลน์โคป 3 เดือนพบว่า ตัวรับรู้ที่โคปด้วยกรดซัลฟูริก 0.1 โมล ให้ผลต่อการตอบสนองแก๊สเอทิลีนในระดับ 10 ส่วนในล้านส่วน โดยมีความไวในการตรวจวัดที่ร้อยละ 2.94 ภายใต้ระยะเวลาเก็บรักษา 3 เดือน การเติมมัลติวอลล์คาร์บอนนาโนทิวบ์ในตัวรับรู้พอลิแอนิไลน์ส่งผลช่วยเพิ่มเสถียรภาพทางความร้อนต่อตัวรับรู้พอลิแอนิไลน์ และที่การเติมมัลติวอลล์คาร์บอนนาโนทิวบ์ ปริมาณร้อยละ 0.2 เพิ่มความไวในการตรวจวัดแก๊สเอทิลีนระดับ 10 ส่วนในล้านส่วน จากร้อยละ 2.94 เป็น 4.39 ภายใต้ระยะเวลาเก็บรักษา 3 เดือน ตัวรับรู้เชิงประกอบของ พอลิแอนิไลน์,มัลติวอลล์คาร์บอนนาโนทิวบ์และอนุภาคนาโนโลหะทินออกไซด์ ถูกขึ้นรูปโดย ทำการฝังตัวของอนุภาคนาโนโลหะทินออกไซด์ด้วยวิธี อิเล็กโตรโพสิซีตและทำการฝังตัวของพอลิแอนิไลน์/มัลติวอลล์คาร์บอนนาโนทิวบ์ โดยให้ศักย์ไฟฟ้าคงที่ในสารละลายของ แอนิไลน์/มัลติวอลล์คาร์บอนนาโนทิวบ์ พบว่า ที่ระดับปริมาณการฝังตัวของอนุภาคนาโนโลหะทินออกไซด์ 60 วินาที ในพอลิแอนิไลน์/มัลติวอลล์คาร์บอนนาโนทิวบ์ให้ความไวในการตอบสนองต่อแก๊สเอทิลีนสูงสุดที่ระดับ 10 ส่วนในล้านส่วน

ภาควิชา วัสดุศาสตร์ลายมือชื่อนิสิต.....
 สาขาวิชา วัสดุศาสตร์ลายมือชื่อ อ.ที่ปรึกษาวิทยานิพนธ์.....
 ปีการศึกษา 2554

5073841923 : MAJOR MATERIAL SCIENCE

KEYWORDS : POLYANILINE/ TIN OXIDE / MUTIWALL CARBON NANOTUBE/ ELECROCHEMISTRY/ELECTROPHORETIC DEPOSITION/ CYCLIC VOLTAMMETRY/ETHYLENE GAS SENSOR

PRASIT PATTANANUWAT: ETHYLENE GAS SENSOR FROM ELECTROCHEMICALLY SYNTHESIZED POLYANILINE/TIN OXIDE/ MULTIWALL CARBON NANOTUBE COMPOSITES. ADVISOR: ASSOC. PROF. DR. DUANGDAO AHT-ONG, PhD., 161 pp.

This research proposed four steps to fabricate and improve sensor for ethylene gas detection based on polyaniline (PANi) and/or PANi composites. The effects of amount of PANi, acid dopant of PANi (i.e., hydrochloric acid (HCl), sulfuric acid (H₂SO₄), phosphoric acid (H₃PO₄), *p*-toluene sulfonic acid (TSA), and dodecyl benzene sulfonic acid (DBSA) at each different concentration of 0.1, 0.075, 0.05, 0.025, and 0.01 M), multiwall carbon nanotubes (MWCNTs at 0.2, 0.4, and 0.8% wt) and tin oxide nanoparticles (Sn₂O NPs at different deposit times of 60, 90, 120, and 150 second) were used to study the sensing property against ethylene gas.

The nanofibril structure of PANi film was easily obtained under applying continuous potential cycle ranging from -0.3-1.0 V with scanning rate 10 mV/s at 10 scans of cyclic voltammetry. The type and concentration of acid dopant had marked influences on the sensing properties against ethylene gas. The sensitivity of PANi with different acid dopants decreased in the order of H₂SO₄> H₃PO₄> TSA> DBSA>HCl. After aging for 3 months, the doping PANi with 0.1 M H₂SO₄ can detect ethylene gas at 10 ppm with sensing magnitudes of 2.94 %. The addition of 0.2 % wt. MWCNT into PANi resulted in an improve sensitivity of PANi against 10 ppm ethylene gas from 2.94% to 4.39% after aging for three months. Multilayer composites of PANi/ MWCNT / SnO₂ NPs were synthesized by electrophoretic deposition of SnO₂ NPs and then chronoamperometric deposition of the PANi/MWCNT. The level of deposition SnO₂ NPs at 60 second in MWCNT/PANi composites exhibited the highest sensitivity for the detection ethylene gas at 10 ppm but its sensitivity decreased with increasing SnO₂ NPs.

Department : Material Science..... Student's Signature

Field of Study : Material Science..... Advisor's Signature

Academic Year : 2011.....

Acknowledgements

I would like to thank my advisor Associate Professor Dr. Duangdao Aht-Ong for her fantastic support throughout the research. She was there whenever I needed any help or ideas. Her comments and suggestions have widened my perspectives in both knowledge and practical applications.

Special thanks are also extended to Assistant Professor Dr. Sirithan Jiemsirilers, Associate Professor Dr. Kawee Srikulkit, and Assistant Professor Dr. Boonchoat Paosawatyanong for reading, proofreading and suggesting on the manuscript, and for their advice, motivating comments, and participation as thesis committee members.

I wish also to extend my sincere thanks to Dr. Anurat Wisitsoraat at the National Electronics and Computer Technology Center (NECTEC), Thailand, for supporting a gas sensor testing system.

I wish grateful recognition in financial support for research work from the 90TH Year Anniversary of Chulalongkorn University Fund (Ratchadaphiseksomphot Endowment Fund) and also thank for scholarship from National Center for Petroleum, Petrochemicals and Advanced Materials, Chulalongkorn University.

My great appreciation goes to all of my friends at the Department of Materials Science who have been encouraging and helping me while I was studying at Chulalongkorn University. Their valuable friendships will last forever.

Last but definitely not least, my deepest gratitude goes to my mother for standing by me regardless of what happened, supporting me, believing in me and encouraging me.

Contents

	Page
Abstract (Thai)	iv
Abstract (English)	v
Acknowledgments	vi
Contents	vii
List of Tables	xi
List of Figures	xii
 Chapter	
I Introduction	1
II Literature Survey	5
2.1 Ethylene gas: structure features and properties	5
2.1.1 Nature of ethylene gas.....	5
2.1.2 Ethylene as a plant hormone.....	6
2.2 Conductive polymer	7
2.2.1 Basic concepts.....	7
2.2.2 Charge storage mechanism.....	9
2.2.3 Charge transfer.....	11
2.3 Polyaniline	13
2.3.1 Structure features.....	13
2.3.2 Doping in polyaniline	14
2.3.3 Charge carrier mechanism of polyaniline.....	16
2.4 Synthesis polyaniline: nanostructure as sensitive layer for gas sensor	18
2.4.1 Electrochemical: principle.....	19
2.4.2 Voltammetry.....	21
2.4.2.1 Potential step voltammetry.....	21
2.4.2.2 Linear Sweep Voltammetry.....	22
2.4.2.3 Cyclic Voltammetry	24

Chapter	Page
2.4.3 Electrochemical synthesis of polyaniline.....	25
2.5 Polyaniline as sensitive layer for gas sensors.....	28
2.5.1 Polyaniline doping: Acid doping	28
2.6 Inclusion of material particles into polyaniline for enhance gas sensing property.....	31
2.6.1 Inclusion of multiwall carbon nanotube into polyaniline.....	31
2.6.1.1 Multiwall carbon nanotube: structure features and Properties.....	31
2.6.1.2 Effect of the presence of gases in contact with the carbon nanotube.....	32
2.6.2 Inclusion of metallic particles into polyaniline.....	34
2.6.2.1 Tin oxide: structure features and properties.....	34
2.6.2.2 Effect of the presence of gases in contact with the tin oxide surface.....	35
2.7 Electrophoretic deposition.....	39
2.7.1 Electrophoresis deposition.....	40
2.7.2 Suspension stability.....	42
 III Experimental.....	 47
3.1 Materials and Chemicals.....	47
3.2 Equipment and Instrument.....	48
3.2.1 Potentiostat/galvanostat	48
3.2.1.1 Gold interdigitated substrate	49
3.2.2 Electrophoretic deposition.....	50
3.3 Experimental Procedure.....	51
3.3.1 Electrochemical Synthesis of Polyaniline as Ethylene Gas Sensor	51
3.3.2 Electrochemical Synthesis of Sensitive Layer of Polyaniline: Effects of acid dopant on ethylene gas sensing.....	53

Chapter	Page
3.3.2.1 Electro-deposition of sensitive layer of polyaniline nanofibers.....	53
3.3.2.2 Preparation of de-doped and doped polyaniline.....	53
3.3.3 In-situ electrochemical synthesis of sensitive layer of polyaniline/multiwall carbon nanotube composite for ethylene gas detection.....	55
3.3.3.1 Dispersion of multi-wall carbon nanotube in aniline monomer.....	55
3.3.3.2 Electro-deposition of sensitive layer of polyaniline nanofibers /multiwall carbon nanotube composite film.....	55
3.3.3.3 De-doped and doped polyaniline/multiwall carbon nanotube.....	55
3.3.4 In-situ electrochemical synthesis of novel sensitive layer of polyaniline/multiwall carbon nanotube/ tin oxide nanoparticles (PANi/MWCNT/SnO ₂ NPs) hybrid materials for ethylene gas detection.....	57
3.3.4.1 Deposition of SnO ₂ NPs onto the interdigitated gold substrate.....	57
3.3.4.2 Chronoamperometric deposition of PANi/MWCNT nanofibers on the thin film of SnO ₂ NPs.....	57
3.3.4.3 De-doped and doped polyaniline/multiwall carbon nanotube/tin oxide nanoparticle.....	58
3.4 Characterization and Testing.....	60
3.4.1 Ultraviolet- Visible Spectrometer (UV-VIS).....	60
3.4.2 Fourier Transform Infrared Spectrometer (FT-IR).....	60
3.4.3 Raman Spectroscopy.....	61
3.4.4 Scanning Electron Microscope (SEM).....	62
3.4.5 Thermo Gravimetric Analyzer (TGA).....	62

Chapter	Page
3.5 Ethylene gas sensing measurement	63
IV Results and Discussion	65
4.1 Electrochemical Synthesis of Polyaniline as Ethylene Gas Sensor ...66	
4.1.1 Electrochemical synthesis of polyaniline.....	66
4.1.2 Characterization of polyaniline.....	68
4.1.2.1 UV-Visible spectral characterization of PANi.....	68
4.1.2.2 Fourier transforms infrared spectroscopy of PANi.....	69
4.1.3 Morphological Studies.....	72
4.1.4 Ethylene gas detection of PANi via resistance measurement...74	
4.2 Electrochemical Synthesis of Sensitive Layer of Polyaniline	
: Effects of Acid Dopant on Ethylene Gas Sensing	77
4.2.1 Electrochemical synthesis of polyaniline.....	77
4.2.2 Characterization of emeraldine salt forms of PANi.....	79
4.2.2.1 UV-Visible spectral characterization of PANi	
and doped PANi.....	79
4.2.2.2 Fourier transforms infrared spectroscopy	
characterization of PANi and doped PANi.....	84
4.2.2.3 Morphological characterization of the deposited PANi	
with different acid dopants.....	91
4.2.2.4 Thermo gravimetric Analysis (TGA).....	98
4.2.3 Ethylene gas detection of doped PANi via resistance	
measurement.....	101
4.3 In-Situ Electrochemical Synthesis of Sensitive Layer of	
Polyaniline/Multiwall Carbon Nanotube Composite for	
ethylene gas detection	114
4.3.1 Electrochemical synthesis of PANi/MWCNT.....	114
4.3.2 Raman characteristic of deposited PANi/MWCNT	
composites.....	116

Chapter	Page
4.3.3 Microstructure characterization of the deposited PANi/MWCNT.....	118
4.3.4 Thermal behavior of PANi/MWCNT composites.....	120
4.3.5 Ethylene gas detection of PANi/MWCNT composites via resistance measurement.....	122
4.4 In-situ electrochemical synthesis of novel sensitive layer of polyaniline/multiwall carbon nanotube/tin oxide hybrid materials for ethylene gas detection.....	126
4.4.1 Deposition of Tin oxide Nanoparticles onto the interdigitated gold.....	126
4.4.4.1 Microstructure characterization of the deposited SnO ₂ NP layer.....	127
4.4.1.2 Elemental analysis of the deposited SnO ₂ NP layer.....	128
4.4.2 Deposition of nanofibers PANi/MWCNT on thin film of SnO ₂ nanoparticle.....	131
4.4.2.1 Microstructure characterization of the deposited PANi/MWCNT layer.....	132
4.4.2.2 Raman characteristic of PANi/MWCNT and PANi/MWCNT/SnO ₂ nanoparticle.....	134
4.4.2.3 Thermal behavior of PANi/MWCNT and PANi/MWCNT/SnO ₂ nanoparticle.....	136
4.4.3 Ethylene gas detection via resistance measurement of PANi/MWCNT and PANi/MWCNT/SnO ₂ nanoparticle.....	138
V Conclusions.....	139
5.1 Conclusions.....	139
References.....	145

Chapter	Page
Appendices	153
Appendix A.....	154
Appendix B.....	160
Biography	161

List of Tables

Table	Page
3.1 Chemical structure of material.....	47
4.1 Weight increase and resistance of deposited PANi films at different potential cycles.....	66
4.2 Infrared vibration and assignments for emeraldine salt of PANi-H ₂ SO ₄	70
4.3 The assignment for UV-Visible absorption peaks of undoped and doped Polyaniline.....	81
4.4 Assignment for IR bands of polyaniline emeraldine base.....	84
4.5 Assignment for IR bands of polyaniline emeraldine salt with different acid dopants.....	90

List of Figures

Figure	Page
2.1 Molecular structure of ethylene	5
2.2 Chemical structure of monomer unit of conductive polymer	7
2.3 Logarithmic conductivity ladder locating some metals and conducting polymers	9
2.4 The mechanism explanation of charge storage of polypryole.....	11
2.5 The chemical structure of polyaniline.....	13
2.6 The different three electronic form bases on polyaniline structure.....	14
2.7 The emeraldine salt formation of polyaniline (a) protonic acid doping of emeraldine base and (b) oxidative doping of lecoemeraldine base.....	15
2.8 Charge carrier evolution of emeraldine base as a function of protonation.....	17
2.9 A galvanic electrochemical cell	20
2.10 Series of linear sweep voltammograms recorded at different scan.....	23
2.11 Voltage as a function of time and current as a function of voltage for CV.....	24
2.12 The current for a reversible electron transfer at different the voltage scan rate.....	25
2.13 Mechanism of oxidative electropolymerization of aniline.....	27
2.14 Mechanism of acid doping of polyaniline.....	29
2.15 The structure of multiwall carbon nanotube consisting of three concentric single walled nanotubes.....	32
2.16 The active site of single wall nanotube for gas absorption.....	33
2.17 Unit cell of SnO ₂	34
2.18 The effect of Walter Schottky of tin oxide in oxygen atmosphere (left) and in reducing gas (right).....	38
2.19 Schematic diagram of the cathodic deposition of electrophoretic deposition....	39
2.20 Electrophoresis double layer in applied electric field.....	40

Figure	Page
2.21 Mechanism stabilization (A) electrostatic (b) steric and (c) electrosteric.....	43
3.1 PGSTAT30 Pentostat/galvanostat	48
3.2 The working substrate for deposition of sensor (a) gold interdigitated substrate (b) gap length between gold gap and insulate gap.....	49
3.3 Schematic illustrates the electrophoretic deposition of SnO ₂ NPs on gold interdigitated substrate.....	50
3.4 Flow diagram for fabrication of PANi sensor for ethylene gas detection.....	52
3.5 Flow diagram for doped PANi sensor fabrication for ethylene gas detection...	54
3.6 Flow diagram for fabrication of PANi/MWCNT sensor for ethylene gas detection.....	56
3.7 Flow diagram for fabrication of PANi/MWCNT/SnO ₂ NP sensor for ethylene gas detection.....	59
3.8 SPECORD S 100 Ultraviolet-visible spectrometer.....	60
3.9 Nicolet 6700 Fourier Transform Infrared Spectrometer.....	61
3.10 GX NIR Raman Spectroscopy.....	61
3.11 JSM 5800 LV Scanning Electron Microscope.....	62
3.12 SDTA 851 ^e Thermo Gravimetric Analyzer.....	63
3.13 Schematic of the gas detection system for testing conductive polymer.....	64
3.14 Gas detection system for testing conductive polymer.....	65
4.1 Cyclic voltammograms of polyaniline film growth at varing 5 to 25 of number of scan with scanning rates of 50 mV/Sec.....	67
4.2 UV-Vis absorption spectra of PANi in N-methyl-2-pyrrolidone solution.....	68
4.3 The chemical structure of emeraldine salt form of sulphonate group of polyaniline.....	69

Figure	Page
4.4 FT-IR spectrum of obtained-PANi after cyclic voltammetry at 10 scans.....	71
4.5 SEM images of PANi prepared by cyclic voltammetry on interdigitated gold substrate at different number of scans of cyclic voltammetry: (a) after 5 scans (b) after 10 scans.....	72
4.6 SEM images of PANi prepared by cyclic voltammetry on interdigitated gold substrate at different numbers scan of cyclic voltammetry: (a) 5 scans (b) 10 scans (c) 15 scans (d) 20 scans (e) 25 scans.....	73
4.7 The resistance response behavior against varying concentrations of ethylene gas of the PANi-H ₂ SO ₄ at different number of cyclic voltammetry scans: (a) 10 scans, (b) 15 scans, (c) 20 scans and (d) 25 scans.....	75
4.8 The sensing magnitude of the PANi-H ₂ SO ₄ against varying concentrations of ethylene gas prepared from different numbers of cyclic voltammetry scan..	76
4.9 Cyclic voltammograms of polyaniline film growth at scanning rate of 50 mV/Sec with varying number of potential scan.....	78
4.10 UV-Vis absorption spectrum of solution undoped PANi solution.....	79
4.11 UV-spectra of PANi dope with HCl at different concentration.....	81
4.12 UV-spectra of PANi dope with H ₂ SO ₄ at different concentration.....	82
4.13 UV-spectra of PANi dope with H ₃ PO ₄ at different concentration.....	82
4.14 UV-spectra of PANi dope with DBSA at different concentration.....	83
4.15 UV-spectra of PANi dope with TSA at different concentration.....	83
4.16 FT-IR spectrum of undoped polyaniline.....	85
4.17 FT-IR spectrum of PANi-HCl at different acid concentration.....	86
4.18 FT-IR spectrum of PANi-H ₂ SO ₄ at different acid concentration.....	86
4.19 FT-IR spectrum of PANi-H ₃ PO ₄ at different acid concentration.....	87
4.20 FT-IR spectrum of PANi-DBSA at different acid concentration.....	87
4.21 FT-IR spectrum of PANi-TSA at different acid concentration.....	88

Figure	Page
4.22 SEM images of PANi : (a) PANi prepared by cyclic voltammetry after 10 scans (b) PANi prepared by cyclic voltammetry after 10 scans and de-doped with 0.1 M NH ₄ OH.....	92
4.23 SEM images of HCl-doped PANi at different concentrations: (a) 0.01 mol (b) 0.025 mol (c) 0.05 mol (d) 0.075 mol (e) 0.1 mol.....	93
4.24 SEM images of H ₂ SO ₄ -doped PANi at different concentrations: (a) 0.01 mol (b) 0.025 mol (c) 0.05 mol (d) 0.075 mol (e) 0.1 mol.....	94
4.25 SEM images of H ₃ PO ₄ -doped PANi at different concentrations: (a) 0.01 mol (b) 0.025 mol (c) 0.05 mol (d) 0.075 mol (e) 0.1 mol.....	95
4.26 SEM image of DBSA-doped PANi at different concentrations: (a) 0.01 mol (b) 0.025 mol (c) 0.05 mol (d) 0.075 mol (e) 0.1 mol.....	96
4.27 SEM image of TSA-doped PANi at different concentrations: (a) 0.01 mol (b) 0.025 mol (c) 0.05 mol (d) 0.075 mol (e) 0.1 mol.....	97
4.28 TGA thermogram of polyaniline emeraldine base (undoped PANi).....	98
4.29 TGA thermogram of polyaniline emeraldine salt (Doped PANi with HCl, H ₂ SO ₄ , H ₃ PO ₄ , DBSA, and TSA).....	100
4.30 The resistance response behavior of the PANi-H ₂ SO ₄ derived from different acid doping concentrations after 1 month: a) 0.01 mol, b) 0.025 mol, c) 0.05 mol, d) 0.075 mol and e) 0.1 mol.....	102
4.31 The resistance response behavior of PANi-H ₃ PO ₄ derived from different acid doping concentrations after 1 month: a) 0.01 mol, b) 0.025 mol, c) 0.05 mol, d) 0.075 mol and e) 0.1 mol.....	103
4.32 The resistance response behavior of PANi-DBSA derived from different acid doping concentrations after 1 month: a) 0.01 mol, b) 0.025 mol, c) 0.05 mol, d) 0.075 mol and e) 0.1 mol.....	104
4.33 The resistance response behavior of PANi-TSA derived from different acid doping concentrations after 1 month: a) 0.01 mol, b) 0.025 mol c) 0.05 d) 0.075 mol and e) 0.1 mol.....	105

Figure	Page
4.34 The resistance response behavior of PANi-H ₂ SO ₄ derived from different acid doping concentrations after 3 months: a) 0.01 mol, b) 0.025 mol, c) 0.05 mol, d) 0.075 mol and e) 0.1 mol.....	108
4.35 The resistance response behavior of PANi-H ₃ PO ₄ derived from different acid doping concentrations after 3 months: a) 0.01 mol, b) 0.025 mol, c) 0.05 mol, d) 0.075 mole and e)0.01 mol.....	109
4.36 The resistance response behavior of PANi-TSA derived from different acid doping concentrations after 3 months: a) 0.01 mol, b) 0.025 mol, c) 0.05 mol d) 0.075 mol and e) 0.1 mol.....	110
4.37 The sensing magnitude of the PANi in term of different acid dopings at various acid concentrations after 1 month: a) H ₂ SO ₄ , b) H ₃ PO ₄ , c) DBSA and d) TSA.....	111
4.38 The sensing magnitude of PANi in term of different acid dopings at various acid concentrations after 3 months: a) H ₂ SO ₄ , b) H ₃ PO ₄ and c) TSA.....	112
4.39 The sensing magnitude of the PANi-H ₂ SO ₄ at different concentrations after 6 Months.....	113
4.40 The cyclic voltammogram of 0.2 % wt of MWCNT in 0.1 M aniline of 1M sulfuric acid at 50 mV/s.....	115
4.41 Raman spectra of the PANi, MWCNT and PANi/MWCNT at MWCNT loading at 0.8% wt.....	117
4.42 Representative SEM micrographs (20,000 x magnification) of the deposited PANi/MWCNT at different MWCNT loadings (a) pure MWCNT (b) PANi (c) 0.2%wt MWCNT/PANi (d) 0.4% wt MWCNT/PANi and (e) 0.8% wt MWCNT/PANi.....	119
4.43 TGA thermograms of the MWCNT, PANi, and PANi/MWCNT composites at different MWCNT loadings.....	121

Figure	Page
4.44 Response-recovery behavior of MWCNT/PANi at different MWCNT loadings after 1 month aging: (A) pure PANi , (B) 0.2% wt MWCNT/PANi, (C) 0.4% wt MWCNT/PANi and (D) 0.8% wt MWCNT/PANi.....	123
4.45 Response-recovery behavior of MWCNT/PANi at different MWCNT loadings after 3 month aging: (A) pure PANi , (B) 0.2% wt MWCNT/PANi, (C) 0.4% wt MWCNT/PANi and (D) 0.8% wt MWCNT/PANi.....	124
4.46 The sensitivity behavior of the PANi/MWCNT composites at different MWCNT loadings times after (a) 1 month and (b) 3 months aging.....	125
4.47 Representative SEM micrographs (20,000 x magnification) of the deposited SnO ₂ NP when deposited at 9 V for (a) 60 sec, (b) 90 sec, (c) 120 sec and (d) 150 second.....	127
4.48 The elemental distributions of deposited SnO ₂ NPs layer at different deposited times (a) 60 second, (b) 90 second, (c) 120 second, and (d) 150 second.....	129
4.48 (cont.) the elemental distributions of deposited SnO ₂ nanoparticle layer at different deposited times (a) 60 second, (b) 90 second, (c) 120 second, and (d) 150 second.....	130
4.49 Chronoamperometric deposition curve of a 0.1 mol aniline/MWCNT in 1.0 M H ₂ SO ₄ solution onto the SnO ₂ NP layer of a gold interdigitated anode.....	131
4.50 Representative SEM micrographs (20,000 x magnification) of the deposited PANi/MWCNT coatings when deposited at 1 V for (a) 90 second, (b) 120 second, (c) 150 second, and (d) 160 second.....	133
4.51 Raman spectra of the PANi/MWCNT and the PANi/MWCNT/SnO ₂ NP composite derived from a SnO ₂ NP deposition time of 90 second.....	135
4.52 TGA thermograms of the PANi/MWCNT and PANi/MWCNT/SnO ₂ NP composite derived from SnO ₂ NP deposition times of 120 and 150 second.....	137

Figure	Page
4.53 The resistance response of PANi/MWCNT/SnO ₂ NP composites derived from different SnO ₂ NP deposition times after (a) 1 month and (b) 3 months ageing.....	139
4.54 The sensitivity behavior of the PANi/MWCNT/SnO ₂ NP composites derived from different SnO ₂ NP deposition times after (a) 1 month and (b) 3 months aging.....	140

CHAPTER I

INTRODUCTION

Ethylene gas, a plant hormone, is the cause of spoilage and over-ripening of fruits as well as the inferior quality of other agricultural products. The shelf life of many fruits is shortened by the hastening of fruit ripening that is induced by ethylene gas at levels of at least 20 ppm [1]. Thus, to prevent the spoilage of fruits in the early stage and to estimate the life expectancy of agricultural product, the ethylene gas level needs to be controlled in the local environment of the fruit, but this requires sensitive evaluation of the actual local gas levels.

The high potential of application for conductive polymers in chemical and biological sensors at room temperature is one of the main reasons for the intensive investigation and development of these materials. Conducting polymers, including polyaniline (PANi), have attracted most attention and become important subject of most research [2]. PANi exists in a variety of forms that differ in chemical and physical properties. The monomer structures of PANi consist of benzenoid diamine (reduced repeating unit) and quinoid diamine (oxidized repeating unit). The difference of oxidation state provide three forms of PANi which are leucoemeraldine base (completely reduced form), emeraldine base (half oxidize form) and pernigraniline base (completely oxidized form). The emeraldine base can be rendered to polysemiquinone radical (metallic form) by acid doping that has potentiality for practical applications in a sustainable way and offers many possibilities for use [3].

During the past decades, PANi and its composites were widely investigated as gas sensing materials for the detection of a number of chemicals such as ammonia (NH₃) [4], nitrogen dioxide (NO₂) [5], carbon monoxide (CO) [6], organic amine [7], chloroform (CHCl₃) [8], hydrazine (N₂H₄) [8], methane (CH₄) [9], methanol vapor [10], and etc.

Typically, after being exposed conductive polymer against analyst gas, the conductivity of conductive polymer is responded by a changing in conductivity. The interaction of gas with conductive polymer can be classified into two classes which are physical absorption and chemical reaction [8]. In case of physical absorption, non-

reactive volatile organic reagents reveal weak interaction between PANi and gas analyst leading to a changing in resistance. For chemical reaction, the oxidation states of PANi can be changed with gas analyst either donor or acceptor electron.

For ethylene gas detection by PANi, the problem is the lack of interfacial reaction between PANi and ethylene gas, due to non-reactive and volatile nature of this gas, leading to a limitation in the sensing performance. The physicochemical modification of this material is required for improving sensing properties. In general, the gas absorption ability, the conductivity of PANi and the effect of counter ion of PANi are considered as majority to improve selectivity and sensing against ethylene gas. [3,7,8]

The synthesis of PANi nanostructure as sensitive layer for gas sensor is of interest because the high surface to volume ratios of nanostructure increase rapid response and reversible resistance change in PANi upon exposure to gas vapor. In situ polymerization of PANi with electrochemical synthesis is one route to obtain the layer of nano structure of PANi. As reported by Zhang and coworkers [11] that the morphology of PANi film prepared by electrochemistry revealed lamellar structure. The bulk film was formed at the bottom whereas the nanostructure of fibrillar was formed at the middle and the top of the film. In addition, this route reveals several advantages compared with the other methods [12]. It is an environmentally friendly process because no need of an oxidant is required in the reaction, the doping level and thickness of PANi film can be controlled via electrode potential, and the obtained-PANi film exhibits good simultaneous deposition compared with the other methods.

A major stimulation for the investigation of alternative paths for type of acid doping PANi was the discovery of a variety of sensing and selectivity of PANi sensor. Emeraldine base form of PANi can be protonated by aqueous acids with a concomitant increase in conductivity of almost 10 orders of magnitude. After doping, the emeraldine salt was created as polysemiquinone radical. The relative content of the benzenoid and quinoid of emeraldine salt can be decorated by the type and concentration of acid. The type of anion acid doping had effect on sensing and selectivity with analyst gas. For example, Ji et. Al. [7] found that doping PANi with three different types of acid including toluene sulfonic acid (TSA), sulfosalicylic acid (SSA) and hydrochloric acid (HCl) showed different response against triethylamine

gas sensing. The order of sensing of doping PANi against triethylamine gas is PANi – TSA, PANi-SSA, and PANi-HCl, respectively.

Besides acid doping, another interesting approach to enhance sensing properties of PANi is to add some additives. Multiwall carbon nanotubes (MWCNTs) have been widely studied as sensing material at room temperature. Thus, the modification PANi with MWCNT is interested to improve sensing properties. The increasing sensitivity of the sensor came from an ability of absorption of these materials. Due to high surface area of MWCNT and functionalization of MWCNT with analyte-specific gas detection, its unique physical and chemical properties can enhance sensing performance.

In addition, PANi modification with metallic particles has been found to improve its performances as sensitive layer. For example, Ulmann et al. [13] found that the incorporation of platinum microparticles into PANi film can enhance its redox switching rate between conducting (oxidized) and isolating (reduced) states. The selection of the metal oxide is very important and is based on the reduction potential of the particular metals of interest. For this research, tin oxide was selected to increase the level of selectivity of the PANi based sensor. Tin oxide (SnO_2) is an n-type semiconductor oxide with wide band gap energy due to electronically oxygen vacancies act as electron donors. Moreover, SnO_2 also has an ability in gas adsorption due to the high reactivity of the SnO_2 surface.

Furthermore, the organic-inorganic hybrid materials have been extensively investigated with a view to obtain composite materials with synergistic or complementary behaviors. The nanocomposites between CNT and metal oxide nanoparticles (NPs) have the potential to be applied in the functional material fields, such as gas detection. For example, Qifei et. al. [14] found that nanocomposites sensor comprising of multiwall carbon nanotubes, gold nano particles, and PANi. Sensor exhibited superior sensitivity, good repeatability and excellent stability in detecting ammonia gas. The sensitivity of sensors displayed a linear response to ammonia gas for concentration ranging from 200 ppb to 10 ppm

This research was divided into four steps which are investigation of the effect of deposited amount of polyaniline on ethylene gas detection by varying a number of cyclic voltammetry, the effect of acid dopant of PANi in terms of acid type and acid

level on ethylene gas detection, the effect of MWCNT nanotube on ethylene gas detection and the effect of tin oxide nanoparticles on ethylene gas detection. A hybrid sensor includes of modified functional PANi, MWCNT and SnO₂ nanoparticles are achieved in the last step. This specific hybrid sensor is invented to increase sensing property against ethylene gas at near room temperature.

Therefore, the aim of this research was to fabricate the ethylene gas sensor based on PANi and PANi composites containing MWCNT and/or SnO₂ by electrochemistry with cyclic voltammetry method. This rational point of research is due to the physicochemical sensitivity of PANi at room temperature, the high surface area of MWCNT and the natural non-stoichiometry of SnO₂ nanoparticle, allowing expected unique physical and chemical properties to enhance the sensing performance of ethylene gas sensors. All of the possible variables including the effect deposited amount of PANi, the effect of acid doping in terms of types and concentrations of acid, the content of MWCNT, and the amount of tin oxide were investigated. The sensitive layer of PANi, PANi/MWCNT and PANi/MWCNT/SnO₂ sensor was fabricated at various amounts of PANi, MWCNT and SnO₂.

CHAPTER II

LITERATURE SURVEY

2.1 Ethylene gas: structure features and properties

2.1.1 Nature of ethylene gas

Ethylene (C_2H_4) is a gaseous unsaturated hydrocarbon. The four hydrogen atoms bound to a pair of carbon atoms that are connected by a double bond. All six atoms that comprise ethylene are coplanar. The angle of H-C-H bond is 119° . It is close to the 120° (sp^2 hybridized carbon). The molecule is also relatively rigid due to the rotation of the C-C bond needs a high energy process to breaking the π -bond [15].

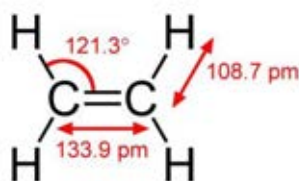


Figure 2.1 Molecular structure of ethylene [2]

Ethylene is a colorless gas with a faint odor, and a slightly sweet taste. The melting is $-169^\circ C$ and the boiling point is $-103.8^\circ C$. The presence of the double bond in its molecule of ethylene gas made its very reactive. The π -bond in the ethylene molecule is responsible for its useful reactivity. The double bond is a region of high electron density, thus it is susceptible to attack by electrophiles. Many reactions of ethylene are catalyzed by transition metals, which bind transiently to the ethylene using both the π and π^* orbitals. Ethylene gas can burn in air with a luminous flame and forms explosive mixtures with pure oxygen. It can combine directly with the halogens such as chlorine to form 1,2-dichloroethane[16].

2.1.2 Ethylene as a plant hormone

Ethylene gas is released from plants as a hormone. The biosynthesis of hormone plants is started from the conversion the amino acid methionine to S-adenosyl-L-methionine (SAM) by the enzyme Met Adenosyltransferase. SAM is converted to 1-aminocyclopropane-1-carboxylic-acid (ACC) by the enzyme ACC synthase (ACS). The ethylene gas is formed by the reaction of the enzyme ACC with oxygen as known as enzyme ACC-oxidase (ACO). The ACS is the key factor to control rate of ethylene gas production [17].

Ethylene production is regulated by a variety of development and environment factor. During the life of the plant, the trace level of ethylene throughout the life of plant is induced at certain stages of growth such as germination, ripening of fruits, abscission of leaves, and senescence of flowers. In addition, a variety of external aspects such as mechanical wounding, environmental stress, and certain chemical including auxin can also induce production of ethylene [18].

Ethylene act physiologically as a hormone and play critically role as ripeness in plants. As well known in the past, Crocker proposed that ethylene was the plant hormone responsible for fruit ripening as well as senescence of vegetative tissues in 1953. In the presence of ethylene, the shelf life of many fruits is shortens by hastening fruit ripening and floral senescence. For example, the concentration of ethylene about 0.1-0.2 ppm is enough to accelerate banana ripening and ethylene at least 0.01 ppm will accurate the blooming of carnation [19]. The flowers and plants which are subjected to stress during shipping release ethylene gas results in reduction of floral display. This problem always found in carnation, geranium, petunia, rose, and many others. It is importance to control and monitor levels of ethylene concentration for long-term storage life of fruit, vegetable and flower. Up to date, there are no suitable and compact ethylene-monitoring systems are available on the market.

2.2 Conductive polymer

The interest of conductive polymers has been recognized by the awarding of Nobel prize in chemistry in 2000 to Heeger [20], Macdiarmid [21], and H. Shirakawa, who synthesized the first conducting polymers and proved their potentialities in a large number of application.

2.2.1 Basic concepts

The common electronic feature of conductive polymers is a π -conjugated structure system which rearranged by the overlap of carbon p-orbital and alternating carbon-carbon sigma bonds. For example, the chemical structure of the most studies through member of the conductive polymer are shown in figure 2.2

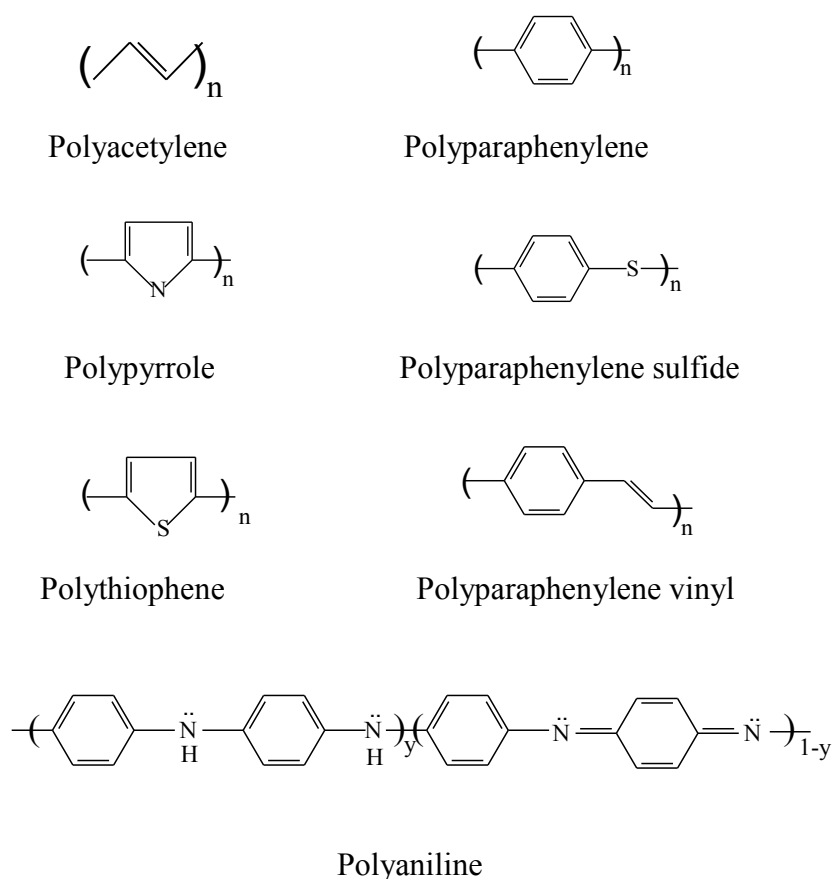


Figure 2.2 Chemical structure of monomer unit of conductive polymer [8]

Conductive polymers are inherently conducting in nature due to the presence of a conjugated electron system in their structure. All above of them have chemical structure for semiconductors. The highest occupied molecular orbital of monomer forms the occupied π -band (valence band) and the lowest unoccupied molecular orbital of the monomer forms the unoccupied π^* -band (conductive band). Conductive polymers have a low energy optical transition, low ionization potential and a high electron affinity. A high level of conductivity (near metallic) can be achieved in conductive polymers through oxidation–reduction as well as doping with a suitable dopant. [22]

The doping process can be increased the conductivity level of conductive polymer. A new energy level is created into band gap energy. The electronic insulator of polymer will be changed into metal form. The electrical conductivity depends on the doping level as donor or acceptor species are incorporated. The electrical conductivity can be n-type or p-type. Dopant atoms are positioned interstitially between chains and donate charges to or accept charges from polymer backbone. For example, Shirakawa et al. [23] found that the conductivity of polyacetylene could be increased by several orders of magnitude through chemical doping and in reality it can be converted from an insulator to a metal like conductor. Following the study on polyacetylene, other polymers such as polypyrrole (PPY), polythiophene, PANI, poly(pphenylenevinylene), and poly(p-phenylene), as well as their derivatives, have been synthesized and. The conductivity of a number of intrinsically conductive polymers relative to copper and liquid mercury is presented in Fig. 2.3

Since it has been found a various conductive polymers and their derivatives, it transited when doped with a weak oxidation agent or reducing agent. The early work has led to an understanding of the mechanisms of charge storage and charge transfer in these systems.

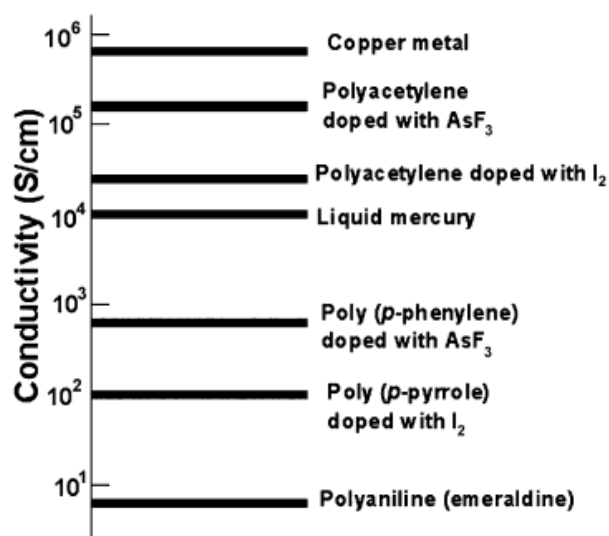


Figure 2.3 Logarithmic conductivity ladder locating some metals and conducting polymers [22]

2.2.2 Charge storage mechanism

The explanation of conducting polymers used band theory method [24]. For concept of conduction of electricity, a half filled valence band was formed from as a continuous delocalized π -system. The bond alteration will lower its energy of polymer (alternating short and long bonds). It introduces a band width of 1.5 eV making it a high energy gap for semiconductor.

In addition, the free spins concentration can increase with dopant. The concentration of free spins levels is higher at higher concentration dopant. To understand the effect of charge is stored along the polymer chain. The polymer may store charge in two ways. In an oxidation process, it could either lose an electron from one of the bands or it could localize the charge over a small section of the chain. Localizing the charge causes a local distortion due a change in geometry, which costs the polymer some energy.

However, the occurring of this local geometry decreases the ionization energy of the polymer chain and increases its electron affinity. This phenomenon made more able to accommodate the newly formed charges. In this way, the band

energy level is increased but its level was less than it would if the charge was delocalized.

The example for typical oxidizing dopants is iodine, NOPF_6 , iron(III) chloride and arsenic pentachloride. Sodium naphthalide is used as typical reductive dopant. The main criteria are its ability to oxidize or reduce the polymer without initiating side reactions that inhibit the polymers ability to conduct electricity.

For example of mechanism explanation, the oxidative doping of polypyrrole proceeds by following steps [25]. First, an electron is removed from the π system of the backbone polymer producing free radical and positive charge. Secondary, the radical and cation can couple to each other via local resonance of the charge and the radical. In this case, a sequence of quinoid-like rings is used. In finally, the distortion was produced and showed higher energy than the remaining portion of the chain. The creation and separation of these defects costs a considerable amount of energy.

This limits of the number of quinoid-like rings that can link these two bound species together. In the case of polypyrrole, it is expected that the lattice distortion extends over four pyrrole rings. This combination of a charge site and a radical is called a "*polaron*". It could be either a radical cation or radical anion. This polaron creates a new localized electronic state in the gap with the lower energy states. It was being occupied by a single unpaired electron. The polaron state of polypyrrole is symmetrically located about 0.5 eV from the band edges.

Upon further oxidation the free radical of the polaron is removed, creating a new spinless defect called a "*bipolaron*". This is lower energy than the creation of two distinct polarons. At higher doping levels, it can be showed that two polarons combine to form a bipolaron. Thus at higher doping levels the polarons are replaced with bipolarons. The band gap of bipolarons symmetrically polypyrrole are located at 0.75 eV. This eventually, with continued doping, forms into a continuous bipolaron bands. Their band gap also increases as newly formed bipolarons are made at the expense of the band edges. For a higher dope level, it is conceivable that the upper and the lower bipolaron bands will merge with the conduction and the valence bands respectively to produce partially filled bands and metallic like conductivity. This mechanism explanation is shown in figure 2.4.

In addition, the ground state structure of such polymers are twofold degenerate, the charged cation are not bound to each other by a higher energy bonding

configuration and can freely separate along the chain. The effect of this is that the charged defects are independent of one another and can form domain walls that separate two phases of opposite orientation and identical energy. These are called solitons and can sometimes be neutral.

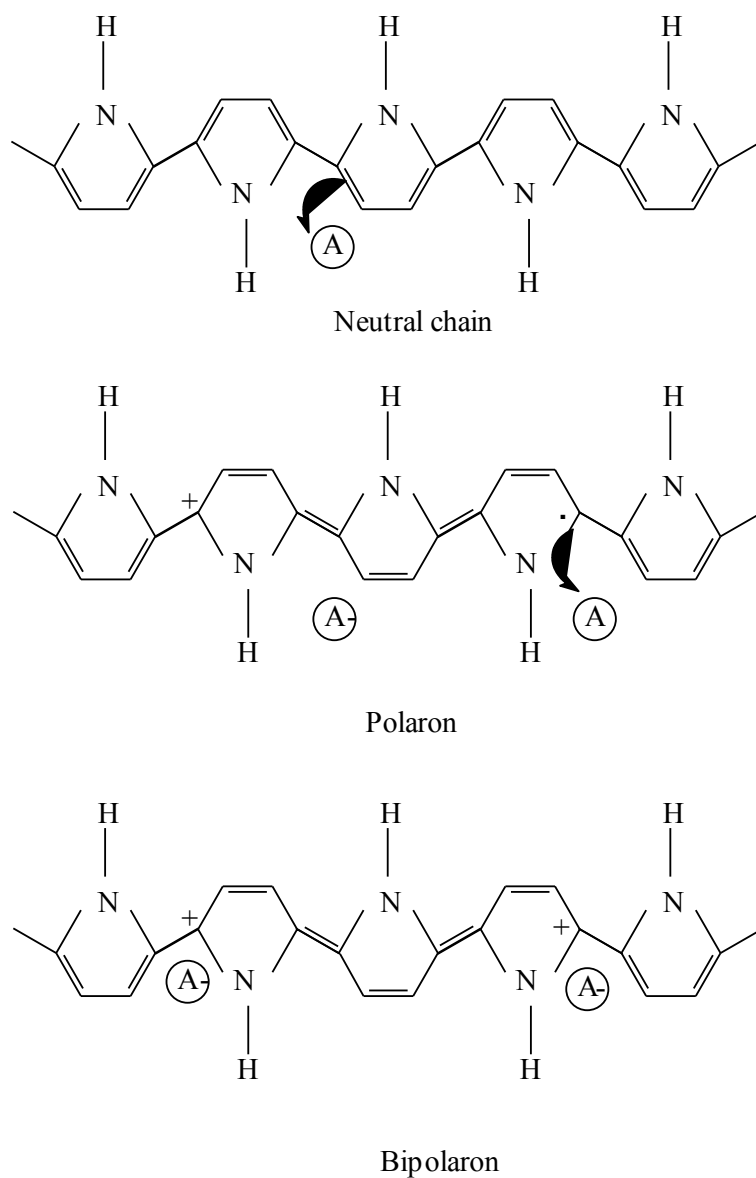


Figure 2.4 mechanism explanation of charge storage of polypyrrole

2.2.3 Charge transfer [25]

The main source of charge carriers are known to be solitons and bipolarons, the precise mechanism is still unsolved. The problem lies in attempting to trace the path of the charge carriers through the polymer. All of these polymers are highly disordered, containing a mixture of crystalline and amorphous regions. It is necessary to consider the transport along and between the polymer chains and also the complex boundaries established by the multiple numbers of phases. This has been studied by examining the effect of doping, of temperature, of magnetism and the frequency of the current used. These test show that a variety of conduction mechanisms are used. The main mechanism used is by movement of charge carriers between localized sites or between soliton, polaron or bipolaron states.

Alternatively, where inhomogeneous doping produces metallic islands dispersed in an insulating matrix, conduction is by movement of charge carriers between highly conducting domains. Charge transfer between these conducting domains also occurs by thermally activated hopping or tunneling. This is consistent with conductivity being proportional to temperature

However, many conducting polymers can degrade even in dry or in free oxygen atmosphere. This intrinsic instability is thermodynamic in origin. It can cause by irreversible chemical reaction between charged sites of polymer. It may be occurred either the dopant counter ion of anion or the π -system of an adjacent neutral chain. It produces a sp^3 carbon, breaking the conjugation. Intrinsic instability can also come from a thermally driven mechanism which causes the polymer to lose its dopant. This happens when the charge sites become unstable due to conformational changes in the polymer backbone.

Among various conducting polymers, polyaniline is unique and promising candidate for practical applications due to its good process ability, environmental stability and reversible control of electrical properties by both charge-transfer doping and protonation. It has attracted most attention and become important subject of most research. Because of potentiality for practical applications, good environment stability, low cost and ease of synthesis. The attention of heterogeneous-conducting polymer nanocomposites has drawn over decade. These materials show special mechanical, electronic, optical and magnetic properties.

2.3 Polyaniline (PANI)

2.3.1 Structure features

Polyaniline is the conductive polymer. Chemical structure of polyaniline is shown in figure 1. It consists of two units. First unit is reduced repeating unit and another one is oxidized repeating units. The different form of polyaniline is proportion to ratio of unit, y-value [26].

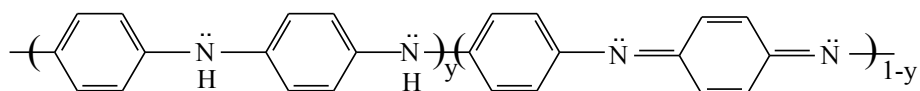
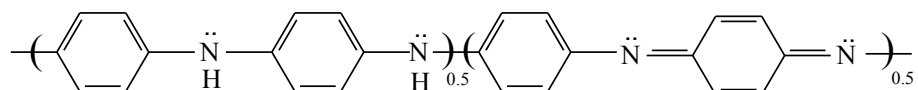


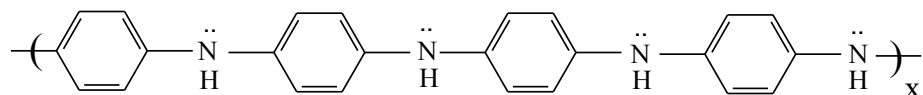
Figure.2.5 The chemical structure of polyaniline

The different repeating units in two forms make 3 forms of polyaniline. First is completely reduced form ($y=1$) of Leucoemeraldine base, second is half oxidized form ($y=0.5$) of emeraldine base and the last form is completely oxidized form ($y=0$) of Pernigraniline base.

For $y = 0.5$; half oxidized form (Emeraldine base)



For $y = 0$; completely reduced form (Pernigraniline base)



For $y=1$; completely oxidized form (Leucoemeraldine base)

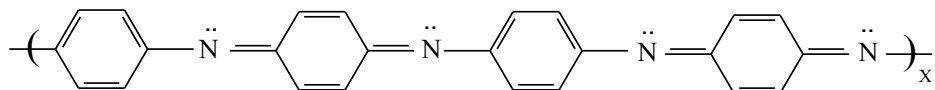


Figure 2.6 the three different electronic form bases on polyaniline structure

Among of three forms of polyaniline, emeraldine base can be rendered into a conductive form of emeraldine salt by chemical or electrochemical doping processes result in increasing electronic conductive about ten orders of magnitude. The emeraldine-based form of PANi is also the most stable of the three states because leucoemeraldine is easily oxidized when exposed to air and pernigraniline is easily degraded.

2.3.2 Doping in polyaniline

The doping process can be achieved by partial oxidation or partial reduction of the π -system of the polymer. In general, the doping process leads to either increase or decrease in the number of electrons associated in polymer [27]. The uniqueness of PANi arises from the sensitivity of its emeraldine oxidation state towards the pH which yields emeraldine base (EB) and emeraldine salt (ES) forms of PANi. An interesting feature of PANi arises from the fact that the non-conducting EB form of PANi can be doped to a highly conducting regime (ES) without changing the total number of electrons associated with it [28]. Such a doping is achieved by a simple protonation of the $-NH$ group of EB by mineral or organic protonic acids and is known as “acid doping”.

The conductivity of PANi is increased more than eight orders of magnitude by acid doping process [29]. Positive charges accumulated on the polymer backbone during protonation of PANi are neutralized by the negatively charged counter ions of the dopant. The protonation is also accompanied by the drastic change

in the electronic structure, crystallinity, solubility, and etc. The degree of protonation and the resulting conductivity can be readily controlled by changing the pH of the dopant acid solution. Inorganic mineral acids such as HCl, H₂SO₄, H₃PO₄, etc. are the most frequently used dopants.

PANi has a special characteristic amongst conductive polymers in the fact that its most highly conducting doped form can be reached by two completely different processes; protonic acid doping of emeraldine base and oxidative doping of leucoemeraldine base as shown in figure 2.7

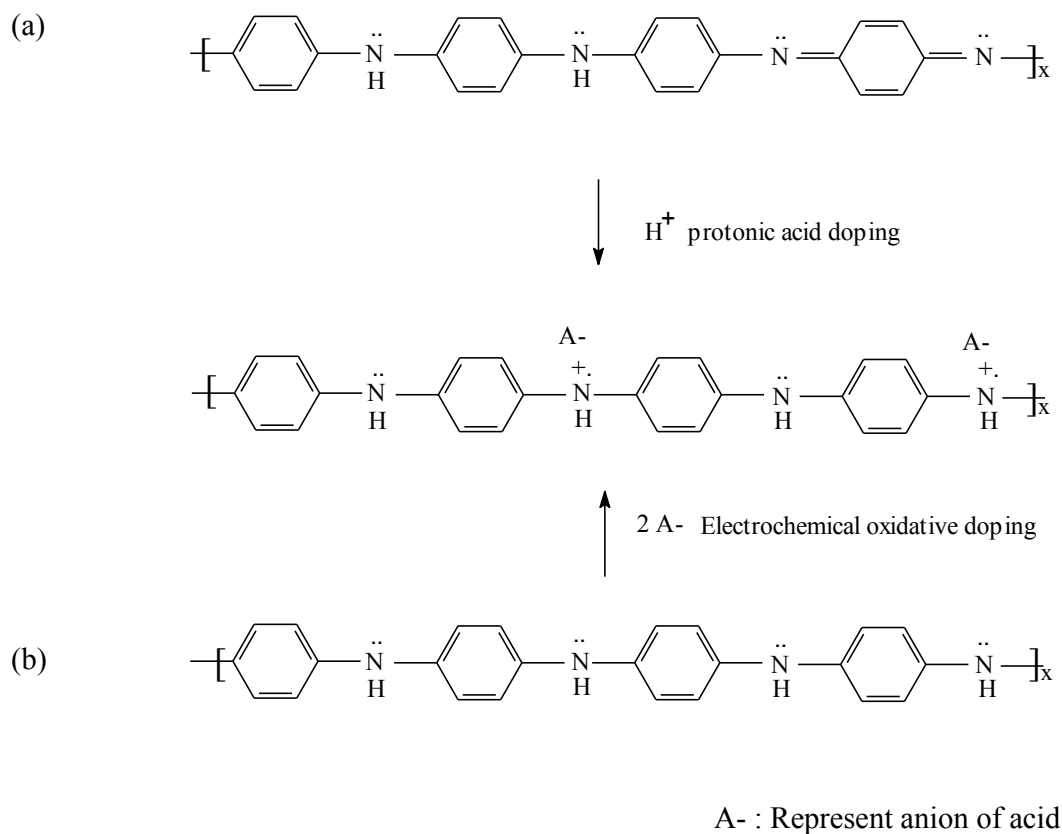


Figure 2.7 the emeraldine salt formation of polyaniline (a) protonic acid doping of emeraldine base and (b) oxidative doping of leucoemeraldine base

2.3.3 Charge carrier mechanism of polyaniline

In polyaniline, nitrogen p_z orbitals and carbon in aromatic rings are also part of the conjugation system. The conjugated double bonds permit easy electron mobility throughout the molecule because the electrons are delocalized. Delocalization is the condition in which π -bonding electrons system are spread over a number of atoms rather than localized between two atoms. This condition allows electrons to move more easily, thus making the polymer electrically conductive.

The undoped PANi is a poor semiconductor that has conductivity of about 10^{-8} S/cm. When it is doped, its conductivity could increase by a factor of 10 S/cm or more depending on the type and concentration of dopant.

For sample [30], doping with acid such as HCl can increase conductivity of PANi due to relocalize charge form of polaron/bipolaron structure. The protonating PANi EB with HCl lead to bipolaron structure. In initiation, the hydrogen ions from HCl will attach themselves to the quinoid nitrogen atoms. This is highly unstable because of the high energy this structure possesses. Thus, the C=N bonds of the quinoid imine structure will break, transforming the quinoid ring into a more stable benzenoid ring, with lower energy, by aromatization, creating the bipolaron structure of doped PANi.

The new benzenoid ring, although more stable than it was previously. However, it still has high energy because of the repulsion force from the adjacent positive charges. To stabilize this structure, the positive charge of one of the hydrogen ions will attract electrons from the neighboring benzene ring, neutralizing the charge. This will create a new positively charged nitrogen group with a neutral nitrogen atom in between the two positive ones. The increased distance between the two positive charges results in the polaron structure, which has a lower energy level than the bipolaron structure.

The overall structure are expected to have extensive spins and charges delocalization resulting in a half-filled polaron conduction band and an increase in the electrical conductivity by over ten orders of magnitude without any changes in in the number of electrons on the polyaniline backbone[31].

Since initially, the ionic interactions between PANi and Cl^- anions are weak, the Cl^- anions are able to migrate to the newly formed positively charged nitrogen atom as the doped PANi complex stabilizes itself by transforming into the polaron

structure. The migration of Cl^- ion tends to be easier when in solution form. This charge carrier mechanism is showed as in figure 2.8

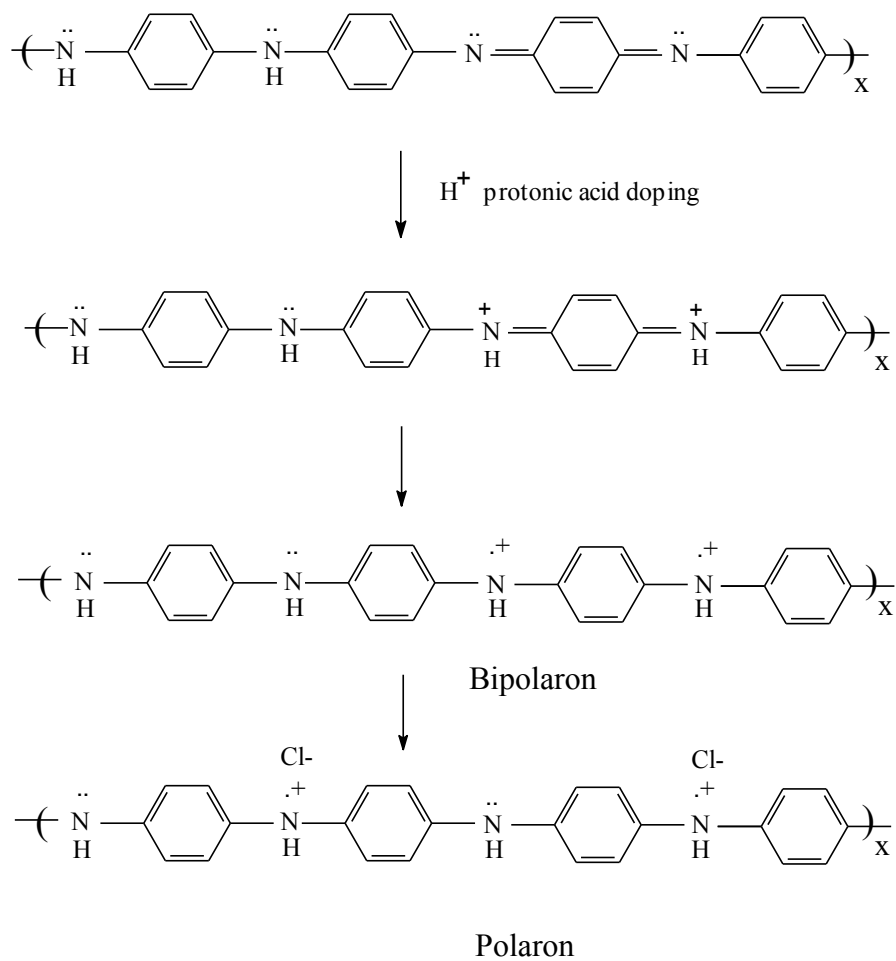


Figure 2.8 charge carrier evolution of emeraldine base as a function of protonation [17]

2.4 Synthesis polyaniline: nanostructure as sensitive layer for gas sensor

The ongoing of synthesis nanostructure of polyaniline as sensitive layer for gas sensor was interested because the high surface to volume ratios of nanostructure increased rapid respond and reversible resistance changed in polyaniline upon exposure to gas vapor. Up to date, the methods to synthesize nanostructure of polyaniline were developed in many ways.

For example, Zhang and coworker [32] synthesized nanofibers polyaniline using toluene as organic solvent, acidic ammonium peroxydisulfates as aqueous phase and camphorsulfonic acid as acid dopant. The average diameter of polyaniline nanofibers were investigated by comparing two type of cis-1,2-alkylethene sulfonate structure (alkyl = C₅H₁₁ or C₇H₁₃). It found that diameter of polyaniline nanofibers decreased in the order 48 nm (no surfactant) > 35 nm (C₅H₁₁-twin-tailed) > 28 nm (C₇H₁₃-twin-tailed).

Yan and coworker [33] synthesized polyaniline nanofibers by an interfacial polymerization method for NO₂ detection. The results showed that the high surface area, porosity and small diameters structures of nanofibers enhance diffusion rate of the molecules resulting into high sensitivity and short response time for NO₂ detection. The nanofibers polyaniline increased in resistance-greater than three orders of magnitude in 100 ppm with comparing bulk polyaniline.

However, the drawback of synthesis nanostructure polyaniline from interfacial polymerization is toxicity of solvent. Therefore, there were many researcher tried to synthesize nanostructure of polyaniline without the presence of organic solution.

For example, in 2001 Wei et.al [34] synthesized nanotube polyaniline without organic phase in the presence of β -naphthalene sulfonic acid (β -NSA) as a dopant. The nanostructures of polyaniline were controlled by mole ratio of β -NSA-aniline. The results showed that the formations of the precipitate β -NSA-aniline salts were formed as “template-like” to create formations of nanotube structure with the mole ratio of β -NSA-aniline was higher than 2. While the “template-like” were played as the NSA-aniline micelle, when the mole ratio of β -NSA-Aniline was lower than 0.5.

Up to date, there are many methods to synthesize and deposit nanostructure of polyaniline such as interfacial polymerization [35], Langmuir-Blodgett [36], electrospinning [37], self-assembly method [38] and etc. Another method to synthesize nano-morphology of polyaniline is electrochemical. The electrochemical is widespread method to synthesize and deposit polyaniline in range of micro to nano-structure scale due to this route presents several advantages compared with other method.

2.4.1 Electrochemical: principle [40,41,42]

Electrochemical is a branch of chemistry that studies chemical reactions which involve electron transfer between the electrode and the electrolyte or species in solution. The electrochemical take place in a solution at the interface of an electron conductor (a metal or a semiconductor) and an ionic conductor (the electrolyte).

The electrochemical reaction is driven by an external applied voltage, as in electrolysis, or chemical reaction created a voltage as in a battery, In contrast, chemical reactions where electrons are transferred between molecules are called oxidation/reduction (redox) reactions. In general, electrochemistry deals with situations where oxidation and reduction reactions are separated in space or time, connected by an external electric circuit.

-At the cathode, ions or molecules are transformed within the interface via reaction with electrons (from the electrode) to produce reduced molecules or ions.

-At the anode, molecule or ions (from the solution) are transformed within the interface to produce electrons (at the electron surface) and oxidized ions and molecules.

The resulting electrons move from the anode though the wire of external circuit to the cathode as electronic current. An electrical circle is required for measuring current and potential (voltage) created by movement of charged particles. Galvanic cell serves as a sample of such system.

For example in figure 2.9, Sample cell consists of solutions of ZnSO_4 and CuSO_4 . The metallic Zn and Cu electrodes are immersed in respective solutions. Electrodes have two contacts:

- a) Through wires connected to voltmeter
- b) Through solutions and salt bridge.

Salt bridge consists of a tube filled with saturated salt solution (e.g. Na_2SO_4 solution). The ends of the tube are capped with porous frits that prevent solutions from mixing, but permit movement of ions

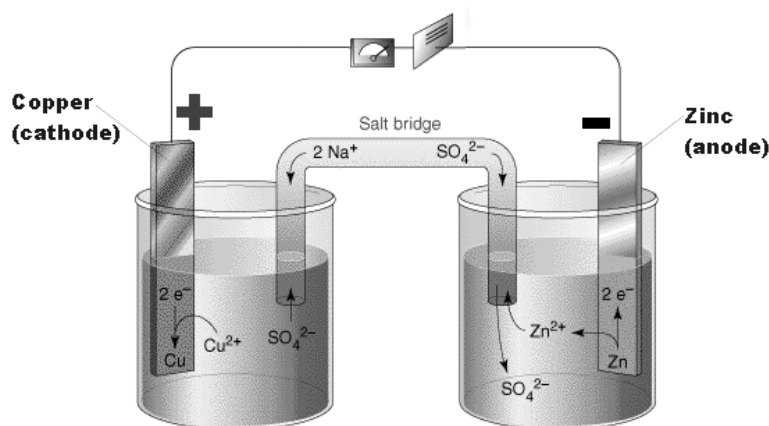
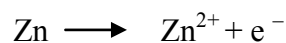


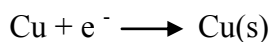
Figure 2.9 A galvanic electrochemical cell [43]

For the system in figure 2.9, three steps of distinct charge transfer processes are described:

1. Electrons transfer in electrodes and wires from zinc electrode to copper electrode
2. Ions transfer in solutions:
 - a. zinc ions move away from the electrode and sulfate ions move towards it.
 - b. copper ions move towards the electrode and negatively charged ions (sulfate) away from it.
 - c. In salt bridge positive ions move right and negative ions left.
3. On the surfaces of electrodes electrons are transferred to ions or vice versa:
 - a. Zinc electrode dissolves



b. Metallic copper is deposited on the electrode surface



There are two types of electrochemical techniques, namely potentiometry and amperometry[44].

Potentiometry is one type of electrochemical analysis methods. Electrochemistry is a part of chemistry, which determines electrochemical properties of substances. Potentiometry is the field of electro analytical chemistry in which potential is measured under the conditions of no current flow (zero). The measured potential may then be used to determine the analytical quantity of interest, generally the concentration of some component of the analyte solution. The potential that develops in the electrochemical cell is the result of the free energy change that would occur if the chemical phenomena were to proceed until the equilibrium condition has been satisfied

The amperometric technique relies on the current passing through a polarizable electrode. The magnitude of the current is direct proportional to the concentration of the electro analyte, with the most common amperometric techniques being polarography and voltammetry. The amperometric measurement can be overly sensitive to impurities such as gaseous oxygen dissolved in the solution, and capacitance effects at the electrode. However, amperometry is a much more versatile tool than potentiometry because the amperometric measurements are generally more precise and more versatile than those made by using potentiometry.

2.4.2 Voltammetry [45,46,47]

Voltammetry is one of the techniques which electrochemists employ to investigate electrolysis mechanisms. There are typically three forms of voltammetry which are potential step, linear sweep and cyclic Voltammetry. For each of these cases a voltage or series of voltages are applied to the electrode and the corresponding current that flows was monitored.

2.4.2.1 Potential step voltammetry

The essential elements needed for an electrolysis measurement are as follows:

- The electrode: made of an inert metal (such as Gold or Platinum)
- The solvent: high dielectric constant solution (such as water or acetonitrile) to enable the electrolyte to dissolve and help aid the passage of current.
- A background electrolyte: This is an electrochemically inert salt (such as NaCl or Tetra butylammonium perchlorate, TBAP) and is usually added in high concentration (0.1 M) to allow the current to pass.
- The reactant: Typically in low concentration 10^{-3} M.

In the potential step measurement, the applied voltage is instantaneously jumped from one value V_1 to another V_2 . The resulting current is then measured as a function time. The current rises instantaneously after the change in voltage and then begins to drop as a function of time.

2.4.2.2 Linear Sweep Voltammetry

In linear sweep voltammetry (LSV) a fixed potential range is employed much like potential step measurements. However in LSV the voltage is scanned from a lower limit to an upper limit. The characteristics of the linear sweep voltammogram depend on a number of factors including:

- The rate of the electron transfer reaction(s)
- The chemical reactivity of the electroactive species
- The voltage scan rate

In LSV measurements, the current response is plotted as a function of voltage. The scan begins from the left hand side of the current/voltage plot where no current flows. As the voltage is swept further to the right (to more reductive values) a current begins to flow and eventually reaches a peak before dropping. To rationalise this behavior, it need to consider the influence of voltage on the equilibrium established at the electrode surface. Here the rate of electron transfer is fast in comparison to the voltage sweep rate. Therefore at the electrode surface equilibrium is established identical to that predicted by thermodynamics.

The exact form of the voltammogram can be rationalised by considering the voltage and mass transport effects. As the voltage is initially swept from V_1 the equilibrium at the surface begins to alter and the current begins to flow. The current rises as the voltage is swept further from its initial value as the equilibrium position is shifted further to the right hand side, thus converting more reactant. The peak occurs, since at some point the diffusion layer has grown sufficiently above the electrode so that the flux of reactant to the electrode is not fast enough to satisfy that required by the Nernst equation [49]. In this situation the current begins to drop just as it did in the potential step measurements.

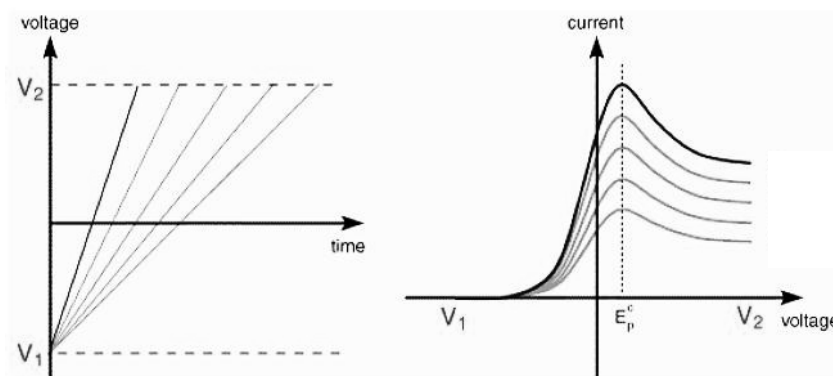


Figure 2.10 Series of linear sweep voltammograms recorded at different scan rates [35]

Each curve has the same form but it is apparent that the total current increases with increasing scan rate. This again can be rationalised by considering the size of the diffusion layer and the time taken to record the scan. Clearly the linear sweep voltammogram will take longer to record as the scan rate is decreased. Therefore the size of the diffusion layer above the electrode surface will be different depending upon the voltage scan rate used. In a slow voltage scan, the diffusion layer will grow much further from the electrode in comparison to a fast scan. Consequently the flux to the electrode surface is considerably smaller at slow scan rates than it is at faster rates. A point to note from the figure is the position of the current maximum, it is clear that the peak occurs at the same voltage and this is a characteristic of electrode reactions which have rapid electron transfer kinetics. These rapid processes are often referred to as reversible electron transfer reactions.

2.4.2.3 Cyclic Voltammetry [50]

Cyclic Voltammetry (CV) is perhaps the most effective and versatile electroanalytical technique available for the mechanistic study of redox systems. It enables the electrode potential to be rapidly scanned in search of redox couples. Once located, a couple can then be characterized from the potentials of peaks on the cyclic voltammogram and from changes caused by variation of the scan rate. CV is often the first experiment performed in an electrochemical study.

Cyclic voltammetry (CV) is very similar to LSV. In this case, the voltage is swept between two values at a fixed rate. However, when the voltage reaches V_2 the scan is reversed and the voltage is swept back to V_1 . The solution contains only a single electrochemical reactant. The forward sweep produces an identical response. When the scan is reversed, converting electrolyte moves back through the equilibrium positions.

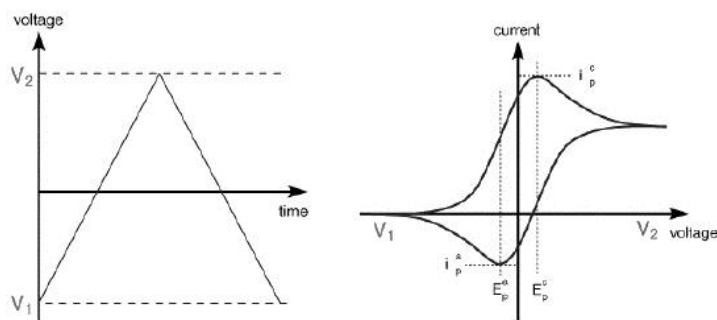


Figure 2.11 Voltage as a function of time and current as a function of voltage for CV [50]

The influence of the voltage scan rate on the current for a reversible electron transfer can be seen in Fig. 2.12. The influence of scan rate is

explained for a reversible electron transfer reaction in terms of the diffusion layer thickness. In case of CV where the electron transfers is not reversible show considerably different behavior from their reversible counterparts.

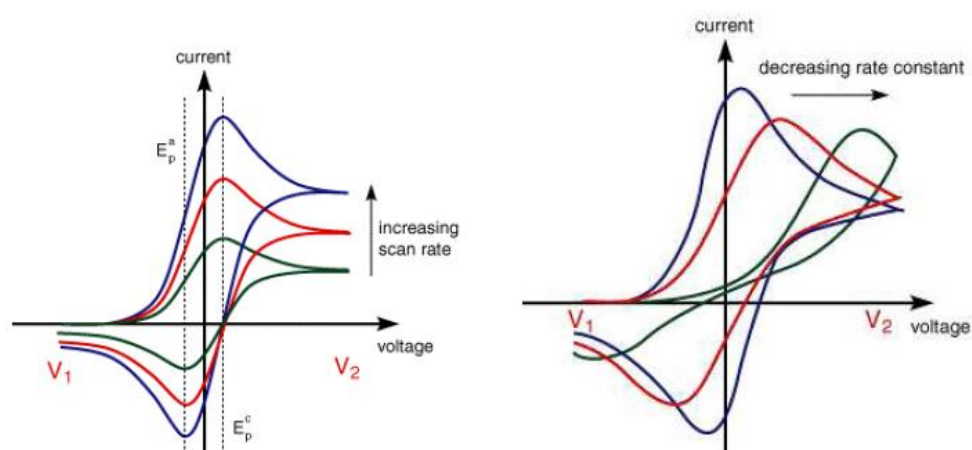


Figure 2.12 the current for a reversible electron transfer at different the voltage scan rate [50]

2.4.3 Electrochemical synthesis of polyaniline

The electrochemical synthesis of polyaniline presents several advantages as cleanness because no extraction from the monomer–solvent–oxidant mixture is necessary, doping and thickness control via electrode potential, simultaneous synthesis and deposition of polyaniline thin layer [51]. With this route, there are three ways for deposition polyaniline on substrate which include the galvanostatic method with a constant current, the potentiostatic method with a constant potential and the potentiodynamic method with current and potential vary with deposite time.

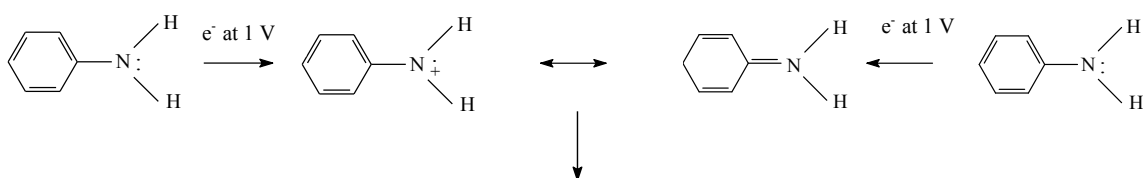
However, whatever the method is used, the three-electrode reactor vessel assembly composes a working electrode on which the polymer is deposited, a counter electrode also named auxiliary electrode (platinum grid) and a reference

electrode (in most cases, a saturated calomel electrode (SCE)). The more common working electrode is a platinum, but PANi depositions have also been realized onto conducting glass (glass covered by indium-doped tin oxide (ITO) electrode), Fe, Cu, Au, graphite, and stainless steel. Polyaniline can be then peeled off from the electrode surface by immersion in an acidic solution.

The electrochemical is a widespread method to synthesis and deposit polyaniline in range of micro to nano-structure scale. As reported by Haibin Zhang and coworkers [52] that the morphology of polyaniline film prepared by electrochemistry revealed lamellar structure. The bulk film was formed at the bottom whereas the nano-structure of fibrillar was formed at the middle and the top of the film. In addition, this route reveals several advantages compared with the other methods [53]. It is an environmentally friendly process because no need of an oxidant is required in the reaction, the doping level and thickness of polyaniline film can be controlled via electrode potential, and the obtained-polyaniline film exhibits good simultaneous deposition compared with the other methods

Moreover, electrochemistry method is the most suitable for fabrication sensor that built in micro circuits. The monomer solution is polymerized and deposited on interdigitated substrate in one step. For example in work of Jens Reemts and et.al., [54] fabricated conductive layers of emeraldine base polyaniline as sensitive layer for organic vapor sensor. These sensing layers were fabricated from drop of aqueous aniline in sulfuric acid solution by cyclic voltammetry electrochemical polymerization. After exposing NH_3 , the sensing layers reveal significant change with a linear dependence of the signal on concentration in the parts per million ranges.

The mechanism for electrochemical synthesis polyaniline was proposed according to work of Am Pharhad hussain et.al., [55] They prepared polyaniline conducting polymer films from an electrolyte containing HCl by potentiodynamic method. The mechanism of oxidative electropolymerization of aniline at 1 V was illustrated as shown in figure 2.13.



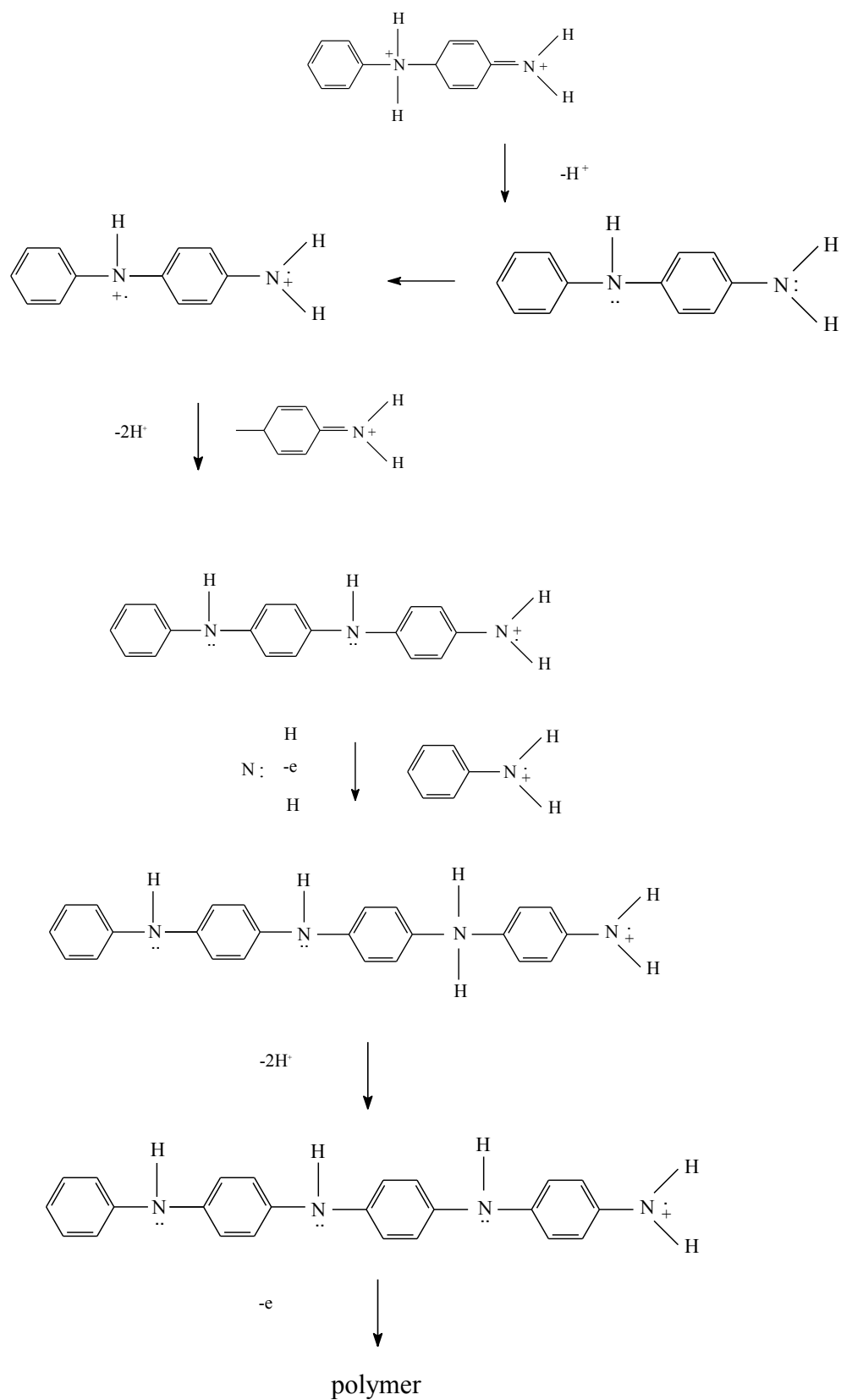


Figure 2.13 mechanism of oxidative electropolymerization of aniline

2.5 Polyaniline as sensitive layer for gas sensors

Most of gas sensors available on the market are semiconducting sensors. The conductivity of these sensors is altered under gas absorption. However, these sensors need to operate at high temperature. To improve gas sensors characteristics, conducting polymer reveal increasingly important role in monitoring due to their applicability at room temperature. It provided that information on industrial manufacturing processes and their emissions, quality control of foods and beverages, and a host of other applications.

Most of gas sensors using PANi as sensitive layer measure, under gas flow, a conductivity change to a direct current. The studies of mechanism of interaction between conductive polymer and gas are of interested. The interaction of gas with conductive polymer can be classified into two classes which are physical absorption and chemical reaction. In case of physical absorption, non-reactive volatile organic reagents (such as hexane [56], alcohol [57]) reveal weak interaction between polyaniline and gas analyst leading to a changing in resistance. For chemical reaction, the changing of conductivity of conductive polymer depends on oxidation states. The oxidation states can either be controlled by synthetic conditions or oxidation-reduction reactions. The conductivity of conductive polymer will be changed after being exposed to gas analyst, if gas analyst is reducing gas (such as hydrazine [53]), emeraldine salt of polyaniline will be donated electron to gas analyst, resulting in an increase of resistance of polyaniline. Oppositely, if gas analyst is oxidizing gas (such as oxygen [56]), emeraldine salt of polyaniline will be accepted electron form gas analyst, resulting in a decrease of polyaniline resistance.

2.5.1 Polyaniline doping: Acid doping

The acidic doping can change the number of electrons associated with the polymer backbone. The acidic doping consists to treat the emeraldine base with a strong acid (HCl, H₂SO₄) that induces the protonation of the imine sites to give the polyemeraldine salt as see through a mechanism illustrated in figure 2.14. Considering the resonant structures, charge and spin can be largely delocalized that explains the observed conductivity

The development sensitivity and selectivity of polyaniline is importance. By doping polyaniline with different type of acid doping, the polyaniline dope revealed different sensitivity and selectivity against various gas detection [53-58].

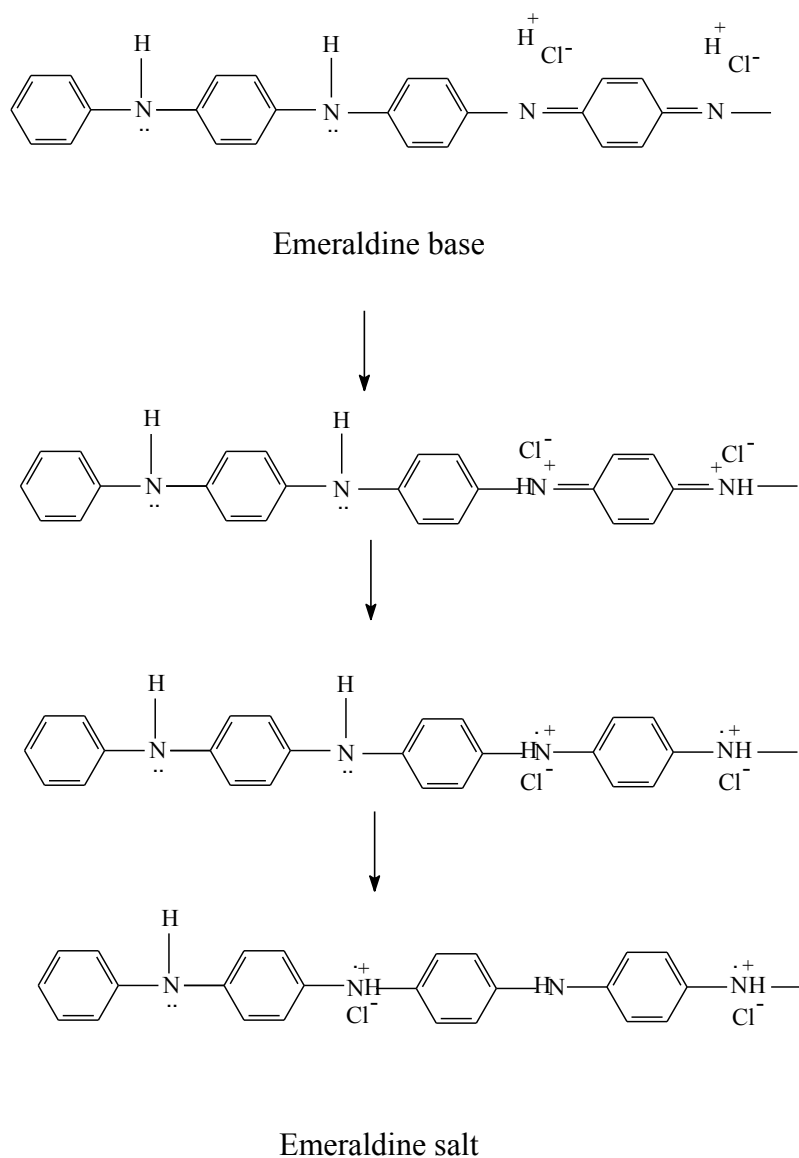


Figure 2.14 Mechanism of acid doping of polyaniline[13]

Moreover, the polyaniline doped with some acid types can react with specific gas analyst. Typically, polyaniline doped with hydrochloric acid reveals de-dope reaction after being exposed to NH_3 , resulted in increasing of its resistance. By

doping polyaniline with different types of acid doping, the doped-polyaniline exhibits different sensitivity and selectivity with gas detections.

As follow work of Shanzuo Ji and coworker[58], they were compared the effect of different three types of acid dope polyaniline which include toluene sulfonyl acid (TSA), sulfosalicylic acid (SSA) and hydrochloric acid (HCl) on sensing triethylamine gas. All three type of doping polyaniline showed linear respond, reversible and reproducible against amine vapor in range of 20-5000 ppm. The order of sensing of doping polyaniline against triethylamine gas is PANi -TSA, PANi-SSA and PANi-HCl, respectively.

Doping polyaniline with some specifics acid type for specifics gas detection is unceasing investigation. For example, polyaniline dope with camphorsulfonic acid (CSA) is one of procedure that is the most refer for hydrogen detection as follow. Shabnam Virji and coworker [59], they fabricated hydrogen sensors from polyaniline dope camphorsulfonic acid by spying polymer solution on interdigitated electrode sensor substrates. The results showed that the resistance of dope-polyaniline decrease 3 % for mixture 1% of hydrogen in nitrogen.

As mention earlier, the effect of acid type for doping polyaniline is an importance factor on selectivity and sensing. There was a report on using the polyaniline dope with ionic liquid (IL) for hydrocarbon detection. For example, as reported by Xiaoxia and coworkers [60], polyaniline was deposited on Quartz crystal microbalance (QCM) gold substrate by electrochemistry and soaked in IL solution. The results revealed an interaction between methane and polyaniline/butylmethylimidazolium camphorsulfonate (PANi/BMICS) ionic liquid composite. The methane molecules absorbed into the PANi/BMICS inserted in the host between the aligned anions and cations of BMICS. This PANi/QCM/BMICS revealed respond frequency linearly changing with methane concentration between 1% and 10% and had current limits detection as low as 115 ppm. This research supports that interactions of polyaniline with some specific doping agent create host for inserting hydrocarbon molecule.

2.6 Inclusion of material particles into polyaniline for enhance gas sensing property

2.6.1 Inclusion of multiwall carbon nanotube into polyaniline

The addition of micro/nanoparticle inclusion such as clays [12], and carbon nanotube [61] is most interesting procedures for improve inorganic semiconductors gas sensor performance, for example, Qifei Chang and coworker [14] were successful preparation of nanocomposites comprise of multiwall carbon nanotubes, gold nano particles and polyaniline. This noble metal was shown to have superior sensitivity and good repeatability used in detecting ammonia gas with excellent stability. The sensitivity of sensors exhibited a linear response of ammonia gas for concentration ranging from 200 ppb to 10 ppm.

2.6.1.1 Multiwall carbon nanotube: structure features and properties [62,63]

Carbon nanotubes (CNTs) are allotropes of carbon with a cylindrical nanostructure. Nanotubes have been constructed with length-to-diameter ratio of up to 132,000,000:1. Multi-walled nanotubes (MWNT) consist of multiple rolled layers (concentric tubes) of graphite or single wall nanotube as shown in figure 2.15. There are two models which can be used to describe the structures of multi-walled nanotubes which are Russian Doll and Parchment model. In the Russian Doll model, the Russian Doll structure is observed more commonly. Its individual shells can be described as SWNTs sheets of graphite are arranged in concentric cylinders, smaller single-walled nanotube in diameter within a larger single-walled nanotube. In the Parchment model, a single sheet of graphite is rolled in around itself, resembling a scroll of parchment or a rolled newspaper. The interlayer distance in multi-walled nanotubes is close to the distance between graphene layers in graphite, approximately 3.4 Å.

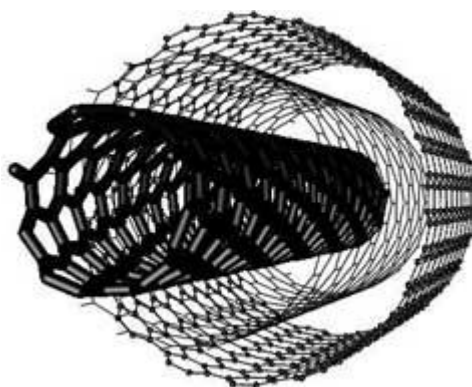


Figure 2.15 the structure of multiwall carbon nanotube consisting of three concentric single walled nanotubes

2.6.1.2 Effect of the presence of gases in contact with the carbon nanotube

Basis on principle of single wall nanotube (SWCNT), the model of gas absorption on SWCNT is usually used to investigate for the changing of the bind energy, tube molecule distance and charge transfer. Peng and Cho [64] studied the absorption of NO_2 on SWCNT. They found that NO_2 gas molecule of this configuration is found to bind with SWCNT with absorption energy of 0.3 eV. And it also found that the molecule has high diffusion kinetics on nanotubes surface. Electron density analysis show that charge transfer induced from C atom to NO_2 gas molecule leading to hole (p-type) semiconducting of nanotubes.

Zhao et al. [65] investigated the effect of absorption of various molecules (NO_2 , O_2 , NH_3 , N_2 , CO_2 , CH_4 , H_2O , H_2 , Ar) on SWCNT. The results of charge transfer, absorption energy show specific value in different gas types. It can be used to identify as physisorption. For the SWCNT, there are four distinct sites for gas absorption

- i. The external surface of the bundle
- ii. The groove formed at the contact between adjacent tube outside bundle

- iii. The interior pore of individual tubes
- iv. Interstitial channel form between adjacent tube within bundle

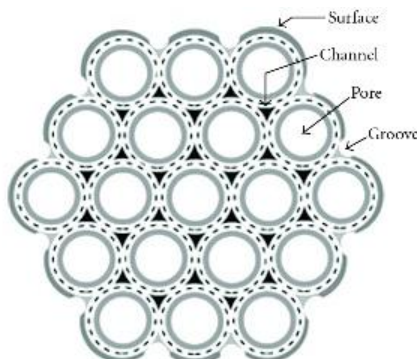


Figure 2.16 the active site of single wall nanotube for gas absorption

The gas absorption on these sites is decided by the binding energy of gas molecule. However, some of these sites are unavailable for some gas absorption because of dimension and size diameter.

In sensor application, the electronic properties of SWCNT were subjected to be investigated due to their sensitivity on environment. For example, Collins et al. [66] showed the electrical resistance of SWCNT can be reversibly tuned after being exposure to oxygen altering with vacuum.

Generally, the electronic properties changes of CNT upon exposure to gas molecules are attributed to the charge transfer between the molecule and nanotube. However, Sumanasekera et al.[67] demonstrated experimentally that the degassed SWCNT resistance can be very sensitive to inert gases (N_2 and He which hardly have electron transfer with CNTs). In this case, it believed that the resistance changes are due to the change in the electron and hole free carrier lifetimes. The large changes in the carrier lifetime can be caused either by increased carrier scattering from dynamic defect states associated with momentarily absorbed gas or due to nonthermal, localized SWCNT phonons generated collisions of the gas molecules with the tube wall.

2.6.2 Inclusion of metallic particles into polyaniline

The addition of some type of metal oxide was used primarily to enhance selectivity of inorganic semiconductors for specific gas sensor. As the results of Monoj Kumar Ram and coworker[38], they fabricated ultrathin conducting polyaniline/ SnO_2 or TiO_2 film for sensing of CO gas via in situ layer-by-layer (LBL) self-assembly technique. Polymerization solution of aniline contained SnO_2 or TiO_2 was absorbed on substrate which contained anionic charge layer of sulfonated polystyrene. The results show that the nano-composite of polyaniline/ metal oxide film revealed excellent candidates for recognition and detection of CO gas.

The study of SnO_2 as gas sensing material is due to its suitable physicochemical properties as, for example, it has a high reactivity to reducing gases at relatively low operating temperatures. It can adsorb oxygen at its surface because of the natural non-stoichiometry of SnO_2 . Moreover, SnO_2 has a lower cost when compared to actual available materials for similar applications.

2.6.2.1 Tin oxide: structure features and properties [67,68]

Tin oxide (SnO_2) is a very stable material which has tetragonal or rutile structure as its most common. In the SnO_2 unit cell as shown in figure 2.17, the Sn atom is surrounded by six oxygen atoms. Furthermore, each of the oxygen anions has four coplanar Sn^{4+} ions as nearest neighbors at the corners of a rectangle plus two next-nearest neighbor on the remaining two corners of the Sn-coordinating distorted octahedron.

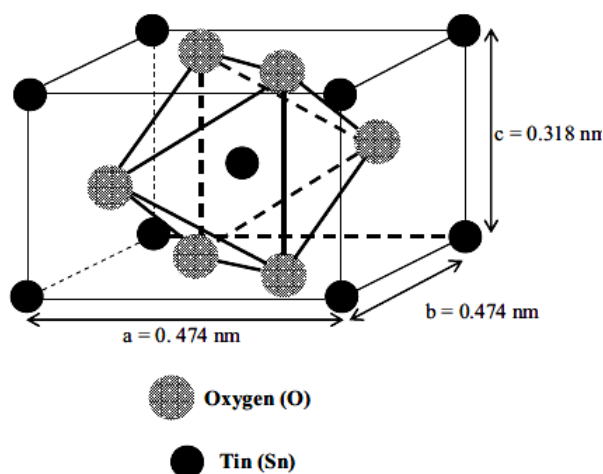


Figure 2.17 Unit cell of SnO_2

Tin dioxide is a semiconductor material, transparent, of high chemical and mechanical stability. Only one stable phase (and no metastable one) is known, which has a tetragonal arrangement of the atoms receiving the names of rutile or cassiterite.

The donor level of Tin oxide have energies of 0.03-0.034eV and 0.14-0.15eV below the conduction band edge, and are generally attributed to single and double ionisation of oxygen vacancies, as unrelaxed vacancies are above, i.e., within the conduction band. The position of the Fermi level is fixed and would be between the conduction band edge and the intrinsic Fermi level position (that is very close to the mid of the band gap), because SnO₂ presents a negligible concentration of electronic band-gap states at their geometrically ideal surfaces.

The existence of surface or interface traps acting as acceptors or donors, each of them having a certain density of states and certain parameters of emission and capture, makes that in the thermodynamic equilibrium at each temperature, the Fermi level position is determined by this region. The charge trapped at grain boundaries or surfaces is compensated by opposite charged depletion regions surrounding them.

However, a direct association between the created states, their activity, their location in the band gap and the type of defects from where they are caused cannot be predicted a priori. Nevertheless, for an n-type semiconductor, in the case of grain boundaries the position of the Fermi level in the grain boundary has to be lower than the corresponding position in the bulk material just to generate the band bending of the surface.

2.6.2.2 Effect of the presence of gases in contact with the tin oxide surface [69,70,71,72]

Tin oxide is an n-type semiconductor due to the presence of oxygen vacancies. The electronically oxygen vacancies act as electron donors. The oxygen vacancies in (110) surfaces can increase the surface conductivity by more than two orders of magnitude with respect to the bulk conductivity. In the same way, it is clearly agreed that the conductance change on exposure to gases arises mainly through a surface phenomenon on the SnO₂ grains

The sensing behavior of SnO₂ can be thought as composed of two steps. Firstly, the reception function recognizes a chemical substance. Another step followed by the transducer function which traduces the chemical signal into an output signal.

When SnO₂ is exposed to an atmosphere at moderate temperatures, two types can occur, namely, *gas adsorption* due to the high reactivity of the SnO₂ surface or *reaction of interaction* of the gas molecules with the molecules chemisorbed at the SnO₂ surface.

- *Gas adsorption*, understood as a direct chemical interaction between the gas molecules and the semiconductor surface is accompanied by charge exchange. Such interchange is interpreted from the electronic point of view as the creation of an inter-band-gap level. Its behavior as acceptor or donor will depend on the type of molecule adsorbed. Thus, gases that capture electrons from the bulk of SnO₂ when they are adsorbed create acceptor levels, while gases that give electrons to the SnO₂ through the creation of an oxygen vacancy introduce donor levels.
- *Reaction of molecules* in the gas phase with those existing already on the semiconductor surface is interpreted as the annihilation of the previously created forbidden band-gap states.

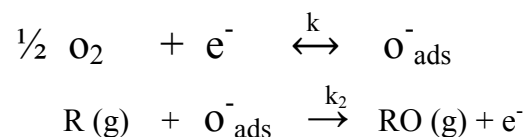
Nevertheless in most cases there is not a direct relationship between the presence of a certain gas in the ambient and the type of level created or annihilated because some intermediate reactions can occur. There are two types of adsorption which are physisorption and chemisorption. The type of absorption depends on the strength of the binding.

- In case of *physisorption*, the species are bonded only by weak physical forces (van der Waals-type forces, dispersion forces, forces of electrostatic nature and electrical image forces) to the surface and is considered when the energy of the bond is of the order of 0.01-0.1eV.

- Meanwhile, *chemical adsorption* is considered when the adsorbed molecules are bound to the semiconductor with bonding energy as large as 1eV. The chemisorption is based on the stronger covalent forces (overlapping between the adsorbate and adsorbent wave functions) and, hence, is connected with a partial electron transfer between adsorbent and adsorbate.

Considering of metal oxide body, when a solid is terminated by a surface, the surface atoms are incompletely coordinated. One or two nearest neighbors are missing, and there are "*dangling bonds*" that are unsatisfied, that is, unshared with neighbors. Specifically, in an ionic crystal like ZnO both cations and anions have poor coordination. The positively charged Zn ions on the surface have an incomplete shell of negative oxide ions around them. There are many mechanism try to illustrate the behavior of sensing gas of metal oxide sensor. A model rationalizing the behavior of the sensor in the measurand environment originally put forward by Mark et al [73] as described below

In basically, the reaction of gas sensing carried out with oxidation-reduction reaction at surface of metal oxide. The conductivity of metal oxide film is controlled by Walter Schottky that block electron transfer between grains of metal oxide. The sensing mechanism was started from the oxygen absorption on the surface at temperature around 200-400 °C. The electrons in tin oxide react with oxygen which leads to reduce state to oxygen anion. The reaction is show as below. [74]



In n-type semiconductor, the electron densities concentrate on the surface of metal oxide. Oxygen adsorbs on the surface and dissociates to form O^- . An electron is extracted from the semiconductor by this O^- . This electron extraction leads to the creation of depletion region near the surface leading to an increase in conductivity of metal oxide. After the reducing gas contact at surface of metal oxide,

the oxygen absorption at surface of metal oxide is decreased. This result leads to decrease in electron density at surface and decrease in conductivity of metal oxide. This phenomenon is illustrated as in figure 2.18.

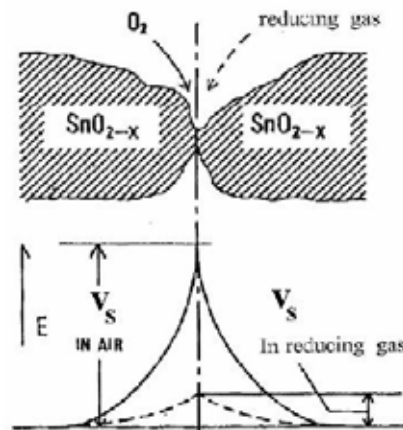


Figure 2.18 the effect of Walter Schottky of tin oxide in oxygen atmosphere (left) and in reducing gas (right) [74]

The changing of Walter Schottky is expressed with relationship as follow equation [75]:

$$V_s = \sigma^2 / 2\epsilon N_D e$$

Where V_s is Walter Schottky

N_D is bulk donor concentration

e is elementary charger

ϵ is dielectric constant

2.7 Electrophoretic deposition [76,77,78,79]

Electrophoretic deposition (EPD) refers as the process that involves the movement of the charged particles in a suspension towards an electrode with an application of an electric field followed by deposition on the electrode. Electrophoretic deposition basically involves two steps which are electrophoresis and deposition. The fine powder that less than $30\ \mu\text{m}$ in size or colloidal suspension can apply for deposition. A characteristic feature of this process is that colloidal particles suspended in a liquid medium migrate under the influence of an electric field (electrophoresis) and are deposited onto an electrode. All colloidal particles in form of stable suspensions that carry a charge can be used in electrophoretic deposition. This includes materials such as polymers, pigments, dyes, ceramics and metals.

There are two Type of electrophoretic deposition, namely cathodic and anodic electrodeposition. The two type of electrophoretic deposition is different in term of charge particle movement deposition. The schematic diagram of the cathodic deposition of electrophoretic deposition was showed in figure 2.19.

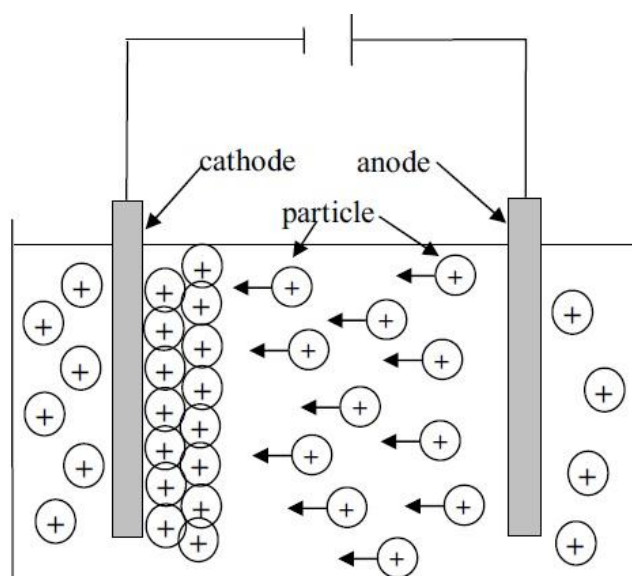


Figure 2.19 Schematic diagram of the cathodic deposition of electrophoretic deposition

2.7.1 Electrophoresis deposition [80,81,82,83]

Electrophoresis is the process in electrophoretic deposition. In this process, the suspended particles carrying electrical charge move through a fluid in response to an applied electric field. Electrophoresis generally occurs when the distance over which the double layer charge falls to zero is large.

According to the double layer theory, all surface charges in fluids are screened by a diffuse layer of ions, which has the same absolute charge but opposite sign depend on the surface charge as shown in figure 2.20. The electric field also exerts a force on the ions in the diffuse layer which has direction opposite to that acting on the surface charge. This latter force is not actually applied to the particle, but to the ions in the diffuse layer, and it is transferred all the way to the particle surface through viscous stress. This part of the force is also called *electrophoretic retardation force*.

When the electric field is applied, the analyzed charged particle is steady to move through the diffuse layer, the total resulting force is zero:

$$F_{total} = 0 = F_{electrostatic\ force} + F_{fiction} + F_{retardation\ force}$$

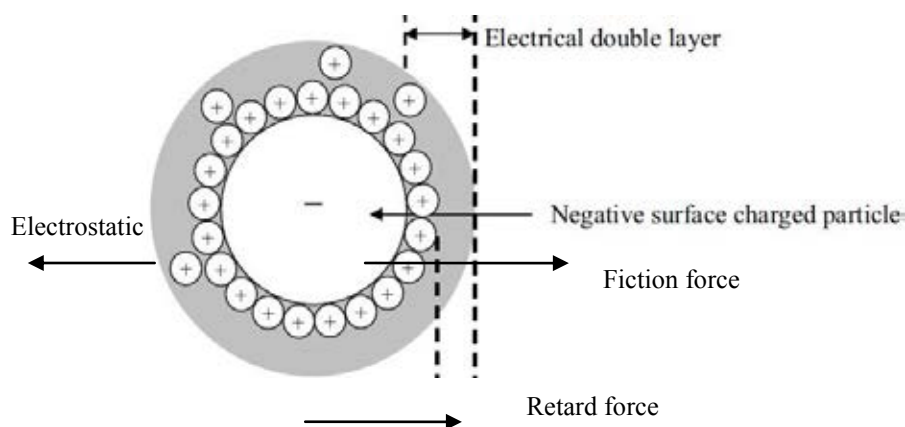


Figure 2.20 Electrophoresis double layer in applied electric field

In addition, when electric field is applied the ions and particles, it will move in opposite directions to each other. However, some ions would also be attracted by the particle and this will be caused the ions to move along with the particle. During eletrophoresis, the same situation exists were a thin layer of liquid around the stern layer (one of two electrically charged layers of electrolyte ions) moves along with the particle. The outer surface of the layer is called the slipping plane and electrostatic potential at sipping plane is called the eletrokinetic potential or zeta potential.

The velocity of particle (v) in an applied electric field is relate to the electrophoretic mobility of the particle (μ_e) and electric field (E) as defined as [78]

$$\mu_e = v/E$$

The most known and widely used theory of electrophoresis was developed in 1903 by Smoluchowski [78].

$$\mu_e = \left(\frac{2 \epsilon_r \epsilon_0 \zeta k}{3 \eta} \right) \cdot f(K)$$

where ϵ_r is the dielectric constant of the dispersion medium

ϵ_0 is the permittivity of free space ($C^2 N^{-1} m^{-2}$)

η is dynamic viscosity of the dispersion medium (Pa s)

ζ is zeta potential

k is dielectric constant

K is inverse Debye length

The Smoluchowski theory can be applied for dispersed particles of any shape and any concentration. Debye length must be important for electrophoresis, it important to note that increasing thickness of the double layer (DL) leads to removing point of retardation force further from the particle surface.

When particle radius a is much greater than the Debye length: $a K \gg 1$; This model of "*thin Double Layer*" offers tremendous simplifications not only for electrophoresis theory but for many other electrokinetic theories. This model is valid for most aqueous systems because the Debye length is only a few nanometers there. It

breaks only for nano-colloids in solution with ionic strength close to water. The $f(\kappa)$ is value to 1.5.

If particle is small, the Smoluchowski theory can be neglected contribution of surface conductivity. This is expressed in modern theory as condition of small Dukhin number. In the effort of expanding the range of validity of electrophoretic theories, the opposite asymptotic case was considered, when Debye length is larger than particle radius. The $f(\kappa)$ is value to 1.

2.7.2 Suspension stability [84,85]

The electrophoretic depositions are consisted of two type suspensions which are aqueous suspension and non –aqueous suspensions. Generally, the stable suspensions present minimal tendency to flocculate and upon eventual settling pack densely owing to the near-absence of irregular agglomerates.

Moreover, there are three mechanisms play important role in dispersing and stabilizing suspensions which are electrostatic, steric and electrostatic mechanism.

-Electrostatic stabilization can be described as repulsive electrostatic double layer force at solid force of the solid-liquid interface. It is more effective in aqueous suspensions because of non-aqueous suspensions. It has lower dielectric constant due to reason that the resultant repulsive energy greatly depends on the surface potential energy of the colloid particles and the dielectric properties of medium

- Steric stabilization can be described as repulsion of polymer chain. The addition of polymer induced force to form polymer layer covering particle. The steric repulsion depends on structure, the thickness layer, and molecular weight of polymer and affinity of polymer on particle surface.

-Electrosteric stabilization is combination of both electrostatic and steric repulsion stabilization.

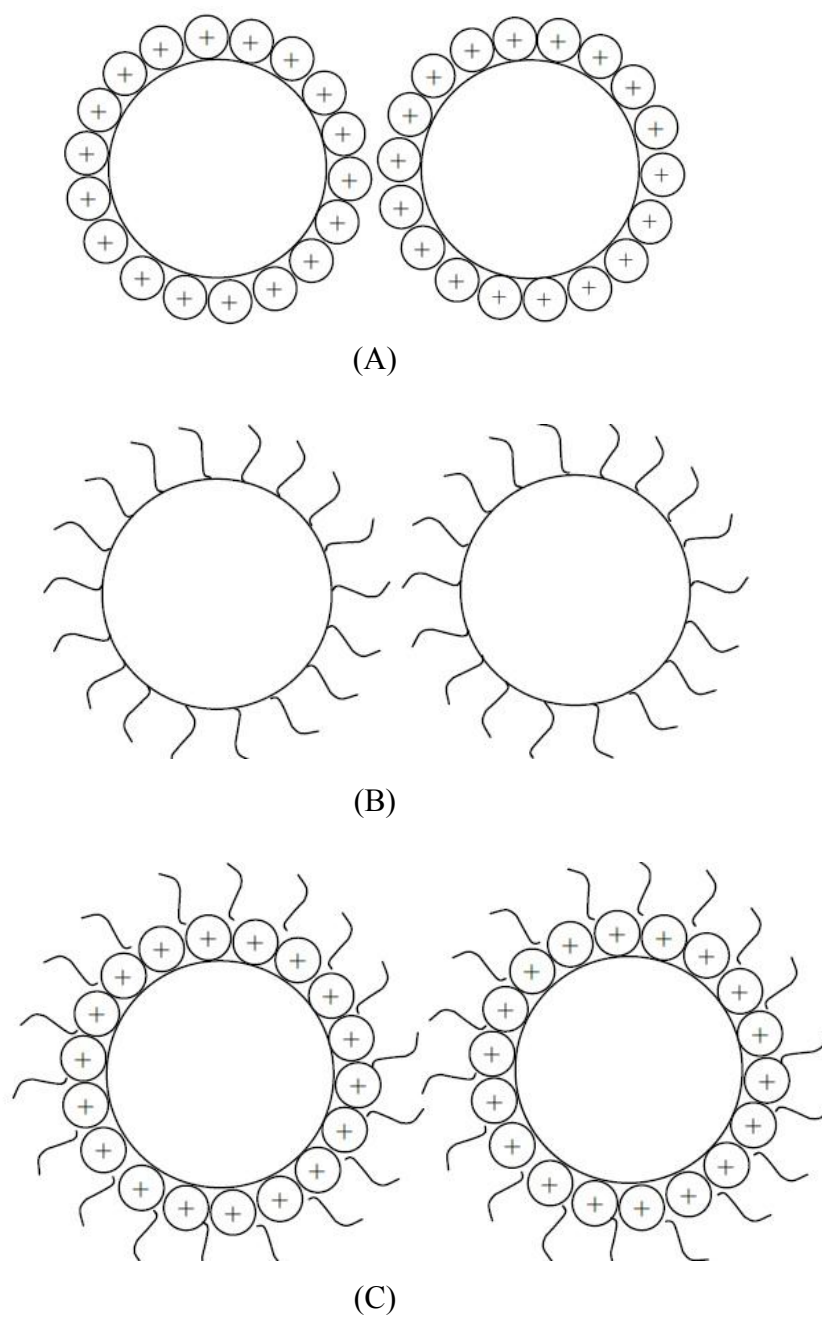


Figure 2.21 Mechanism stabilization (A) electrostatic (b) steric and (c) electrosteric [85]

In aqueous suspension, Partho [86] has outline four charging mechanism of particle dispersed in water:

- i) Dissociation of the surface to yield an ion to the suspension
- ii) Nernstian charging through specific adsorption or desorption of lattice ions
- iii) Metal hydrolysis reaction at metal hydroxide and metal oxide surface
- iv) Metal hydrolysis with incongruent of at least one cation species

However, to prepare suspension in EPD, the most usual practice employed to stabilize an aqueous suspension is by changing the pH of the suspension to values that are far from pH at the isoelectric point. The isoelectric point is the isoelectric point.

CHAPTER III

EXPERIMENTAL AND PROCEDURE

3.1 Materials and Chemicals

The chemicals used in this experiment were normal analytical grade and listed as follows. Some chemical structures are shown in Table 3.1.

1. Aniline monomer (ANi)

Aniline monomer was manufactured by Fluka Chemie A. G. Switzerland. It was purified by distillation under reduced pressure and used as monomer for electrochemically synthesis of polyaniline (PANi).

2. Sulfuric acid (H_2SO_4)

Sulfuric acid was purchased from Labscan Asia Co.Ltd., Thailand. H_2SO_4 was used as solvent for preparing aniline solution and as acid dopant for PANi.

3. Hydrochloric acid (HCl)

Hydrochloric acid was purchased from Labscan Asia Co.Ltd., Thailand. HCl was used as acid dopant for PANi.

4. Phosphoric acid (H_3PO_4)

Phosphoric acid was purchased from Labscan Asia Co.Ltd., Thailand. H_3PO_4 was used as acid dopant for PANi.

5. *p*-toluenesulfonic acid (*p*-TSA)

p-toluenesulfonic acid was purchased from Labscan Asia Co.Ltd., Thailand. *p*-TSA was used as acid dopant for PANi.

6. Dodecyl benzene sulphonic acid (DBSA)

Dodecyl benzene sulphonic acid was purchased from Labscan Asia Co.Ltd., Thailand. DBSA was used as acid dopant for PANi.

7. Ammonium hydroxide (NH_4OH)

Ammonium hydroxide was purchased from Labscan Asia Co.Ltd., Thailand. 0.1 %w/v of ammonium hydroxide solution was used for tuning emeraldine salt PANi to emeraldine base PANi.

8. Multi-wall carbon nanotube (MWCNT)

Multi-wall carbon nanotube was purchased from Labscan Asia Co.Ltd., Thailand. The outer diameter was 10-15 nm with length 0.1-10 μm and wall 5-15. MWCNT was used as additive for fabrication of PANi/MWCNT composite.

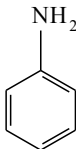
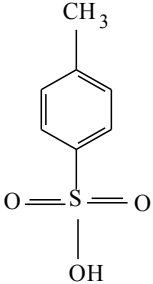
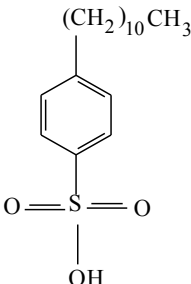
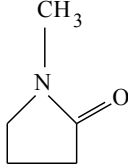
9. Tin oxide Nanoparticle (SnO_2 NP)

Tin oxide Nanoparticle was manufactured by Fluka Chemie A. G. Switzerland. The diameter of SnO_2 NP was 100-200 nm. SnO_2 NP was used as additive for fabrication of PANi/MWCNT/ SnO_2 NP composite.

10. N-methyl-2-pyrrolidone (NMP)

N-methyl-2-pyrrolidone was purchased from Labscan Asia Co.Ltd., Thailand. NMP was used as solvent to dissolve PANi for investigation of UV-Visible spectroscopy.

Table 3.1 chemical structure of material

Chemical	Chemical structure
Aniline monomer	 <chem>Nc1ccccc1</chem>
<i>p</i> -toluenesulfonic acid	 <chem>Cc1ccc(S(=O)(=O)O)cc1</chem>
Dodecyl benzene sulphonic acid	 <chem>CCCCCCCCCCCCc1ccc(S(=O)(=O)O)cc1</chem>
N-methyl-2-pyrrolidone	 <chem>CN1CC(=O)CC1</chem>

3.2 Equipment and Instrument

Details of each equipment and instrument are described according to the experimental procedure as follows.

3.2.1 Potentiostat/galvanostat

The potentiostat/galvanostat (PGSTAT30, Metrohm Autolab, Utrecht, Netherlands) interfaced with General Purpose Electrochemical System (GPES), as shown in Figure 3.1, was used to electrochemically synthesize polyaniline (PANi) and polyaniline composites. A potentiostat is the electronic hardware used to control conventional three-dimensional electrodes cells which are working electrode, reference electrode, and counter electrode. In this research, cyclic voltammetry technique was used to electrochemically synthesize PANi and PANi/MWCNT, whilst chronoamperometric technique was used to electrochemically synthesize PANi/MWCNT/SnO₂. The first technique is functioned by giving sweeping potential of the working electrode with respect to that of the reference electrode (in case of the deposition of the PANi and PANi/MWCNT on interdigitated substrate). And second technique, the systems is functioned by maintaining the potential of the working electrode at a constant level with respect to the potential of the reference electrode by adjusting the current at an auxiliary electrode (in case of the deposition of PANi/MWCNT on SnO₂ NP/interdigitated substrate). The hardware system consists of an electrical circuit which is usually described in terms of simple op amps.



Figure 3.1 PGSTAT30 Potentiostat/galvanostat

3.2.1.1 Gold interdigitated substrate

Gold interdigitated substrate was manufactured by National Electronics and Computer Technology Center, Thailand. It was used as a working electrode. The rectangle board size was 1.5 cm x 2.0 cm with 0.5 cm thickness. The printed wire board of interdigitated substrate was showed in Figure 3.2. The pattern on board was consisted of gold pattern overlapping with insulating gap. The total overlap electrode length was 25 mm which consisting of 14 μm wide of the gold pattern alternating with 10 μm wide of the insulating gap.

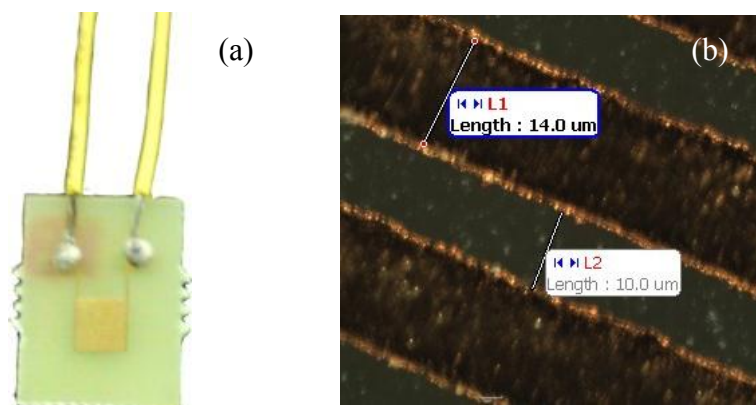


Figure 3.2 The working substrate for deposition of sensor (a) gold interdigitated substrate (b) gap length between gold and insulate gap

3.2.2 Electrophoretic deposition

Electrophoretic deposition technique is used to deposit tin oxide nanoparticle (SnO_2) on interdigitated substrate. The 5% (w/v) SnO_2 NPs conductive colloidal in distilled water was prepared by sonification and the pH was adjusted to 2 with sulfuric acid. A gold pattern coated wire board of interdigitated was used as the anode, whilst aluminum sheet having the size of 2.0 cm x 3.0 cm with 2.0 mm in thickness was used as the cathode. The process involves the movement of SnO_2 NPs charge particle in suspension towards to deposit on anode under electric field at 9 V.

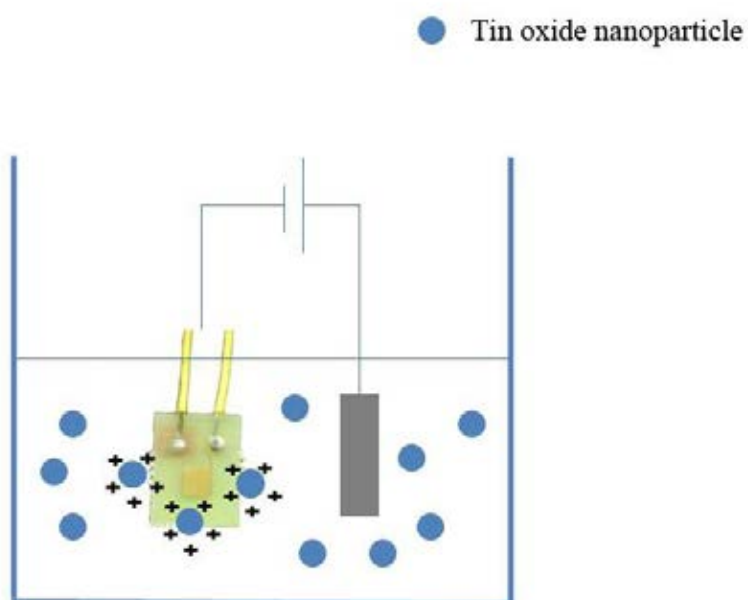


Figure 3.3 Schematic illustrates the electrophoretic deposition of SnO_2 NPs on gold interdigitated substrate

3.2 Experimental Procedure

In this research work, the sensors for ethylene gas detection were fabricated based on PANi. This research proposed the four step methodologies in order to fabricate and improve sensing of ethylene sensor based on PANi and/or PANi composite.

1. To fabricate PANi sensor and investigate the effect of deposited amount of polyaniline on ethylene gas detection by varying a number of cyclic voltammetry
2. To investigate the effect of acid dopant of PANi in terms of acid type and acid level on ethylene gas detection
3. To fabricate PANi/MWCNT and investigate the effect of multiwall carbon nanotube (MWCNT) on ethylene gas detection
4. To fabricate PANi/MWCNT/SnO₂ and investigate the effect of tin oxide nanoparticles on ethylene gas detection

The details of synthesis and fabrication PANi and PANi composite sensor were described as follows:

3.3.1 Electrochemical Synthesis of Polyaniline as Ethylene Gas Sensor

The objective of this part was to fabricate PANi sensor and investigate the effect of deposited amount of polyaniline on ethylene gas detection by varying a number of cyclic voltammetry

The deposited film of sensitive layer of PANi was electrochemically synthesis by cyclic voltammetry method [4]. Aniline monomer was purified by distillation under the reduced pressure before being used by keeping it was kept under the N₂ atmosphere at 5 °C. The electrolyte solution was prepared from the solution of 0.1 M Aniline monomer in 1M aqueous sulfuric solution. The interdigitated electrode sensor substrate consisting of gold pattern coated on printed wire board was used as a working electrode for deposition. The electrolyte solution containing aniline monomer deposited PANi was polymerized by applying sweeping potential within the range of -0.3-1.0 V at the scanning rate of 50 mV/s relative to the silver reference electrode and

platinum counter electrode. The numbers of cycle scan of cyclic voltametry were varied start from 5, 10, 15, 20 and 25 scans. The growth of deposited-PANi film on interdigitated gold substrate was expected to cover insulating gaps between the neighboring electrodes.

The experimental flow diagram for fabrication of PANi sensor for ethylene gas detection is showed in Figure 3.4.

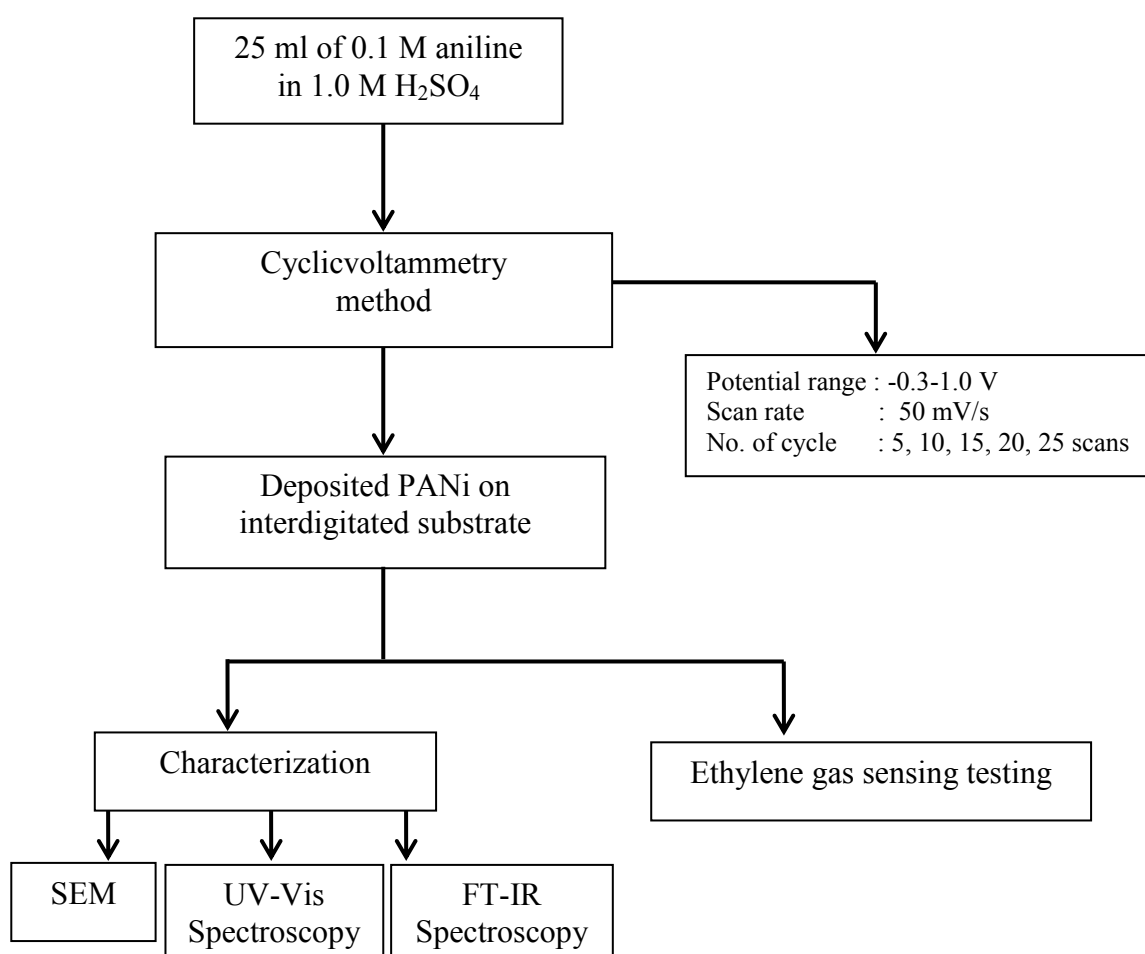


Figure 3.4 Flow diagram for fabrication of PANi sensor for ethylene gas detection

3.3.2 Electrochemical Synthesis of Sensitive Layer of Polyaniline: Effects of acid dopant on ethylene gas sensing

The purpose of this step was to investigate the effect of acid dopant of PANi in terms of acid type and acid level on ethylene gas detection. The experiment was divided into 2 steps as follows.

3.3.2.1 Electro-deposition of sensitive layer of polyaniline nanofibers

The deposition of sensitive layer of PANi was fabricated by cyclic voltammetry method as previously described in section 3.3.1. The number of cyclic voltammetry for deposition PANi was chosen from the optimum condition as will be discussed in section 4.1.

3.3.2.2 Preparation of de-doped and doped polyaniline

The emeraldine salt form of polyaniline-sulfuric (PANi-H₂SO₄) on interdigitated substrate obtained from section 3.3.2.1 was washed with distilled water. Then, the emeraldine salt form of PANi-H₂SO₄ on interdigitated was de-doped to emeraldine base by soaking interdigitated substrate in 0.1 M ammonium hydroxide for 3 hours. After that, the emeraldine base of PANi was treated with specific acid dopant of particular concentration for 12 hours at room temperature. Five different acids which are hydrochloric acid (HCl), sulphuric acid (H₂SO₄), phosphoric acid (H₃PO₄), *p*-toluenesulfonic acid (TSA), and dodecyl benzene sulphonic acid (DBSA) were used as acid dopant at different concentrations of 0.1, 0.075, 0.05, 0.025 and 0.01M.

The experimental flow diagram for fabrication of doped PANi sensor for ethylene gas detection is showed in Figure 3.5.

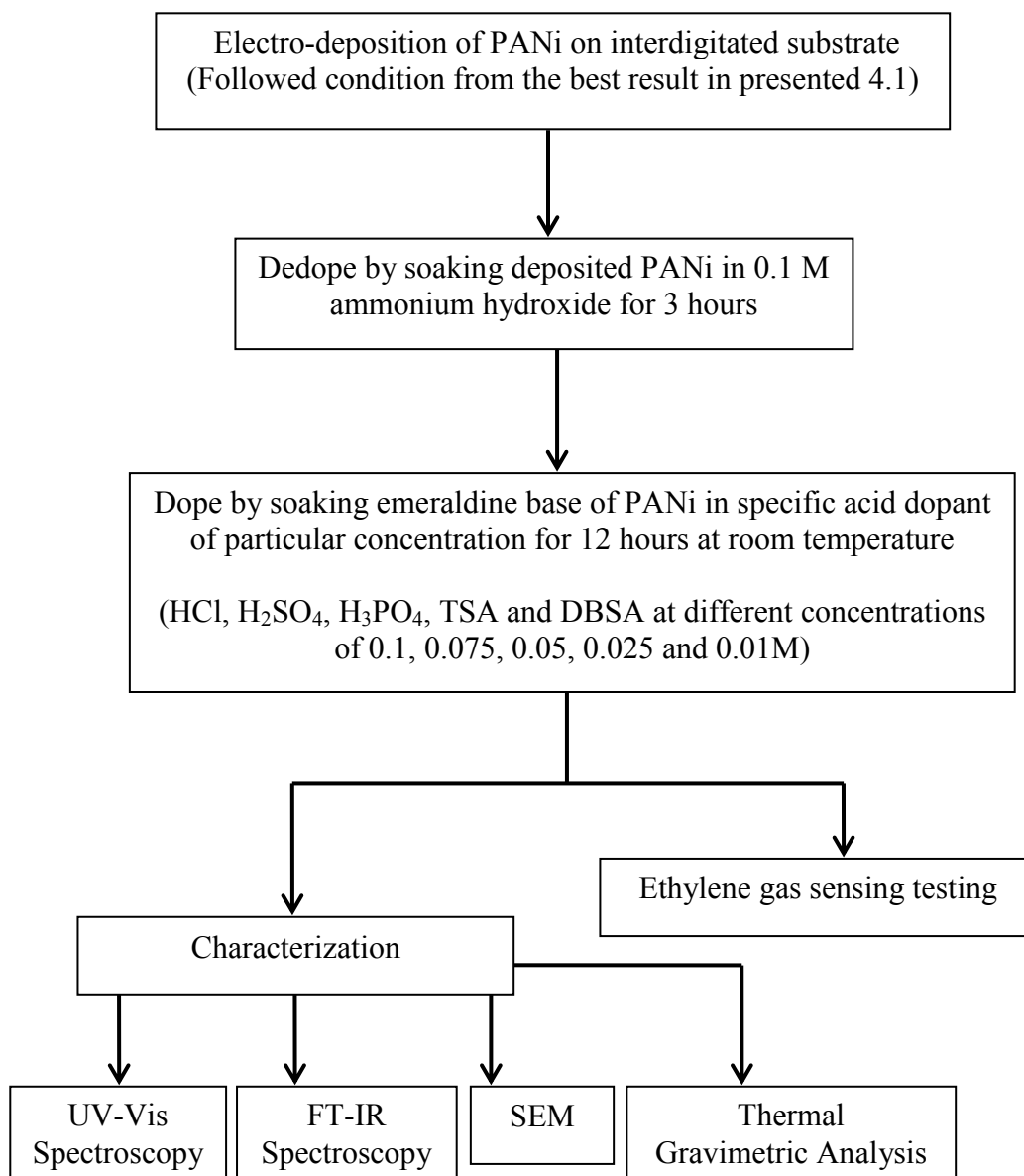


Figure 3.5 Flow diagram for doped PANi sensor fabrication for ethylene gas detection

3.3.3 In-situ electrochemical synthesis of sensitive layer of polyaniline/multiwall carbon nanotube composite for ethylene gas detection

The aim of this part was to fabricate PANi/MWCNT and investigate the effect of multiwall carbon nanotube (MWCNT) on ethylene gas detection. Four steps for fabrication of PANi/MWCNT sensor were detailed as follows.

3.3.3.1 Dispersion of multi-wall carbon nanotube in aniline monomer

To prepare electrolyte solution from aniline/MWCNTs, the MWCNTs were weighted in different percentage weight per volume of aniline at 0.2, 0.4, and 0.8. The suspension of MWCNT in aniline monomer was heated to reflux in aniline for 7 hours in the dark [87]. The mixing solution was turned to dark red and used as the suspension solution.

3.3.3.2 Electro-deposition of sensitive layer of polyaniline nanofibers /multiwall carbon nanotube composite film

The deposition of sensitive layer of PANi/MWCNT was fabricated by cyclic voltammetry method as previously explained in section 3.3.1. The electrolyte solution was prepared from the solution of 0.1 M aniline/MWCNT (0.2, 0.4, and 0.8 % w/v of MWCNT in aniline monomer) in 1M aqueous sulphuric acid solution.

3.3.3.3 De-doped and doped polyaniline/multiwall carbon nanotube

The obtained emeraldine salt form of polyaniline-sulfuric/multiwall carbon nanotube (PANi-H₂SO₄/MWCNT) on interdigitated substrate was washed with distilled water. Then, the emeraldine salt form of PANi-H₂SO₄/MWCT was de-doped to emeraldine base by soaking in 0.1 M ammonium hydroxide for 3 hours. After that, the emeraldine base of PANi/MWCNT was treated with acid dopant at particular concentration for 12 hours at room temperature. The five specific acids dopants at particular concentration were chosen from the optimum result from section 4.2.

The experimental flow diagram for PANi/MWCNT sensor fabrication for ethylene gas detection is showed in figure 3.6.

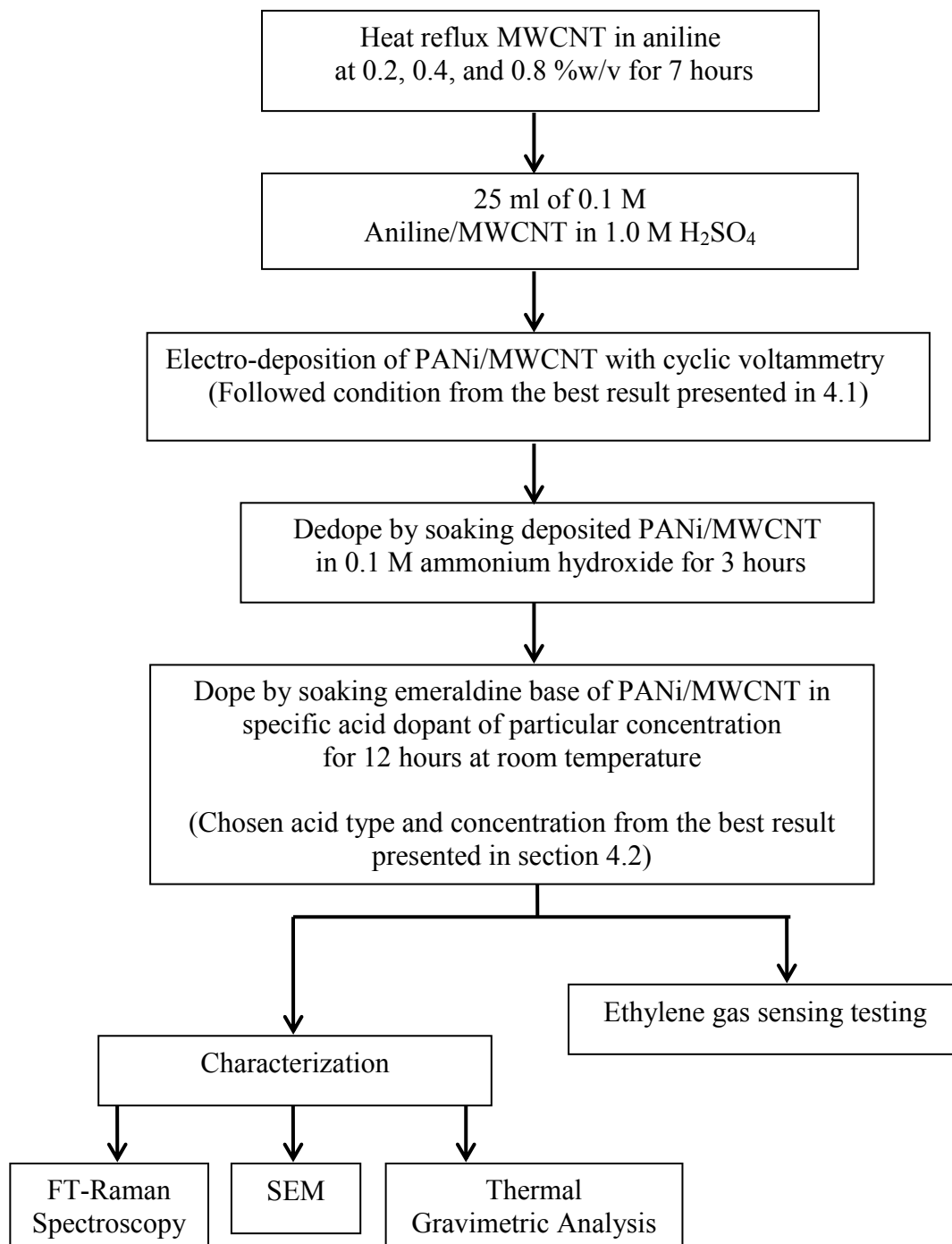


Figure 3.6 Flow diagram for fabrication of PANi/MWCNT sensor for ethylene gas detection

3.3.4 In-situ electrochemical synthesis of novel sensitive layer of polyaniline/multiwall carbon nanotube/tin oxide nanoparticles (PANi/MWCNT/SnO₂ NPs) hybrid materials for ethylene gas detection

The aim of this part was to fabricate PANi/MWCNT/SnO₂ NP and investigate the effect of tin oxide nanoparticles on ethylene gas detection. A sensitive multilayered PANi/MWCNT/SnO₂ NP composite material for ethylene gas detection was synthesized in two steps. Firstly, SnO₂NPs were electrophoretically deposited onto a gold interdigitated substrate and then secondly a PANi/MWCNT layer was chronoamperometrically deposited on top of the SnO₂NP/gold interdigitated substrate. The details of each step are as follows.

3.3.4.1 Deposition of SnO₂NPs onto the interdigitated gold substrate

A colloidal suspension of 5% (w/v) SnO₂NPs in distilled water was prepared by sonification and the pH was adjusted to 2 with sulfuric acid. A gold pattern coated wire board, comprised of a 25 mm overlapping electrode length and 10 μm insulating gap, was used as the anode, whilst aluminum foil was used as the cathode. The colloidal suspension of SnO₂NPs was electrophoretically deposited onto the gold interdigitated substrate at 9 volts, but with different deposition times (0, 60, 90, 120 and 150 sec) to cause different SnO₂NP loadings.

3.3.4.2 Chronoamperometric deposition of PANi/MWCNT nanofibers on the thin film of SnO₂NPs

A 0.2% (w/w) suspension of MWCNT was dispersed in aniline by refluxing at 180 °C for 12 hours. The mixing solution turned dark red and was used as the suspension solution. The *in-situ* polymerization of PANi/MWCNT onto the thin layer of SnO₂NPs was conducted by chronoamperometric deposition using a conventional three-electrode set-up in an undivided cell (potentiostat/galvanostat of autolab model PGSTAT30 and interfaced with General Purpose Electrochemical System). The electrolyte medium was 25 ml of 1.0 M sulfuric acid solution containing a suspension of 0.1 mol aniline/MWCNT. This electrolyte medium was polymerized to yield a deep

green MWCNT/PANi film, that was deposited on the thin anodic film of SnO₂NPs on top of the interdigitated gold, by polarizing at 1 V for 150 sec relative to the Ag/AgCl reference electrode and the platinum counter electrode.

3.3.4.3 De-doped and doped polyaniline/multiwall carbon nanotube/tin oxide nanoparticle

The oxidizing state of PANi, the emeraldine salt form of PANi-H₂SO₄ was changed into emeraldine base (insulator/semi conductive form) by soaking into 0.1 M ammonium hydroxide for 3 hr. Then, the emeraldine base form of PANi was treated with 0.1 M sulfuric acid for 12 hours in order to convert the emeraldine base form of PANi into the conductive emeraldine salt (PANi-H₂SO₄). This oxidized state of the MWCNT/PANi-H₂SO₄ was the optimum condition for ethylene gas detection as reported and discussed in section 4.2.

The experimental flow diagram for PANi/MWCNT/SnO₂NP sensor fabrication for ethylene gas detection is showed in Figure 3.7.

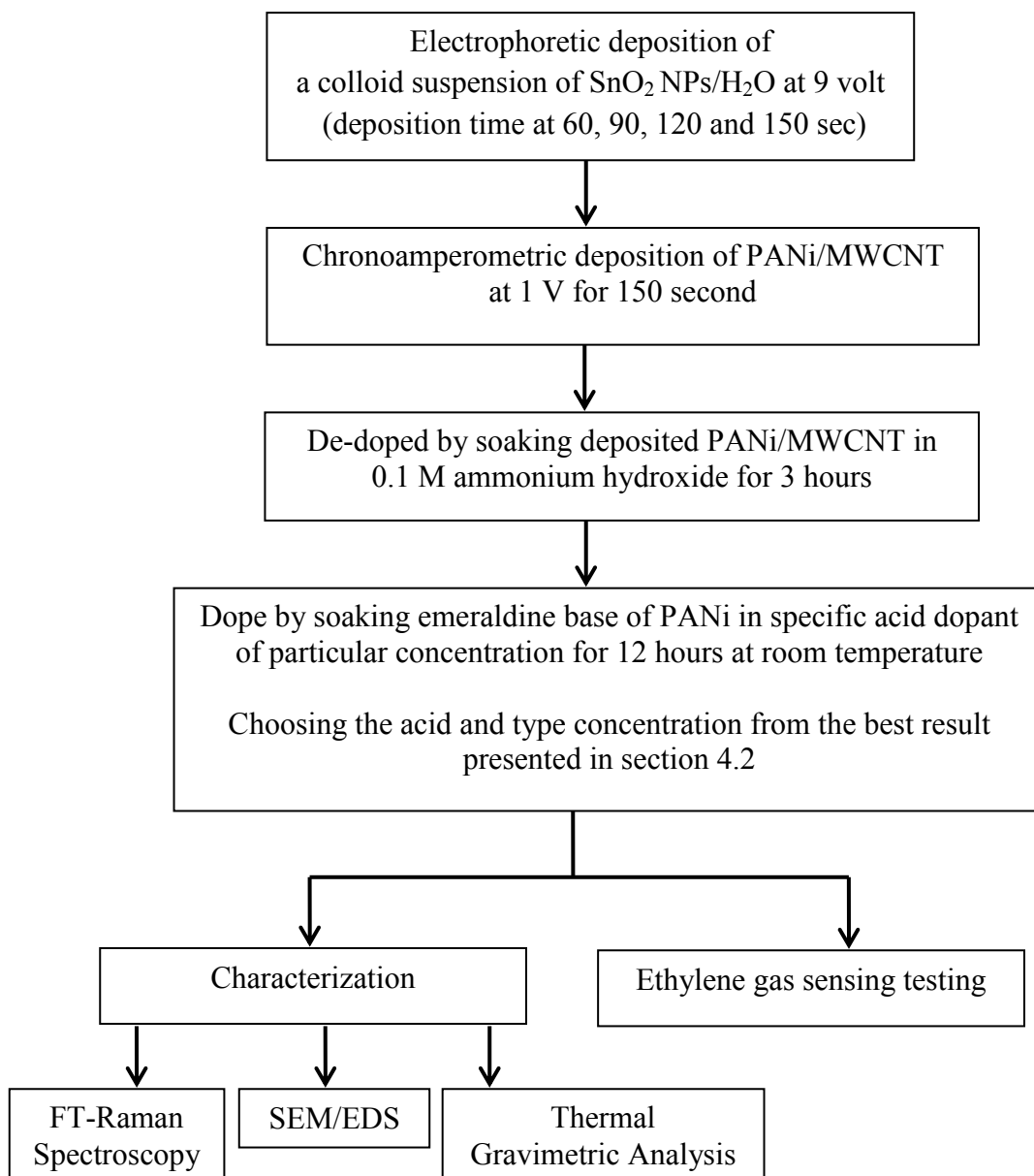


Figure 3.7 Flow diagram for fabrication of PANi/MWCNT/SnO₂NP sensor for ethylene gas detection

3.4 Characterization and Testing

3.4.1 Ultraviolet- Visible Spectrometer (UV-VIS)

The Ultraviolet-Visible spectra of polyaniline and doped polyaniline were recorded with UV-VIS spectrometer (SPECORD S 100, Analytikjena, Jena, Germany) to investigate the polaron and bipolaron state of polyaniline (emeraldine base of polyaniline) and polyaniline-doped (emeraldine salt of polyaniline). The solution of polyaniline was prepared by dissolution of polyaniline in N-methyl-2-pyrrolidone at concentration of 0.1g/l. The light transmission or absorbance was recorded as a function of wavelength in the range of 300-900 nm.



Figure 3.8 SPECORD S 100 Ultraviolet-visible spectrometer

3.4.2 Fourier Transform Infrared Spectrometer (FT-IR)

The FT-IR spectra have been taken by using Nicolet 6700, Thermo scientific, Madison, Wis. This technique was used to characterize the functional group of undoped polyaniline (emeraldine base of polyaniline) and doped polyaniline (emeraldine salt of polyaniline). The sample was mixed with KBr at the ratio of 50:1(KBr:PANi) and pelletized into pellet shape by using hydraulic press. The absorbance was recorded as a function of wavelength in a range of 400 -4000 cm^{-1} with 64 scans at a resolution of 4 cm^{-1} .



Figure 3.9 Nicolet 6700 Fourier Transform Infrared Spectrometer

3.4.3 Raman Spectroscopy

The functional groups of MWCNT/PANi and MWCNT/PANi/SnO₂ NPs were characterized with Raman spectroscopy (Spectrum-GX NIR, Perkin-Elmer (Madison, Wis.)). The sample was mixed with KBr and pelletized into pellet shape by using hydraulic press. This pellet was spinned with high speed to protect degradation from laser beam. The He-Ne laser was used at 633 nm and recorded wavelength in range 0-2000 cm⁻¹.



Figure 3.10 GX NIR Raman Spectroscopy

3.4.4 Scanning Electron Microscope (SEM)

The morphology of polyaniline, doped polyaniline and polyaniline composites was characterized by SEM (JSM 5800 LV, JEOL, Tokyo, Japan). The scanning electron microscopy was operated at 15 KV. The surface of the sample was sputter-coated with a thin layer of gold before being scanned to avoid surface charging under electron beam.



Figure 3.11 JSM 5800 LV Scanning Electron Microscope

3.4.5 Thermo Gravimetric Analyzer (TGA)

TGA (SDTA 851^e, Mettler Toledo, Greifensee, Switzerland) was used to study the thermal stability and decomposition temperature of undoped polyaniline, doped polyaniline and polyaniline composites. TGA analysis of samples was carried out under nitrogen (in case of PANi and doped PANi) or oxygen (in case of PANi composites) atmosphere from 50 °C to 600 °C with a heating rate of 10 °C/min. The samples were removed from interdigitated substrate and weighted in the range of 5-10 mg. Prior to do the experiment, the samples were dried in an oven at 60°C overnight. The thermal degradation temperature (Td) was reported as the onset of weight loss of heated sample.



Figure 3.12 SDTA 851^e Thermo Gravimetric Analyzer

3.5 Ethylene gas sensing measurement

The ethylene gas detection of PANi samples was measured by monitoring a change in resistance of PANi sample. All measurements were monitored a changing in resistance of sample by sequentially changing concentration of ethylene gas at 1000, 500, 200,100, 50,20 and 10 ppm alternating with nitrogen gas. The schematic of gas detection system used in this experiment is shown in Figure 3.14.

The sensing magnitude of the sensors (S) is defined as [7]

$$S = \frac{(R_{\text{nitrogen}} - R_{\text{gas}}) \times 100}{R_{\text{gas}}} \quad (\text{Eq.3.1})$$

Where R_{gas} is the resistance of the sensors in ethylene gas.

R_{nitrogen} is the resistance of the sensors in nitrogen gas.

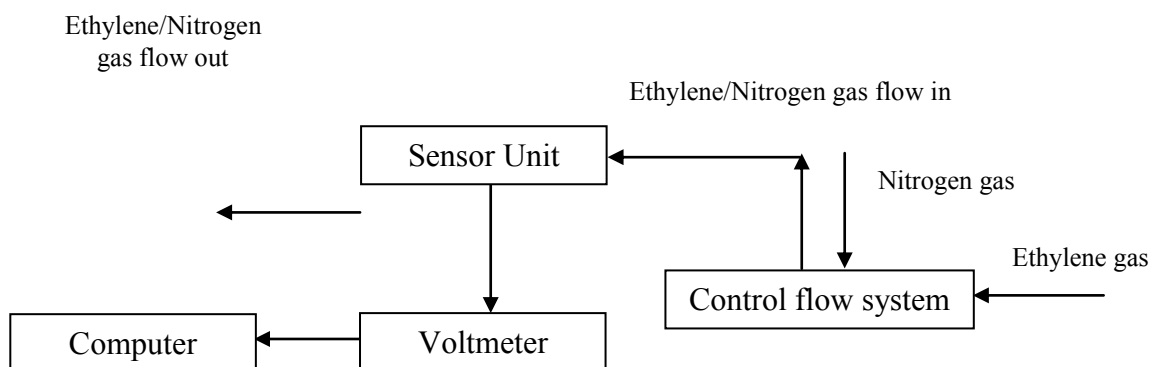


Figure 3.14 Schematic of the gas detection system for testing conductive polymer

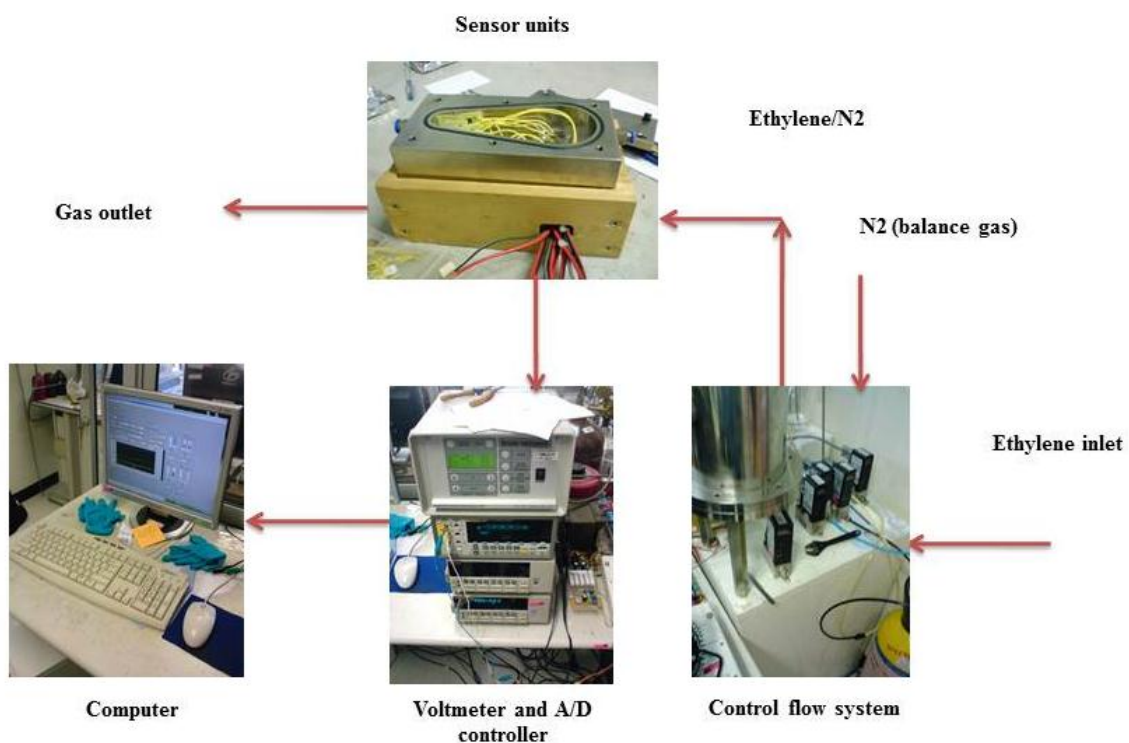


Figure 3.15 Gas detection system for testing conductive polymer

CHAPTER IV

RESULTS AND DISCUSSION

In this research, the sensors for ethylene gas detection were fabricated based on PANi. The effects of deposited PANi, acid dopant PANi and some additives (i.e., MWCNT and SnO₂ NP) on ethylene gas detection were investigated. This research was divided into four parts as list below in order to fabricate and improve sensing of ethylene gas sensor base on PANi and/or PANi composites.

1. To fabricate PANi sensor and investigate the effect of deposited amount of polyaniline on ethylene gas detection by varying a number of cyclic voltammetry

2. To investigate the effect of acid dopant of PANi in terms of acid type and acid level on ethylene gas detection

3. To fabricate PANi/MWCNT and investigate the effect of multiwall carbon nanotube (MWCNT) on ethylene gas detection

4. To fabricate PANi/MWCNT/SnO₂ and investigate the effect of tin oxide nanoparticles on ethylene gas detection

The details of synthesis and fabrication of PANi and PANi composites sensor were described as follows:

4.1 Electrochemical Synthesis of Polyaniline as Ethylene Gas Sensor

4.1.1 Electrochemical synthesis of polyaniline

Electrochemical depositions of PANi films were carried out with cyclic voltammetry method within the range of -0.3-1 V. The effect of deposited amount of PANi on ethylene gas detection was investigated by varying the number of potential cycle at 5, 10, 15, 20, and 25 scans. The sensitive layer of PANi was deposited on interdigitated gold substrate in order to bridge the gaps between insulating and conductive gold pattern with cyclic voltammetry method.

The resultant amount and resistivity of deposited PANi at different numbers of cycle scan from cyclic voltammetry were showed in Table 4.1. The electrolyte solution from 0.1 mole aniline monomer in 1M H₂SO₄ was oxidized and polymerized to polyaniline in potential range of -0.3-1.0 V. The growth of PANi film was deposited on interdigitated gold substrate and yielded a deep green film. The neighboring gaps between insulating and gold pattern were connected to each other by the deposited amount of PANi after applying ten potential cycles.

With increasing number of potential cycle, weight of deposited-PANi film was increased whereas the resistance of the deposited-PANi film was decreased. The decrease of resistance of PANi with increasig number of potential cycle was resulted from the regular growth of conductive PANi.

Table 4.1 Weight increase and resistance of deposited PANi films at different potential cycles

Number of cycle	Weight increase [mg]	Resistance [Ω]
5	less than 25	-
10	71.45 \pm 6.99	8.37 $\times 10^4$ \pm 81.82
15	80.59 \pm 16.12	3.55 $\times 10^4$ \pm 43.62
20	122.09 \pm 0.02	5.72 $\times 10^2$ \pm 0.75
25	158.64 \pm 16.70	49.9 \pm 0.42

The redox behavior of cyclic voltammogram recorded was investigated during applying continuous potential cycle in ranging from -0.3-1V as shown in Figure 4.1. The upper peak revealed anodic region and the lower peak revealed cathodic region. The voltammogram revealed that the slight shifts of the upper peak to the higher potential of anodic peak with the increasing number of potential cycles were resulted from the increasing of the regular growth of PANi films during electrochemical polymerization. The increasing of their peak height with the increasing number of potential cycle was an indication of deposited conductive form of PANi (Emeraldine salt) on substrate and also electroactive. Meanwhile, the slight shifts to the lower potential of cathodic peak with the increasing number of potential cycles were attributed to the autocatalytic polymerization occurs during electrolysis of aniline (Genies et al., 1985) [88].

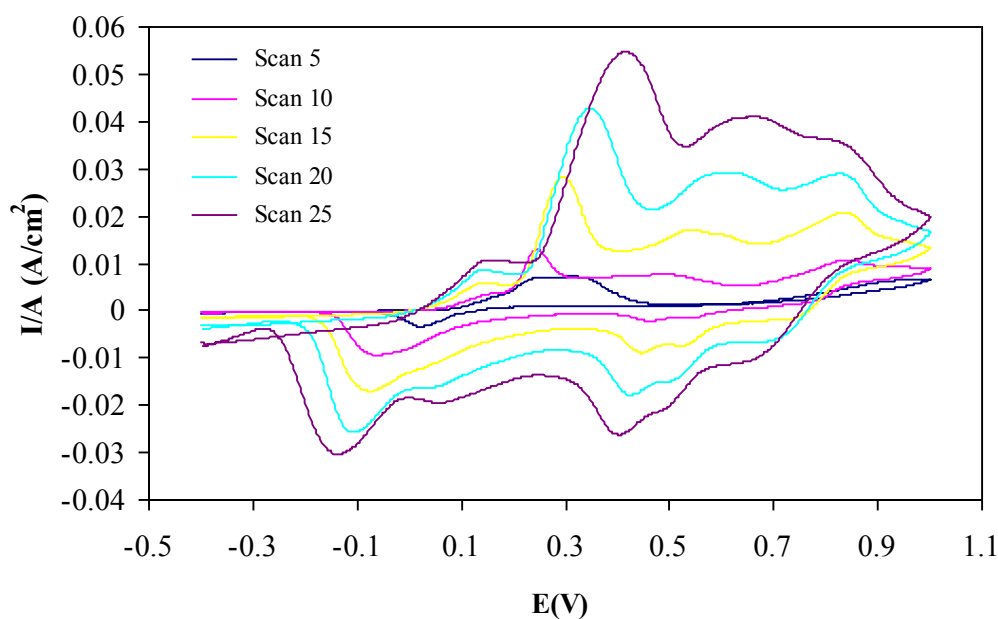


Figure 4.1 Cyclic voltammograms of polyaniline film growth at varying 5 to 25 of number of scan with a scanning rates of 50 mV/Sec

In addition, the cyclic voltamogram can be expressed in term of redox characteristic behavior. First, the polymerization carried out by oxidation at 0.2-0.3 V as a formation of polaron state of PANi. The reaction continually proceeded by formation of diradical dications of bipolaron state of PANi at 0.5 and 0.8-1.0 V,

respectively. And the reductive peak in reverse direction at 0.4-0.6 and -0.1-0.2 V revealed reduction of polaron state as redox reactions of dimers, oligomers, and the degradation products such as p-aminophenol and quinoneimine [88].

4.1.2 Characterization of polyaniline

4.1.2.1 UV-Visible spectral characterization of PANi

In this experiment, the UV-Vis absorption was used to investigate the optical properties of conductive PANi in term of the absorption wavelength.

The PANi sample was dissolved in N-methyl-2-pyrrolidone at the concentration of 0.1g/l. The UV-Vis absorption spectrum of solution PANi was investigated as shown in Figure 4.2. The deposited PANi was obtained from the polymerization of aniline monomer in H₂SO₄ solution with cyclic voltammetry method. The obtained-PANi after polymerization is formed as emeraldine salt form of sulphonate group as shown in Figure 4.3.

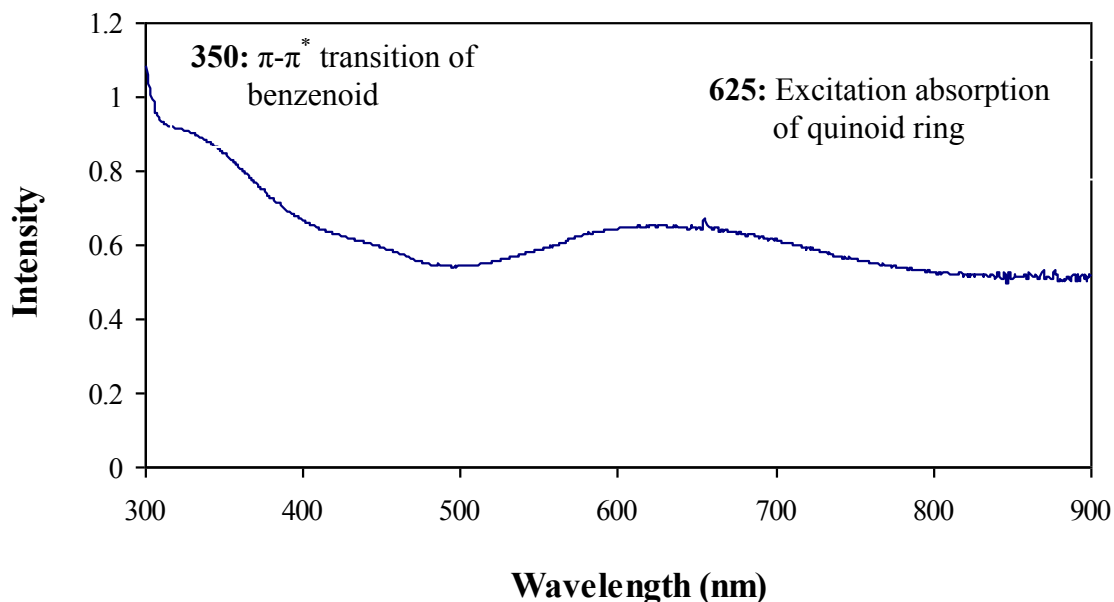


Figure 4.2 UV-Vis absorption spectra of PANi in N-methyl-2-pyrrolidone solution

As shown in Figure 4.2, the characteristic absorption bands of PANi-H₂SO₄ revealed broad peaks around 625 and 350 nm due to the π - π^* transition of benzenoid ring and the excitation absorption of quinoid ring, respectively [89]. In addition, the existence of broad peak around 450 nm confirmed the presence of polaron/bipolaron state. This characteristic peak indicated the conducting behavior of polyaniline. This result was due to the quinoid ring of PANi was converted to semi-quinoid radical. The nitrogen atom on imine groups were protonated with hydrogen atom as seen in Figure 4.3

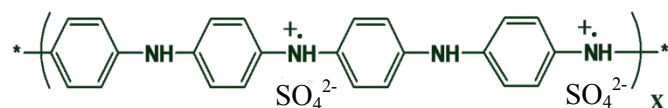


Figure 4.3 the chemical structure of emeraldine salt form of sulphonate group of polyaniline

4.1.2.2 Fourier transforms infrared spectroscopy of PANi

Besides UV-Vis spectroscopy, functional groups of the PANi-H₂SO₄ were characterized using FT-IR technique. The IR vibrations of PANi-H₂SO₄ are given in Table 4.2, whereas its spectrum is shown in Figure 4.4.

Table 4.2 Infrared vibration and assignments for emeraldine salt of PANi-H₂SO₄ [90]

Major IR Bands of PANi-H₂SO₄	
Wavenumber (cm⁻¹)	Assignment and Remarks
1569	C=N stretching of quinoid ring
1470	C-H stretching of benzenoid ring
1303	C-N stretching of benzenoid ring
1237	C-N stretching of benzenoid ring
1135	C-H bending of quinoid ring
1078	SO ₄ ²⁻ substitution
874	C-H bending of aromatic ring
800	C-H bending of aromatic ring

The FT-IR spectrum of PANi-H₂SO₄ was presented in Figure 4.4. The results showed eight important transmittance peaks. The first peak at 1569 cm⁻¹ corresponded to the stretching peak of C=N of quinoid ring. The peak at 1470 cm⁻¹ was due to the C-H stretching of benzenoid ring. The characteristic peaks at 1303 and 1237 cm⁻¹ can be assigned to C-N stretching of benzenoid ring. The peak at 1135 cm⁻¹ was due to the C-H stretching of quinoid ring. The presence of band at 878 cm⁻¹ and 800 cm⁻¹ was due to C-H bending of aromatic ring of benzenoid structure. The strong peak at 1078 cm⁻¹ indicated SO₄²⁻ group on polyaniline which compensated the positive charges on the benzenoid ring.

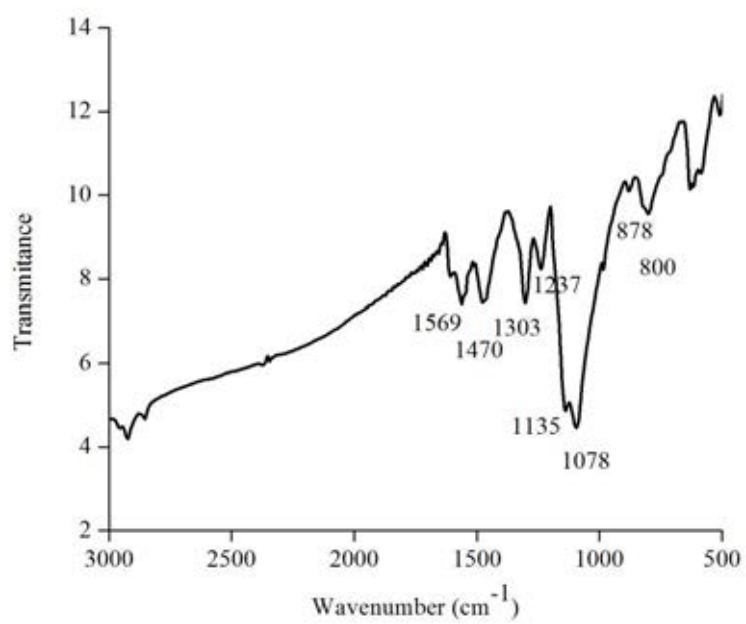


Figure 4.4 FT-IR spectrum of obtained-PANi after cyclic voltammetry at 10 scans

4.1.3 Morphological Studies

The PANi was deposited by electrochemistry via cyclic voltammetry method at different numbers of cyclic scan (i.e., 5, 10, 15, 20 and 25 scans). The SEM images were used to investigate the morphology of deposited PANi on interdigitated gold electrode as shown in Figure 4.5 and 4.6.

The increasing number of cyclic voltammetry scan led to an increase amount of the deposited PANi on the substrate. As seen in figure 4.5, after 5 scans, the deposited amount of PANi was not enough to bridge the gaps between conductive and insulating gaps of interdigitated substrate. The gaps between conductive and insulating gaps of interdigitated substrate was bridged by deposited amount of PANi after at least 10 scans of cyclic voltammetry.

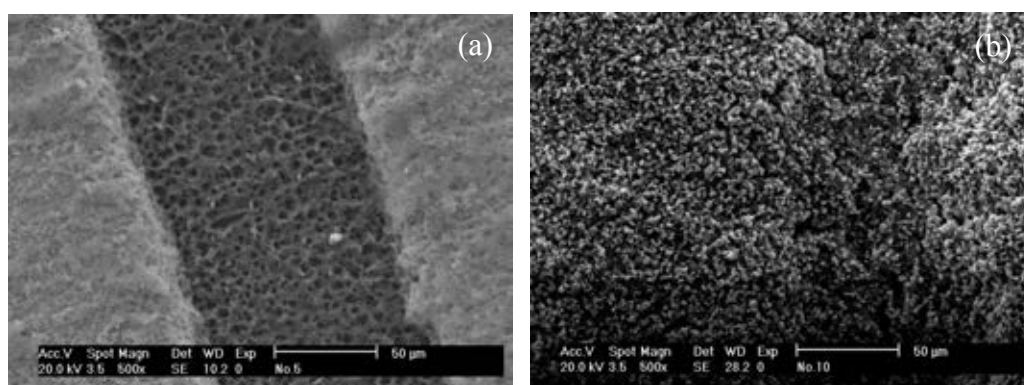


Figure 4.5 SEM images of PANi prepared by cyclic voltammetry on interdigitated gold substrate at different number of scans of cyclic voltammetry: (a) after 5 scans (b) after 10 scans

The effect of number of cyclic voltammetry scan on morphology of PANi was shown in Figure 4.6. The morphology of PANi showed porous film with bulk microstructure after deposition at 5 scans. The increasing amount of deposited PANi from 5 to 10 scans revealed development of microstructure of porous film into nanofibril structure.

In addition, the morphology of PANi film exhibited a combination of micro/nano fibril and micro beads after increasing number of cyclic voltammetry up to 15 scans as seen in Figure 4.6(c). The increasing number of potential cycles of

electrochemical polymerization to 25 scans led to greater amount of micro beads appearing on the substrate. These results indicated that, upon increasing number of potential cycles, the micro/nano fibril structure in PANi was transformed into micro beads during regular growth of PANi.

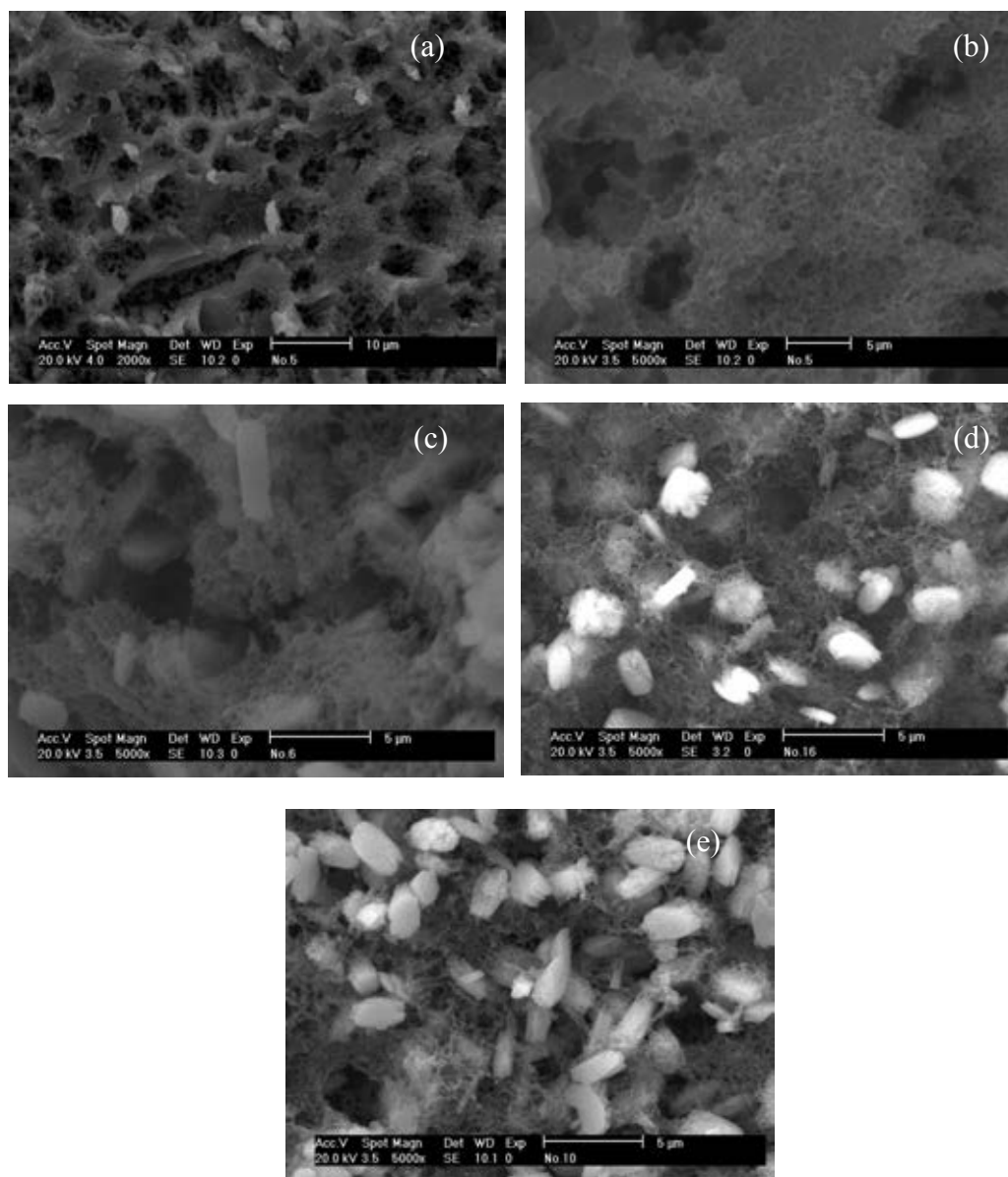


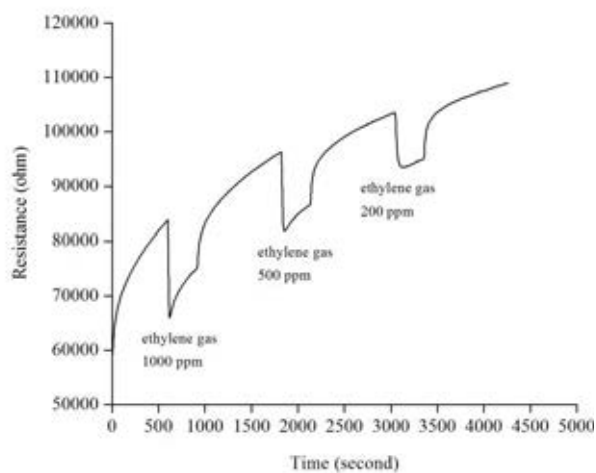
Figure 4.6 SEM images of PANi prepared by cyclic voltammetry on interdigitated gold substrate at different numbers scan of cyclic voltammetry: (a) 5 scans (b) 10 scans (c) 15 scans (d) 20 scans (e) 25 scans

4.1.4 Ethylene gas detection of PANi via resistance measurement

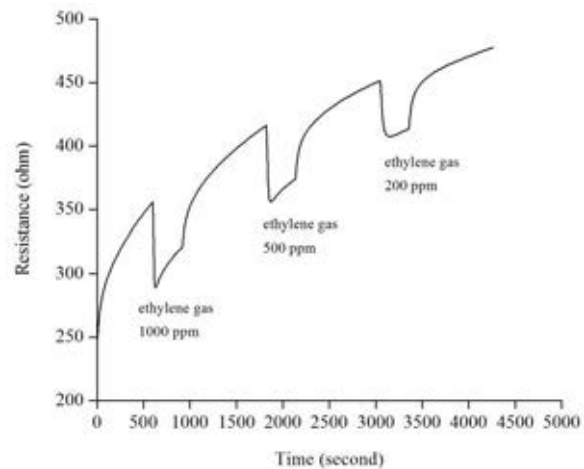
The response–recovery characteristics of the PANi-H₂SO₄ sensor to ethylene gas at 1000, 500, and 200 ppm were shown in Figure 4.7. It should be noted that, the baseline of PANi-H₂SO₄ shifted toward higher resistance with constant rate in nitrogen atmosphere. After being exposed to ethylene gas, the entire PANi-H₂SO₄ films responded by undergoing a decrease in its resistance. The resistance of PANi-H₂SO₄ recovered to baseline after being exposed to nitrogen gas.

These results may be due to the interaction of small molecule of ethylene diffuses into the PANi-H₂SO₄, leading to an expansion of the compact PANi-H₂SO₄ chain into linear form of PANi-H₂SO₄ chain backbone (Anjali A et al., 2000 [57]). The sensing magnitude against the concentration of ethylene with different numbers of cyclic voltammetry scan was shown in Figure 4.8. The sensitivity of the deposited PANi-H₂SO₄ at 10 cyclic voltammetry (CV) scans showed the highest sensitivity, and this sensitivity was decreased in the order of the number of cyclic voltammetry scan as 10 CV > 15 CV > 20 CV > 25 CV > 5CV. The deposited PANi-H₂SO₄ with 10 scans exhibited the highest sensitivity for the detection of ethylene gas at 200 ppm, with a change in the sensing magnitude of about 10.79 %.

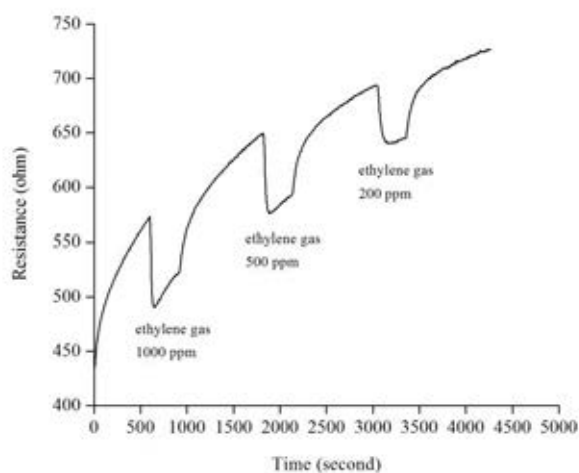
In addition, as evidenced by SEM analysis, the less micro beads and more micro/nano fibril morphology of the PANi synthesized at in 10 scans facilitate greater absorption of ethylene gas than the one synthesized at 15 scans, resulting in higher sensitive toward ethylene gas than the others. The increasing number of cyclic voltammetry scans to higher than 20 scan leading to a decrease in the sensitivity because of the bulky morphology of PANi films.



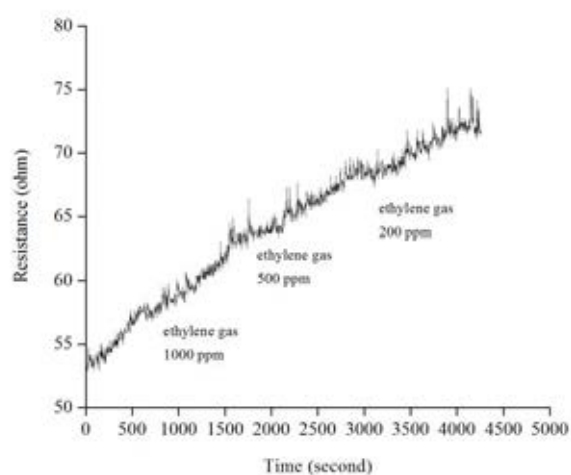
(a)



(b)



(c)



(d)

Figure 4.7 The resistance response behavior against varying concentrations of ethylene gas of the PANi-H₂SO₄ at different number of cyclic voltammetry scans: (a) 10 scans, (b) 15 scans, (c) 20 scans and (d) 25 scans

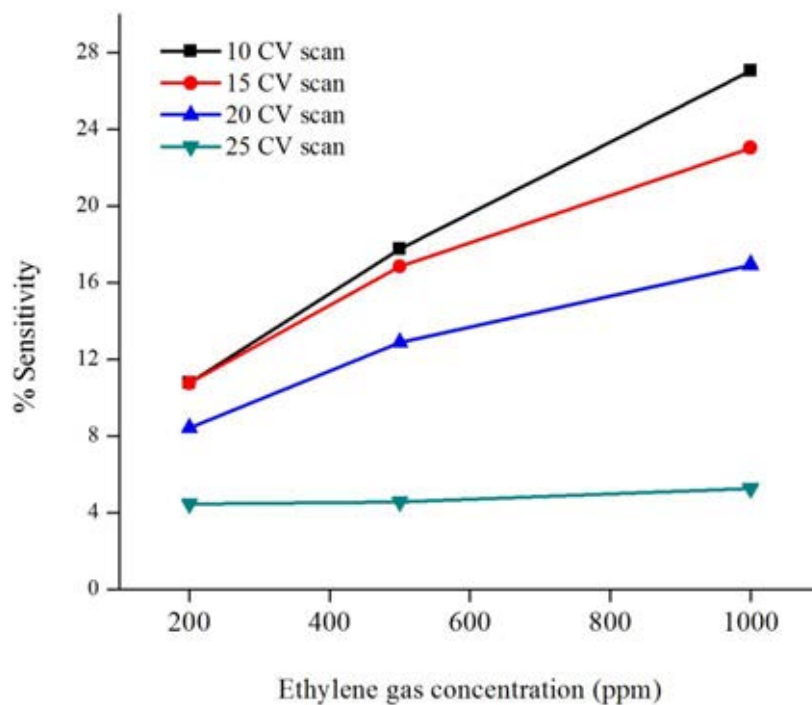


Figure 4.8 The sensing magnitude of the PANi-H₂SO₄ against varying concentrations of ethylene gas prepared from different numbers of cyclic voltammetry scan

4.2 Electrochemical Synthesis of Sensitive Layer of Polyaniline: Effects of Acid Dopant on Ethylene Gas Sensing

This section investigated the effect of acid dopant on sensing property against ethylene gas. As previously reported in section 4.1.4, the deposited PANi at 10 scans cyclic voltammetry revealed the highest sensitivity against ethylene gas detection. This condition was used as optimum condition to fabricate PANi on gold interdigitated substrate. However, without modification, this PANi sensor had been limited to detect ethylene gas at lower level than 100 ppm. Generally, the modification of PANi with acid doping process was used to improve sensing property. By changing the acid doping level and specific acid type, the conductivity of PANi can be tuned for enhancing sensing properties.

Thus, in this part, the sensitive layer of PANi was modified by acid doping process after the deposition of polyaniline at 10 cyclic voltammetry scans. The emeraldine salt form of PANi- H_2SO_4 was changed into emeraldine base (insulator/semi conductive form) by soaking in ammonium hydroxide for 3 hr. And then The emeraldine base of PANi was treated with five different acids which are hydrochloric acid (HCl), sulfuric acid (H_2SO_4), phosphoric acid (H_3PO_4), *p*-toluenesulfonic acid (TSA) and dodecyl benzene sulphonic acid (DBSA) at various concentrations of 0.1, 0.075, 0.05, 0.025 and 0.01M overnight.

4.2.1 Electrochemical synthesis of polyaniline

The deposited-PANi on interdigitated substrate was a prepared by electro-deposition of 0.1 M aniline monomer in 1M aqueous sulfuric solution at sweeping potential in the range of -0.3-1.0 V at 50 mV/s with 10 scan of cyclic voltammetry relative to the silver reference electrode and platinum counter electrode. The working electrode is interdigitated electrode sensor substrate consisting of gold pattern coating on printed wire board. The overlap electrode length was 25 mm and the insulating gap was 10 μm .

The cyclic voltammograms record was monitored during electro-polymerization, as shown in Figure 4.9. The radical cations were formed through oxidation as polaron state of PANi at 0.1-0.3 V. The oxidation at 0.5-0.6 and 0.8-1.0 V indicated further oxidation with the formation of diradical dications of bipolaron

state of PANi. The reductive peak in reverse direction at 0.4-0.6 and -0.1-0.2 V revealed reduction of polaron state as redox reactions of dimers, oligomers, and the degradation products such as p-aminophenol and quinoneimine [88].

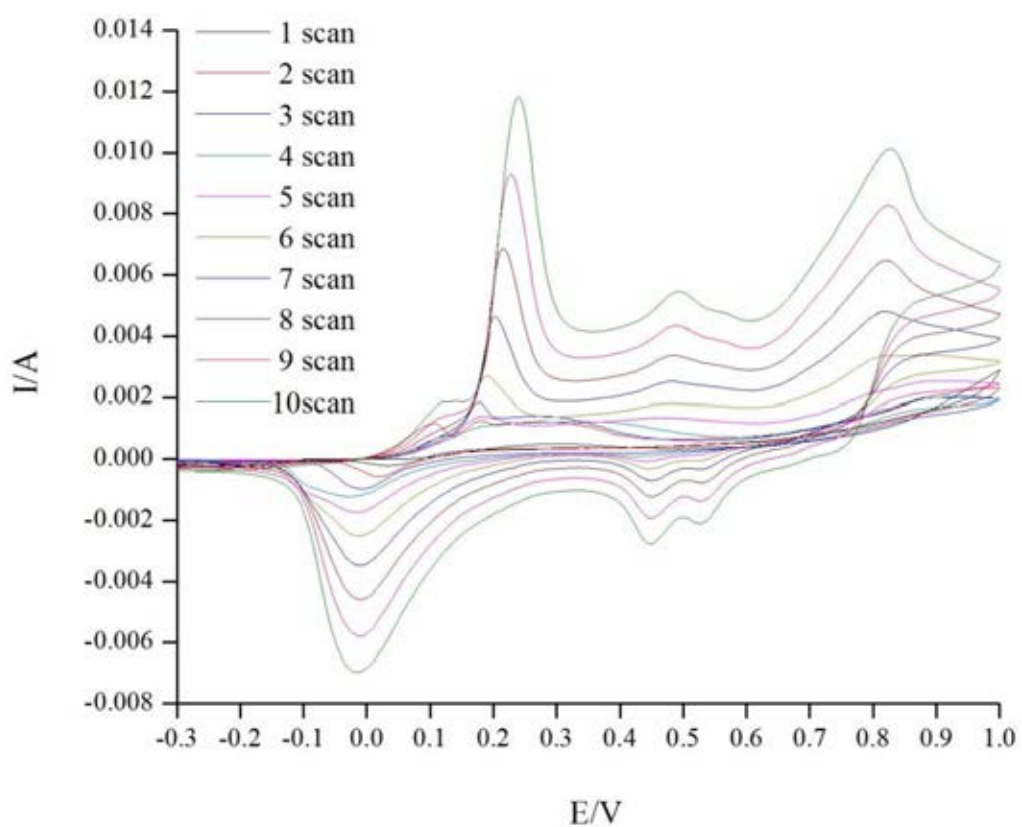


Figure 4.9 Cyclic voltammograms of polyaniline film growth at scanning rate of 50 mV/Sec with varying number of potential scan

4.2.2 Characterization of emeraldine salt forms of PANi

4.2.2.1 UV-Visible spectral characterization of PANi and doped PANi

The UV-Vis absorption was used to illustrate the optical properties of conductive polyaniline in term of absorption wavelength. The chemical properties of deposited PANi were modified by doping process. The emeraldine salt form of PANi-H₂SO₄ was turned into emeraldine base by soaking in 0.1 M ammonium hydroxide for 3 hours. After that, the emeraldine base of PANi was treated with five different acids (e.g. hydrochloric acid (HCl), sulfuric acid (H₂SO₄), phosphoric acid (H₃PO₄), *p*-toluenesulfonic acid (*p*-TSA), and dodecyl benzene sulphonic acid(DBSA) at various concentrations of 0.1, 0.075, 0.05, 0.025 and 0.01M overnight.

For UV-Vis experiment, the samples were prepared at concentration 0.1g/l in N-methyl-2-pyrrolidone. The UV-Vis absorption spectrum of solution undoped PANi (emeraldine base) was presented in Figure 4.10. As seen, the characteristic bands of undoped PANi were observed at 325 and 640 nm due to the π - π^* transition of benzenoid ring and the excitation absorption of quinoid ring.

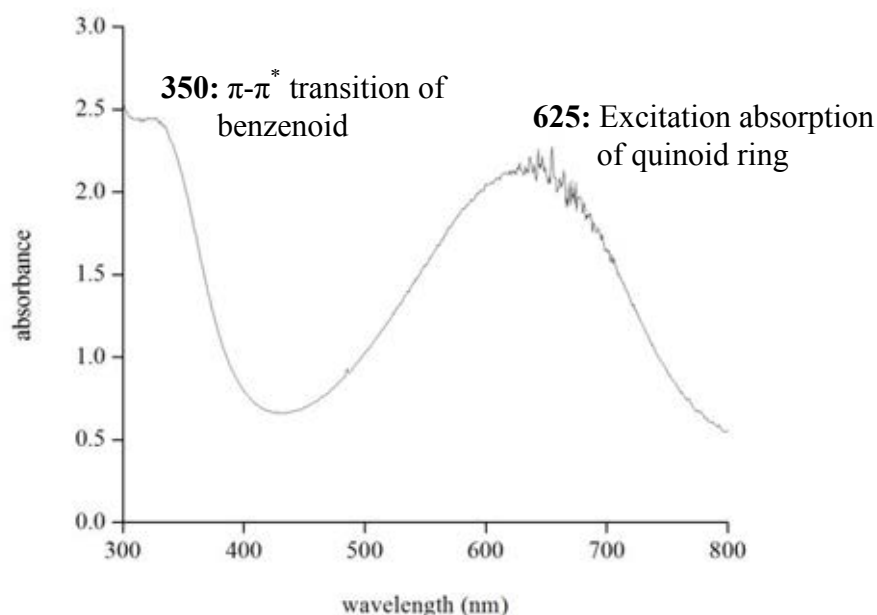


Figure 4.10 UV-Vis absorption spectrum of solution undoped PANi solution

The effect of acid dopant types and acid concentration on the optical properties was investigated by doping emeraldine base with different acid dopant types and concentrations. Figure 4.11-4.16 showed the UV-Vis spectra of polyaniline emeraldine base doped with different acid dopants; hydrochloric acid (HCl), sulfuric acid (H₂SO₄), phosphoric acid (H₃PO₄), *p*-toluenesulfonic acid (*p*-TSA) and dodecyl benzene sulphonic acid (DBSA) at various concentrations at 0.1, 0.075, 0.05, 0.025 and 0.01M.

The characteristic optical property of PANi doped with all different acids showed similarly significant changes related to acid concentration. As seen in Figure 4.11-4.15, at lower acid doping concentration, the characteristic bands of PANi doped were observed at 325 and 640 nm. The increasing of acid doping concentration led to these shift of bands to lower intensity, while the curve at 825 nm was slightly shifted to higher intensity.

The characteristic optical property with increasing concentration of acid dopants can be implied that at lower acid doping concentration, the π - π^* transition of benzenoid ring and the excitation absorption of quinoid ring are the main characteristic structure in molecule. The increasing acid concentration led to the protonation of nitrogen atom on imine. The quinoid ring of PANi was converted to semiquinoid radical cations as the presence of polaron/bipolaron states of emeraldine salts form of polyaniline. This result leads to a decrease in the intensity of excitation absorption peak at 640 nm and generates new absorption peaks at 825 nm. This new peak confirmed that of presence of polaron/bipolaron state and indicated the conducting behavior of polyaniline (Chen S.A. et al., 1995 [89]).

In addition, this behavior can be clearly observed in strong acid dopants such as sulfuric acid and phosphoric acid as seen in Figure 4.12 and 4.13, respectively. The sulfuric acid and phosphoric acid dopants revealed higher efficiency to protonate emeraldine base of PANi due to high efficient dissociation ability of acid [91]. The shift of absorbance band at 825 nm to higher absorbance was resulted from the higher efficiencies to protonate H⁺ on polymer chain. These results confirmed a changing structure of quinoid ring emeraldine base to polaron/bipolaron states of emeraldine salt.

Table 4.3 The assignment for UV-Visible absorption peaks of undoped and doped polyaniline

Wavelength (nm)	Assignment
325	π - π^* transition of benzenoid ring
640	π - π^* transition of quinoid ring
825	Polaron state

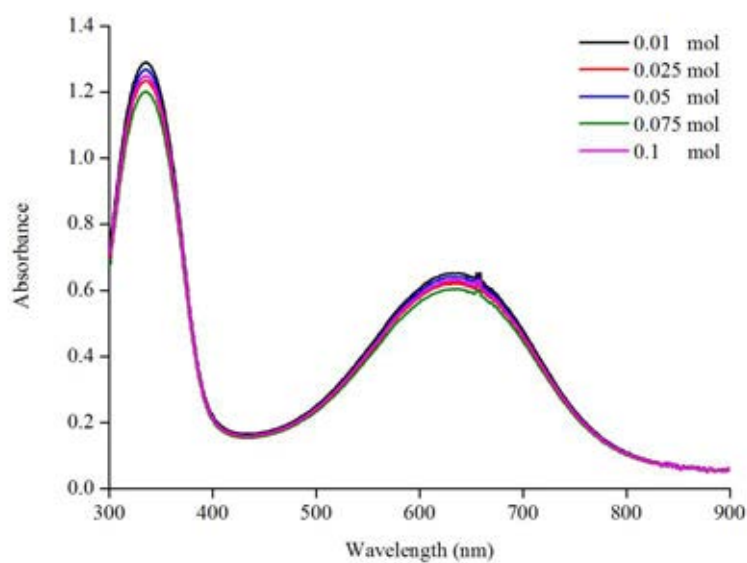


Figure 4.11 UV-spectrum of PANi doped with HCl at different concentrations

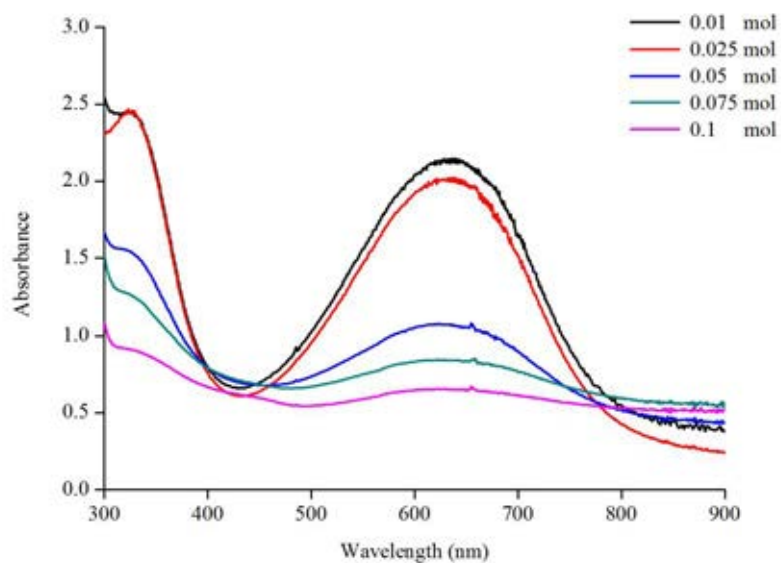


Figure 4.12 UV-spectrum of PANi doped with H₂SO₄ at different concentrations

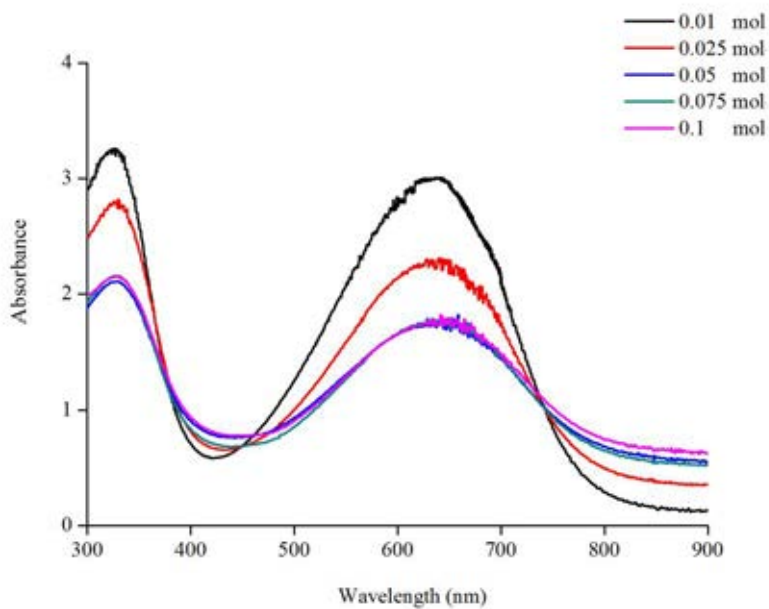


Figure 4.13 UV-spectrum of PANi doped with H₃PO₄ at different concentrations

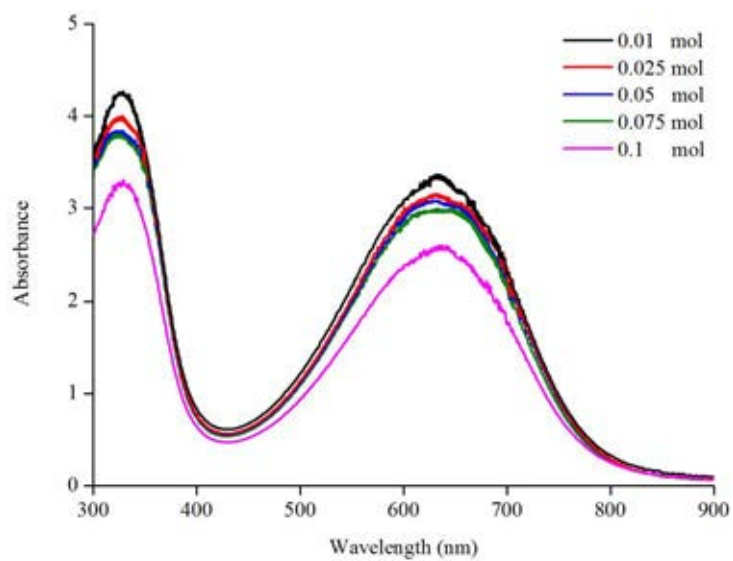


Figure 4.14 UV-spectrum of PANi doped with DBSA at different concentrations

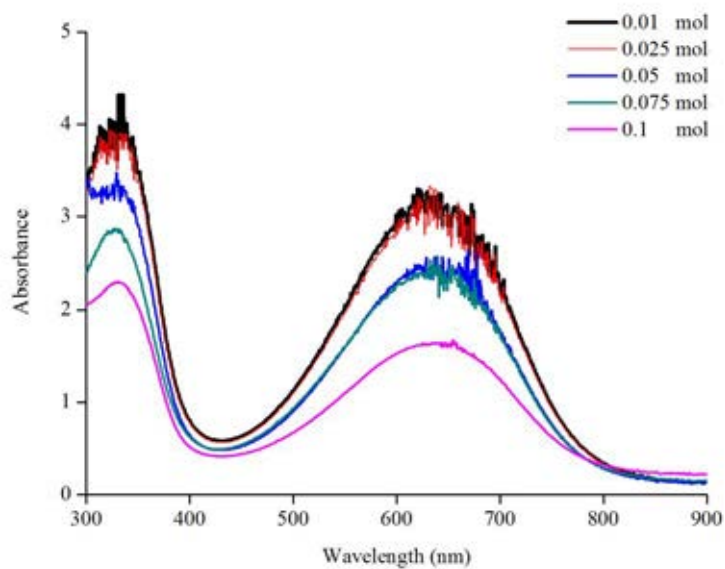


Figure 4.15 UV-spectrum of PANi doped with TSA at different concentrations

4.2.2.2 Fourier transforms infrared spectroscopy characterization of PANi and doped PANi

Functional groups of undoped PANi and doped-PANi were investigated by FT-IR technique. The assignments for FT-IR vibration of undoped PANi are given in Table 4.4.

Table 4.4 Assignment for IR bands of polyaniline emeraldine base

Major IR Bands of Components	
Wavenumber (cm^{-1})	Assignment and Remarks
1560	C=N stretching of quinoid ring
1472	C-H stretching of benzenoid ring
1300	C-N stretching of benzenoid ring
1081	C-H bending of quinoid ring
803	C-H out of plane of aromatic ring

The FTIR spectrum of undoped polyaniline is showed in Figure. 4.16. The spectrum of undoped polyaniline exhibited five important transmittance bands. The first peak at 1560 cm^{-1} corresponded to stretching peak of C=N of quinoid ring. The peak at 1472 cm^{-1} was due to the C-H stretching of benzenoid ring. The characteristic peak at 1300 cm^{-1} can be assigned to the C-N stretching of benzenoid ring. The presence of in-plane C-H bending of quinoid ring and C-H out-of-plane in aromatic ring can be seen by the intensity at 1081 and 803 cm^{-1} , respectively.

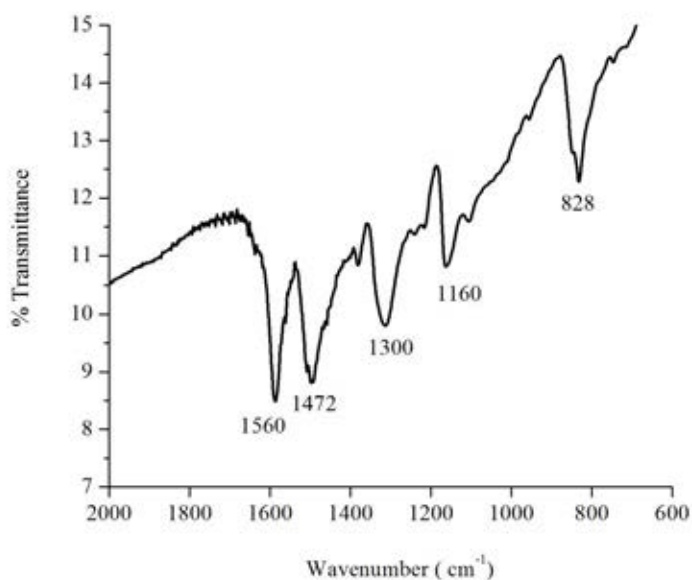


Figure 4.16 The FT-IR spectrum of undoped polyaniline (Emeraldine base)

The emeraldine base of PANi was doped with five different acids type. The characteristic peak of anion acid on doped PANi with different types of acid was illustrated in Figure 4.17-4.21 and Table 4.5.

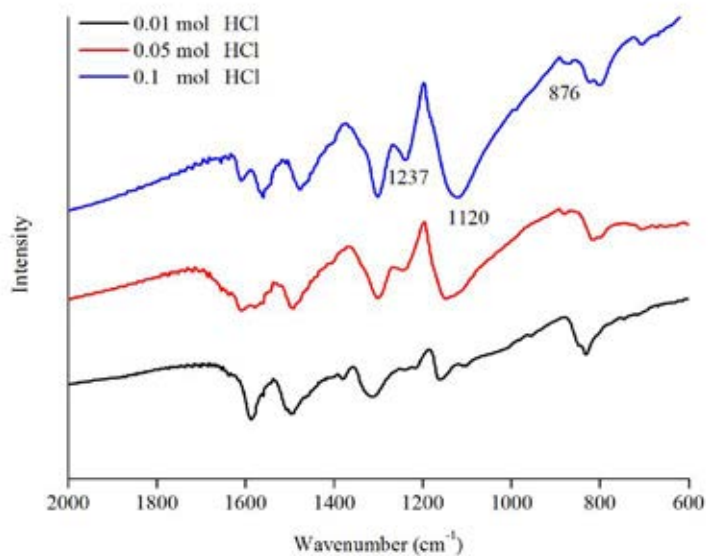


Figure 4.17 FT-IR spectrum of PANi-HCl at different acid concentration

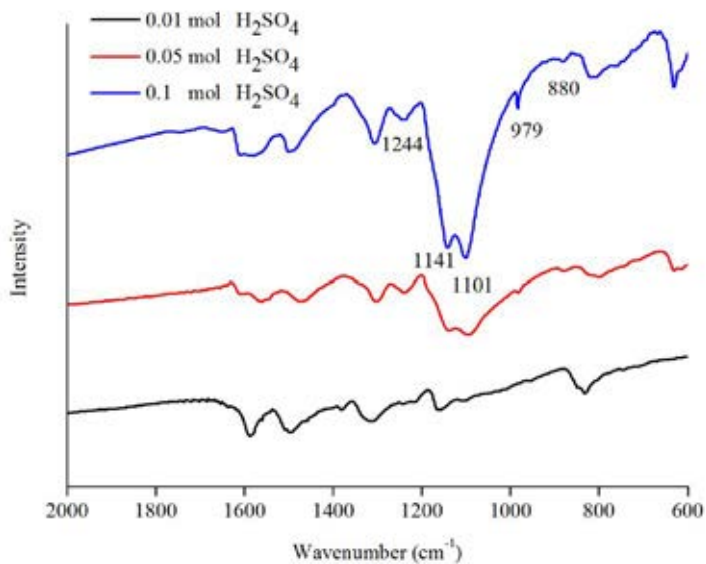


Figure 4.18 FT-IR spectrum of PANi-H₂SO₄ at different acid concentration

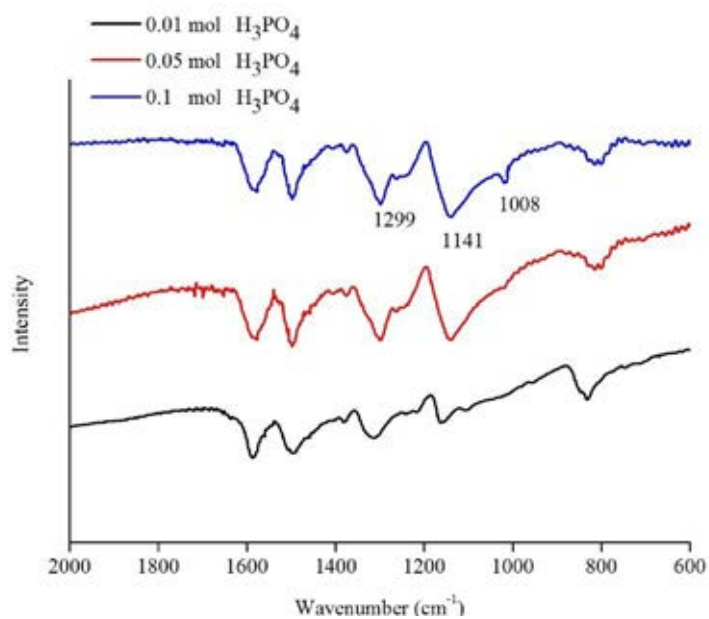


Figure 4.19 FT-IR spectrum of PANi-H₃PO₄ at different acid concentration

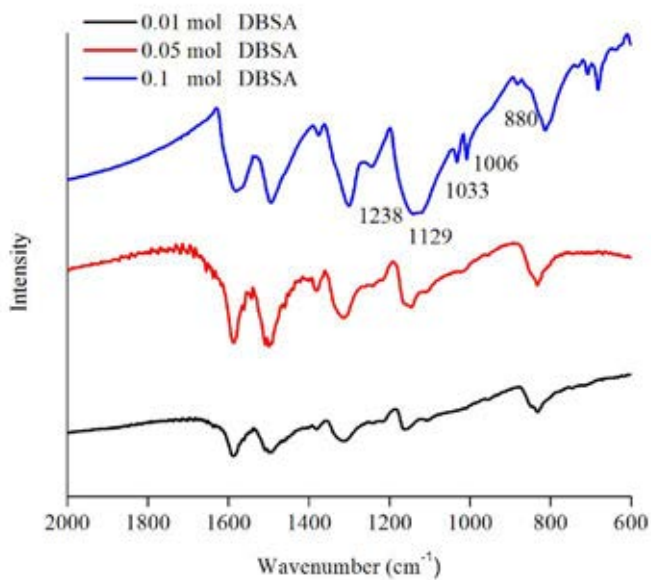


Figure 4.20 FT-IR spectrum of PANi-DBSA at different acid concentration

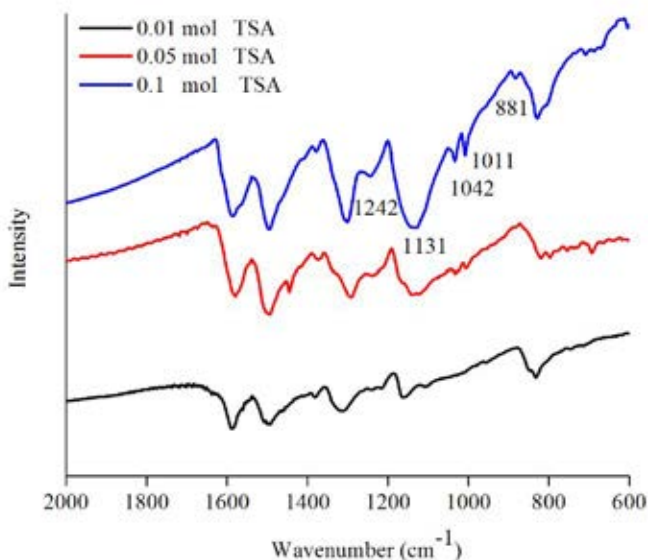


Figure 4.21 FT-IR spectrum of PANi-TSA at different acid concentration

The FTIR spectra of doped PANi at different HCl concentrations were shown in Figure 4.17. The FT-IR spectrum of 0.01 mol HCl doped PANi showed similar characteristic to undoped PANi due to low acid concentration doping, which its efficiency was not enough to protonate H^+ on PANi molecule. At 0.01 mol of HCl doping, the spectrum of PANi showed five important transmittance bands at 1588, 1497, 1315, 1165 and 829 cm^{-1} , which were corresponded to C=N stretching of quinoid ring, C-H stretching of benzenoid ring, C-N stretching of benzenoid ring, C-H in-plane bending of quinoid ring and C-H out-of-plane in aromatic ring, respectively.

Obviously, as the concentration of HCl doping increased to 0.05 and 0.1 mol, the new bands were appeared at 1237, 1120, and 876 cm^{-1} . The appearance of these peaks increased with increasing of acid concentration due to the high level of acid protonation. The presence of new peaks at 1237 and 1120 cm^{-1} indicated the broken symmetry mode of quinoid structure to benzenoid structure as a presence of C-N stretching of benzenoid ring. The peak at 1120 cm^{-1} can be assigned to Cl^-

substitution [55]. The appearance of band at 876 cm^{-1} resulted from more C-H stretching of aromatic ring structure.

The FTIR spectra of doped PANi at H_2SO_4 different concentrations were presented in Figure 4.18. The FT-IR spectrum of 0.01 mol PANi- H_2SO_4 showed five important transmittance bands at 1585, 1490, 1310, 1160 and 830 cm^{-1} similar to undoped PANi due to low efficiency to protonate H^+ at low acid concentration. At higher H_2SO_4 concentration (0.05 and 0.1 mol), the news bands were appeared at 1240, 1141, 1101, 979 and 877 cm^{-1} . The band at 1240, 1141 and 1101 cm^{-1} indicated the broken symmetry mode of quinoid structure to benzenoid structure as a presence of C-N stretching of benzenoid ring. The presence of new peak at 979 cm^{-1} of PANi doped with H_2SO_4 can be designated as SO_4^{2-} on PANi, while the band at 877 cm^{-1} resulted from C-H stretching of aromatic ring structure [92].

The FTIR spectra of doped PANi at different H_3PO_4 concentrations were displayed in Figure 4.19. At 0.01 mol of H_3PO_4 doping, the FTIR spectrum showed similar result with the undoped PANi and PANi doped with 0.01 mol HCl and H_2SO_4 . At higher H_3PO_4 concentration (0.05 and 0.1 mol), the news bands were appeared at 1299, 1141, and 1108 cm^{-1} . The presence at 1299 and 1119 cm^{-1} indicated the broken symmetry mode of quinoid structure to benzenoid structure as a presence of C-N stretching of benzenoid ring. The peak around 1119 cm^{-1} revealed vibration mode of P=O anion on PANi molecule [92, 93].

The FTIR spectra of PANi doped with DBSA at different concentrations were exhibited in Figure 4.20. At 0.01 mole PANi-DBSA, the FTIR spectrum showed similar result with the undoped and other acids doped PANi at 0.01 mol. As the concentration of DBSA doping increased to 0.05 and 0.1 mol, the presence at 1238 and 1129 cm^{-1} indicated a presence of C-N stretching of benzenoid ring. The band at 877 cm^{-1} was resulted from C-H stretching of aromatic ring structure. The presence band at 1033 and 1006 cm^{-1} revealed S=O stretching of sulphinic ester anion and sulphoxide anion on PANi, respectively [92, 93].

The FTIR spectra of PANi doped with TSA were shown in Figure 4.21. The designation of its FTIR spectra were similar to those of PANi-DBSA due to the similar structure of acid dope. The S=O stretching of sulphinic ester anion and sulphoxide anion on PANi was observed at 1042 and 1011, respectively.

Table 4.5 Assignment for IR bands of polyaniline emeraldine salt with different acid dopants

Major IR Bands of Components	
Wavenumber (cm ⁻¹)	Assignment and Remarks
Emeraldine salt of polyaniline	
1590	C=N stretching of quinoid ring
1495	C-H stretching of benzenoid ring
1299,1237	C-N stretching of benzenoid ring
874,804	C-H bending of aromatic ring
polyaniline doped with HCl	
1120	Cl ⁻
polyaniline doped with H ₂ SO ₄	
979	SO ₄ ²⁻
polyaniline doped with H ₃ PO ₄	
1008	PO ₄ ³⁻
polyaniline doped with TSA ,(DBSA)	
1033,(1072)	sulphinic ester anion
1006,(1011)	sulphoxide anion

4.2.2.3 Morphological characterization of the deposited PANi with different acid dopants

The SEM images were used to investigate the morphology of undoped PANi and doped PANi. The morphology of deposited PANi and undoped PANi on interdigitated gold substrate was shown in Figure 4.22. The deposited PANi (at 10 CV) revealed a formatted three-dimensional nanofibril network structure as shown in Figure 4.22(a). Likewise, the undoped PANi also showed similar morphology as nanofibril structure Figure 4.22(b). It can then be concluded that the de-doped PANi with ammonium hydroxide had no effect on morphology of PANi structure.

The effects of different types and concentrations of acid dope on morphology of PANi were investigated as show in Figure 4.23-4.27. Clearly, the type and concentration of acid dope had strong effect on the morphology of PANi. In case of using HCl, the morphology of PANi-HCl revealed fibril network structure when doping at concentration 0.01 mol. The increasing of HCl acid concentration, however, led to an agglomeration of nanofibril on substrate as seen in Figure 4.23(b-d). This result may be attributed to the large Cl^- group in HCl incorporated with PANi chain.

On the other hand, the doping PANi with H_2SO_4 and H_3PO_4 revealed fibril network structure at all concentrations of acid doping as shown in Figure 4.24-4.25. It is cleared that both of SO_4^{2-} and PO_4^{3-} anion groups had no influence on the morphology of PANi molecule.

Similar to PANi doped with HCl, the SEM image of PANi doped with DBSA showed nanofibril network structure at 0.01 mol of DBSA (as shown in Figure 4.26(a)). The increase of DBSA doping concentration also led to an agglomeration of nanofibril structure. Meanwhile, in case of TSA doped PANi (as seen in Figure 4.27), the morphology of PANi-TSA revealed fibril network structure at TSA doping concentration of 0.01, 0.025 and 0.05 mol. Then, the agglomerated nanofibril PANi was observed at TSA doping concentration of 0.75 and 0.1 mole. The higher agglomeration of nanofibril PANi was observed in PANi-DBSA than in PANi-TSA, which may be resulted from long chain of aliphatic group in sulphinic ester anion of DBSA incorporated with PANi.

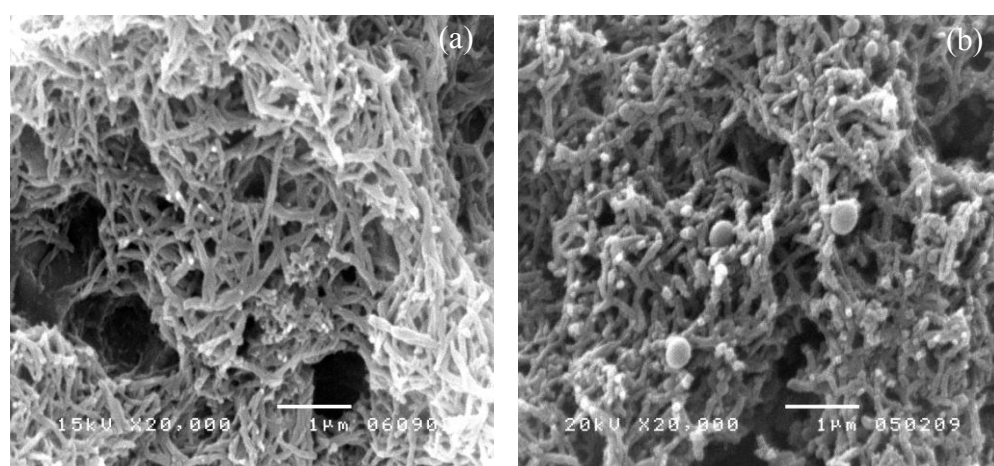


Figure 4.22 SEM images of PANi : (a) PANi prepared by cyclic voltammetry after 10 scans (b) PANi prepared by cyclic voltammetry after 10 scans and de-doped with 0.1 M NH_4OH

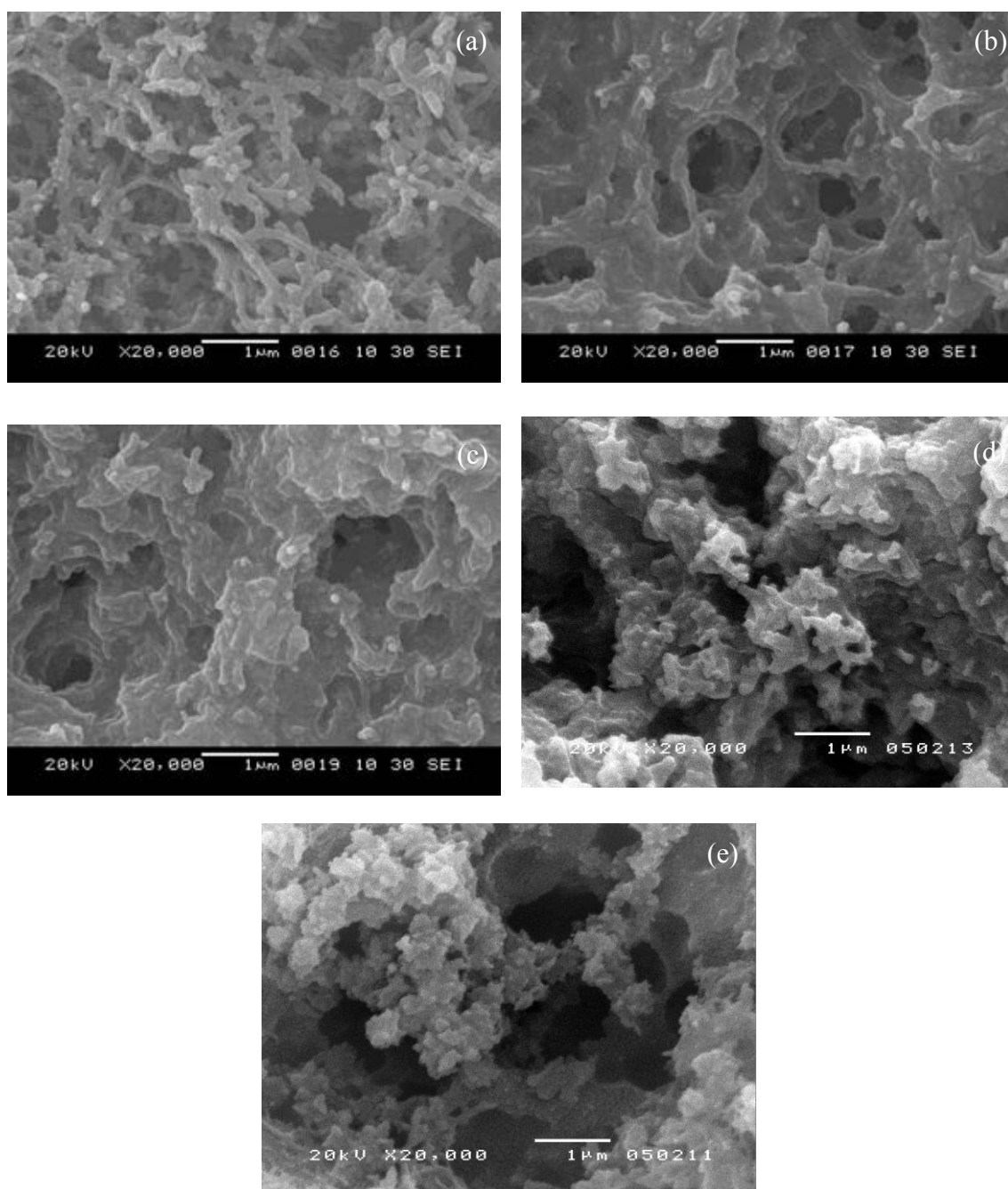


Figure 4.23 SEM images of HCl-doped PANi at different concentrations: (a) 0.01 mol (b) 0.025 mol (c) 0.05 mol (d) 0.075 mol (e) 0.1 mol

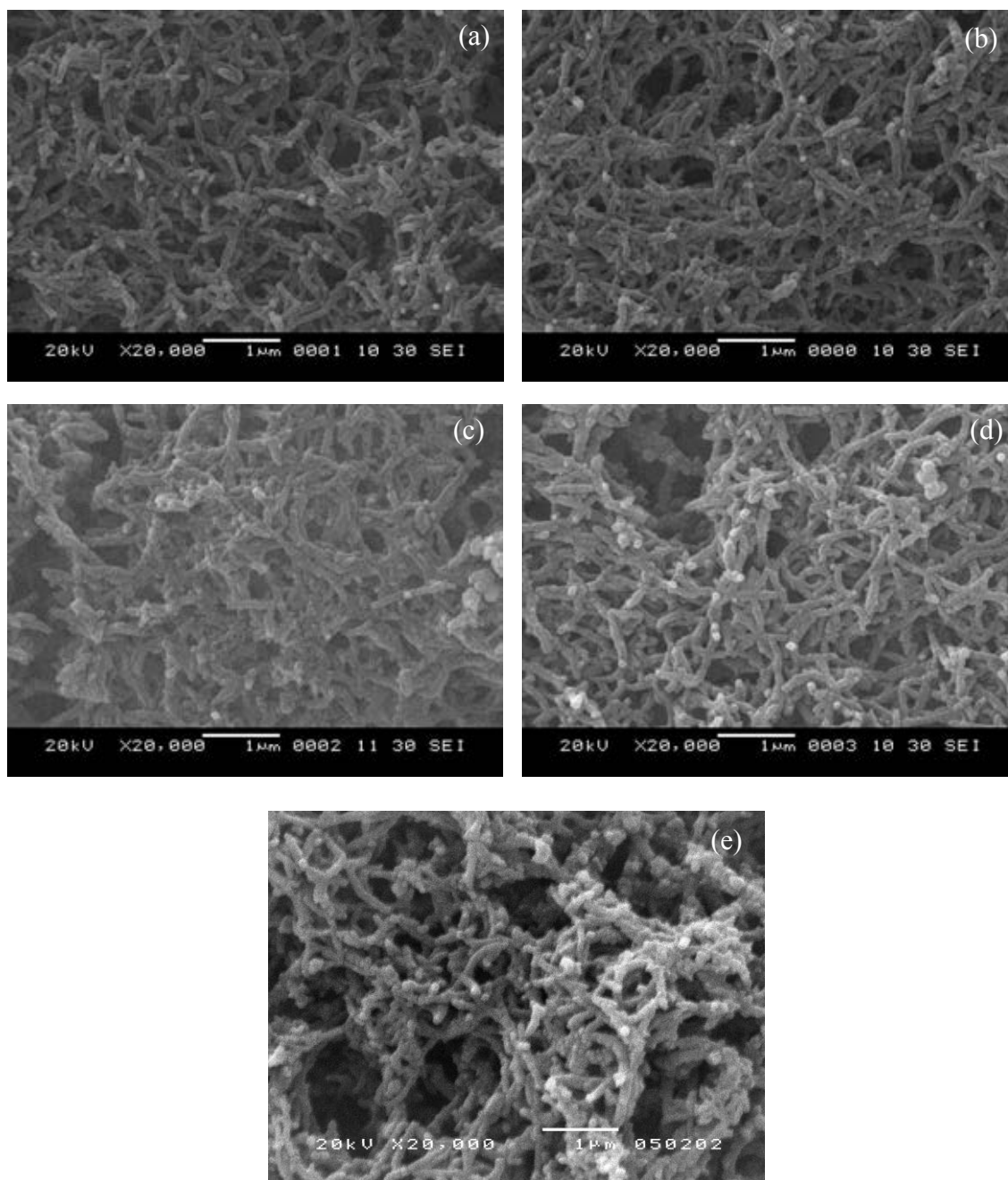


Figure 4.24 SEM images of H₂SO₄-doped PANI at different concentrations:
(a) 0.01 mol (b) 0.025 mol (c) 0.05 mol (d) 0.075 mol (e) 0.1 mol

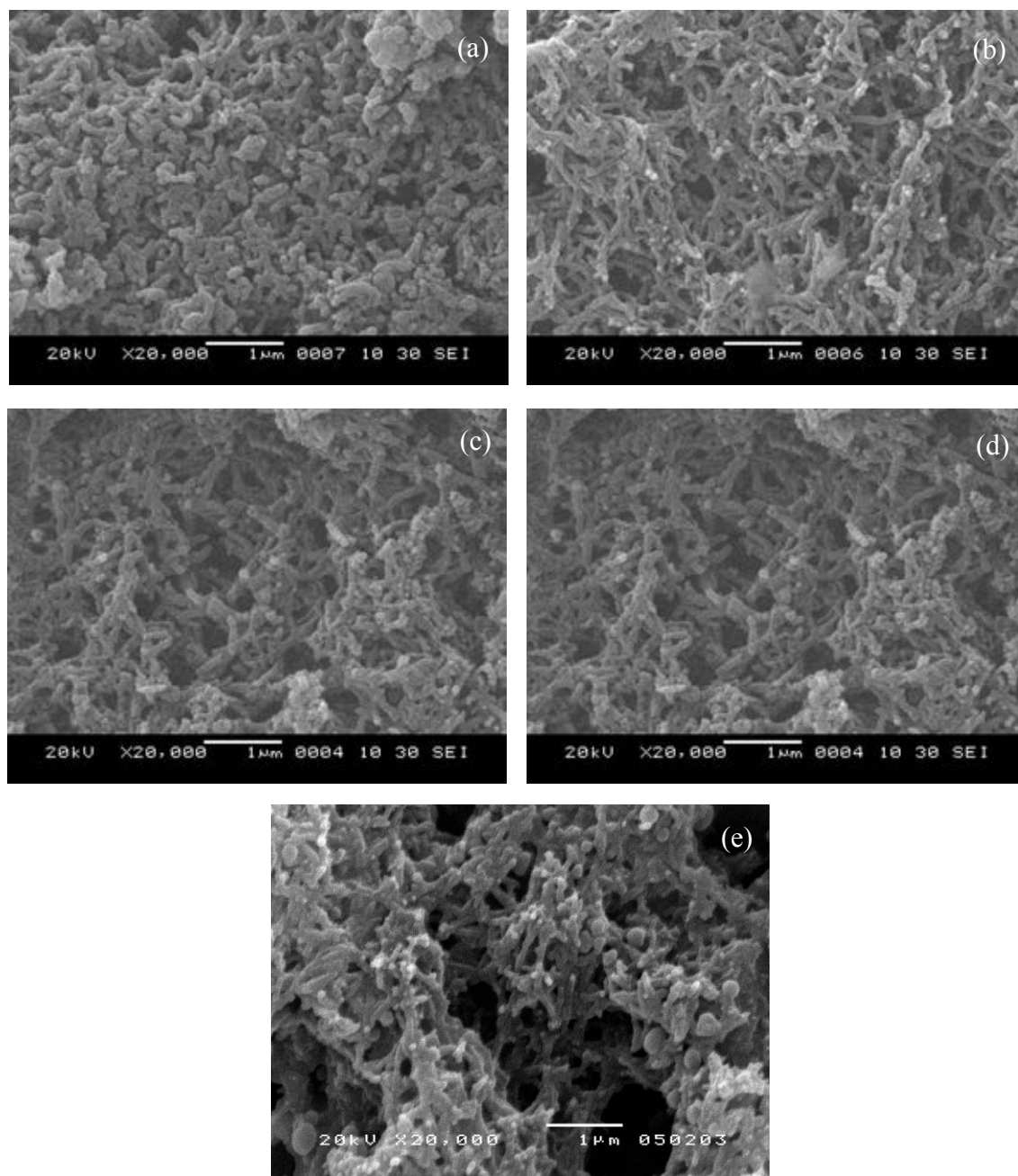


Figure 4.25 SEM images of H_3PO_4 -doped PANi at different concentrations: (a) 0.01 mol (b) 0.025 mol (c) 0.05 mol (d) 0.075 mol (e) 0.1 mol

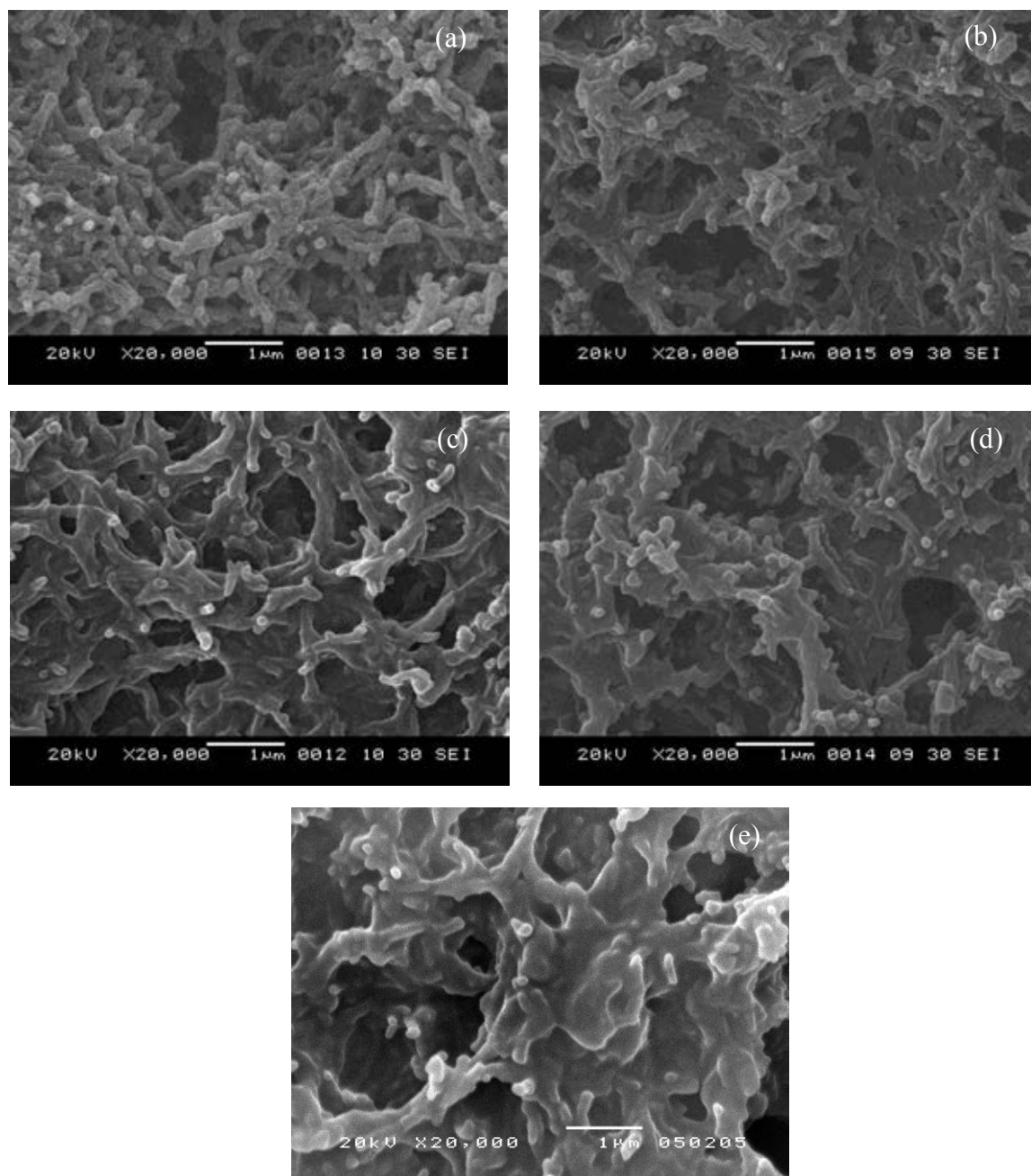


Figure 4.26 SEM image of DBSA-doped PANi at different concentrations: (a) 0.01 mol (b) 0.025 mol (c) 0.05 mol (d) 0.075 mol (e) 0.1 mol

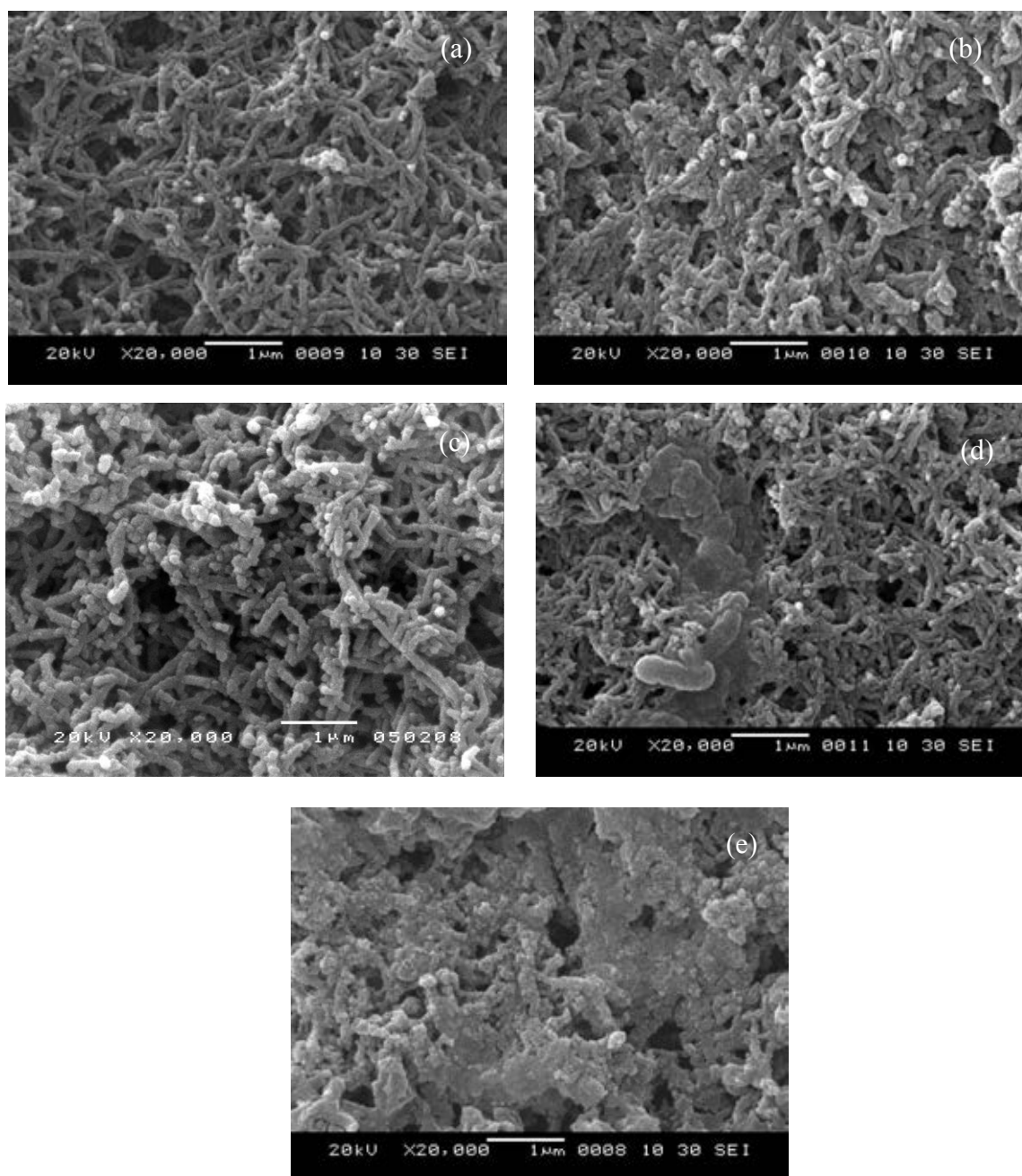


Figure 4.27 SEM image of TSA-doped PANi at different concentrations: (a) 0.01 mol (b) 0.025 mol (c) 0.05 mol (d) 0.075 mol (e) 0.1 mol

4.2.2.4 Thermo gravimetric Analysis (TGA)

Thermogravimetric analysis of undoped PANi and doped PANi was investigated under nitrogen atmosphere at $10\text{ }^{\circ}\text{C min}^{-1}$ from $50 - 600\text{ }^{\circ}\text{C}$. TGA curves of undoped and doped PANi are showed in Figure 4.28 and 4.29.

The polyaniline emeraldine base of undoped PANi of revealed a typical three-steps weight loss. The first step can be attributed to the loss of water molecules at temperature up to $100\text{ }^{\circ}\text{C}$. After the initial weight loss, the TGA thermogram revealed the loss of low molecular weight oligomer at $250\text{ }^{\circ}\text{C}$. A dramatic weight loss of the thrid-order transition temperature began approximately at $480\text{ }^{\circ}\text{C}$ due to the skeleton of polyaniline backbone started to decompose. These results are in good agreement to the work of Lili Ding et al.,1999 [94].

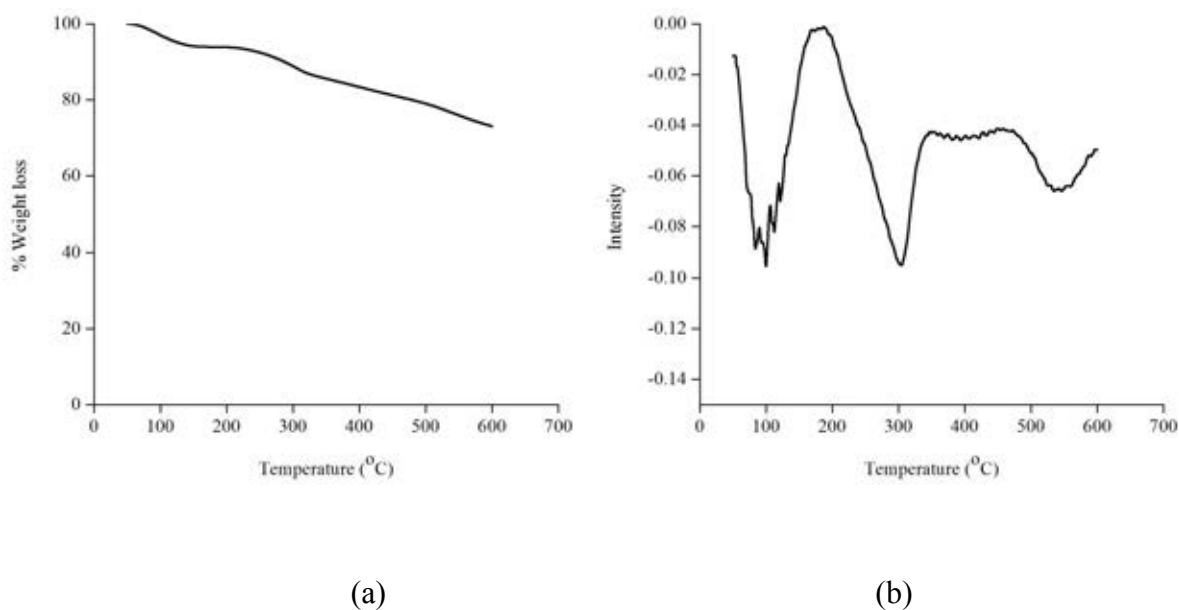


Figure 4.28 TGA thermogram of polyaniline emeraldine base: (a) (undoped PANi) and (b) first order derivative of thermogram of polyaniline emeraldine base

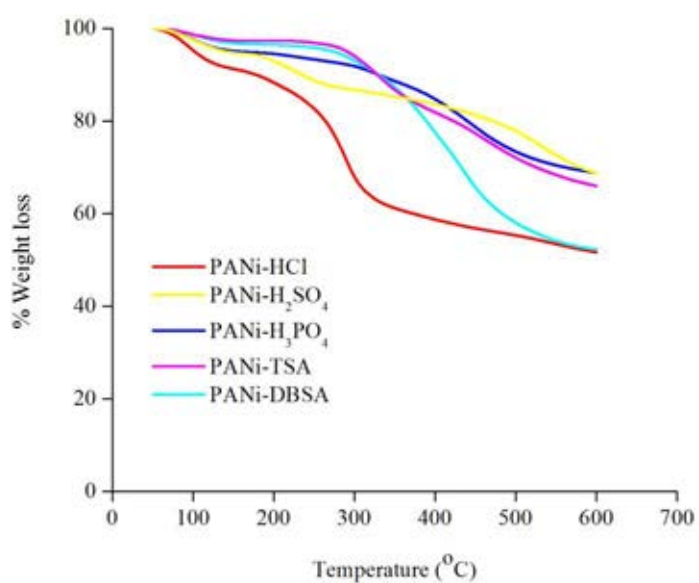
Figure 4.29 showed TGA thermogram of doped PANi (emeraldine base salt) with HCl, H₂SO₄, H₃PO₄, DBSA and TSA. Comparing with polyaniline emeraldine base, thermal stability of all polyaniline emeraldine salt was significantly lowered than polyaniline emeraldine base particularly in term of residual weight.

It is cleared that the thermal stability of PANi was strongly dependent upon on the counter ions. In case of PANi-H₃PO₄, the first 5% of weight loss associated with water at the temperature between 50 and 100 °C. The large second step of thermal degradation transition between 200 and 600 °C was due to the loss of acid dopant and the decomposition of polymer backbone. The PANi-H₃PO₄ shows residual weight 70% of its original weight after 600 °C. This result may be attributed to come from the higher boiling point of H₃PO₄ which is inert towards oxidation and reduction. Another reason is the formation of phosphoamide that occurring from benzene segment of reacted with H₃PO₄ that can stabilize PANi chain.

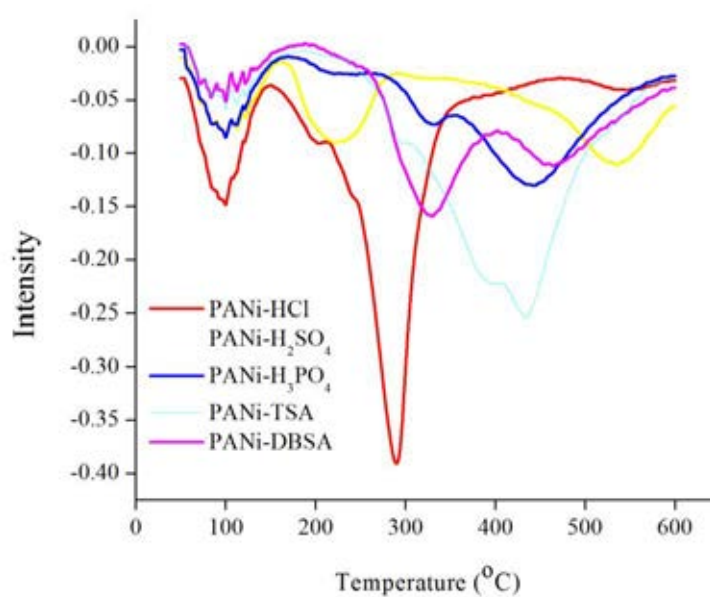
For PANi-H₂SO₄, its thermogram also showed three steps of weight loss. Similar to PANi- H₃PO₄ the first step of weight loss (5%), occurring between 50 and 100 °C was due to water decomposition, followed by the loss of acid dopant at 168 °C. The third step of weight loss observed at 400 °C was resulted from the decomposition of PANi backbone chain. . The PANi-H₂SO₄ shows residual weight 70% of its original weight after 600 °C. This result may be attributed to come from the higher boiling point of H₂SO₄ as similar result with PANi-H₃PO₄.

For PANi-HCl, its thermogram showed three separate decomposition temperatures. The first decomposition step exhibited about 8-10% weight loss at the temperature between 50 and 100 °C due to the water evaporation. Next, the loss of solvent was observed at the temperature between 180 and 300 °C. The third step of weight loss corresponded to the decomposition of PANi backbone chain began around 350°C and it showed residual weight 50% of its original weight after 600 °C.

In the case of PANi-DBSA and PANi-TSA, their thermograms shows of two step weight loss. The first TGA step showed 2-4% weight loss of water at temperature between 50-100 °C, followed by the loss of acid dopant at approximately 250 °C. The PANi-TSA showed higher thermal stability than PANi-DBSA in terms of % weight residue after 600 °C.



(a)



(b)

Figure 4.29 TGA thermogram of polyaniline emeraldine salt: (a) TGA of Doped PANi with HCl, H₂SO₄, H₃PO₄, DBSA, and TSA (b) first order derivative of thermogram of doped PANi

4.2.3 Ethylene gas detection of doped PANi via resistance measurement

The respond-recovery characteristics of doped PANi after 1 and 3 months aging with different acid dopant against various ethylene concentrations (i.e., 1000, 500, and 200 ppm) were showed in Figure 4.30-4.33. The respond-recovery characteristic of doped PANi after 3 month aging with different acid against ethylene concentration at 200, 100, 50, 20 and 10 ppm were showed in fig 4.34-4.36. The sensing magnitude of PANi after 1 month aging against ethylene concentration at 1000, 500, and 200 ppm were showed in fig 4.37. The sensing magnitude of PANi after 3 month aging against ethylene concentration at 200, 100, 50, 20, and 10 ppm were showed in fig 4.38.

After being exposed to ethylene gas, every sensors except PANi-HCl responded by undergoing a decrease in their resistance. The PANi-sensors recovered into baseline under nitrogen atmosphere. However, it can be observed that the baseline of PANi- sensor showed slight increase with constant rate under nitrogen atmosphere. These results were due to an expansion of compact PANi chain into linear form of PANi chain backbone. The lack of response for PANi-HCl against ethylene gas may be due to the large size of Cl⁻ atom on PANi molecule that disturbed the expansion of PANi chain. During the first month of aging, every sensors revealed good response against ethylene gas concentration as low as 200 ppm.

The doping PANi with H₂SO₄, H₃PO₄ and DBSA within the range of acid doping between 0.01-0.01 mol showed good response to detect ethylene gas as lowest concentration as 200 ppm. But in case of PANi-TSA, where the TSA concentration was higher than 0.05 mol, the sensor had no had not efficiency to detect ethylene gas, as displayed in Figure 4.33(e).

In addition, the concentration of acid had strongly affected on conductivity of PANi. The conductivity increased with increasing of acid doping concentration. It was cleared that that conductivity of PANi-sensor can be turned with acid concentration.

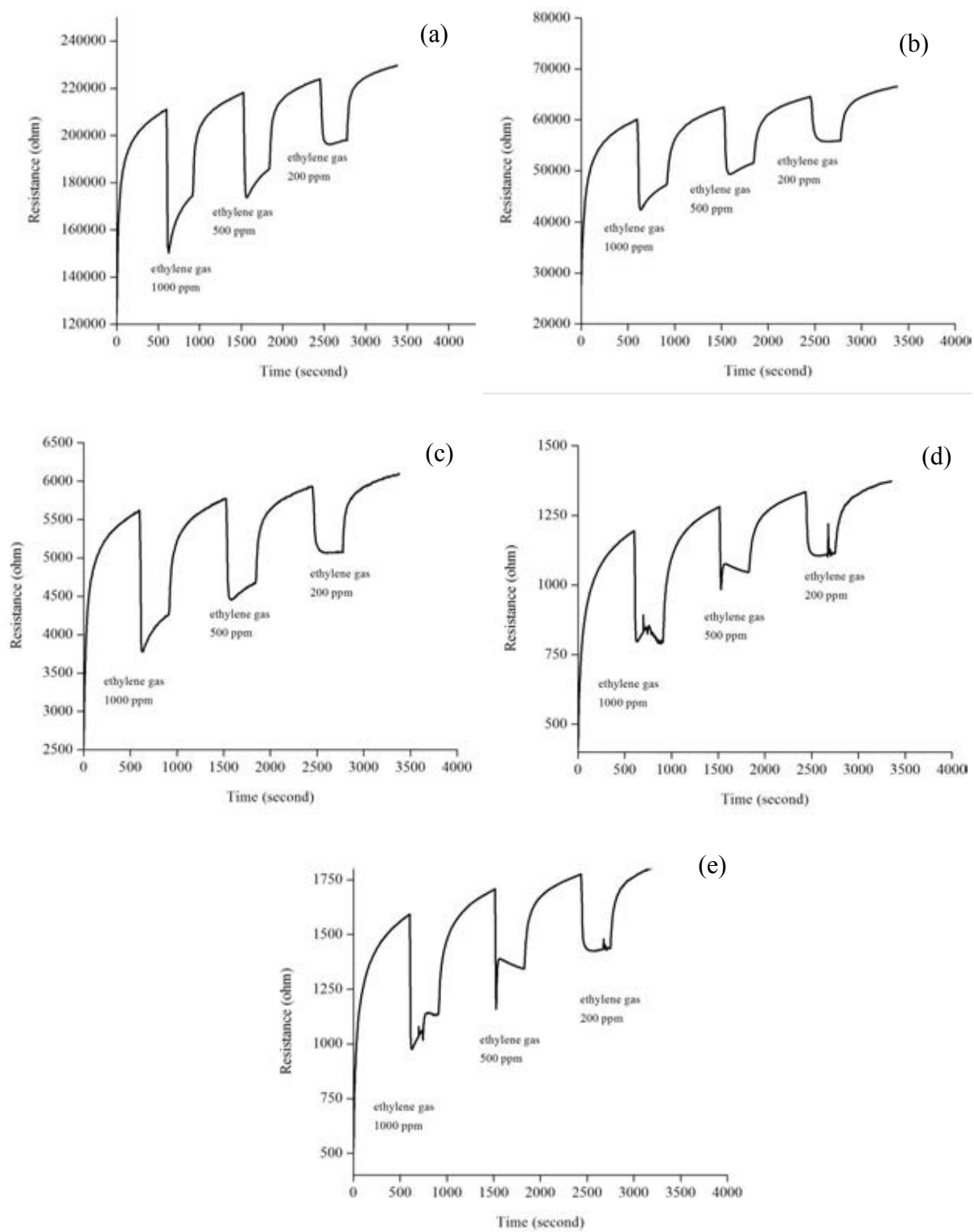


Figure 4.30 The resistance response behavior of the PANi-H₂SO₄ derived from different acid doping concentrations after 1 month: a) 0.01 mol, b) 0.025 mol, c) 0.05 mol, d) 0.075 mol and e) 0.1 mol

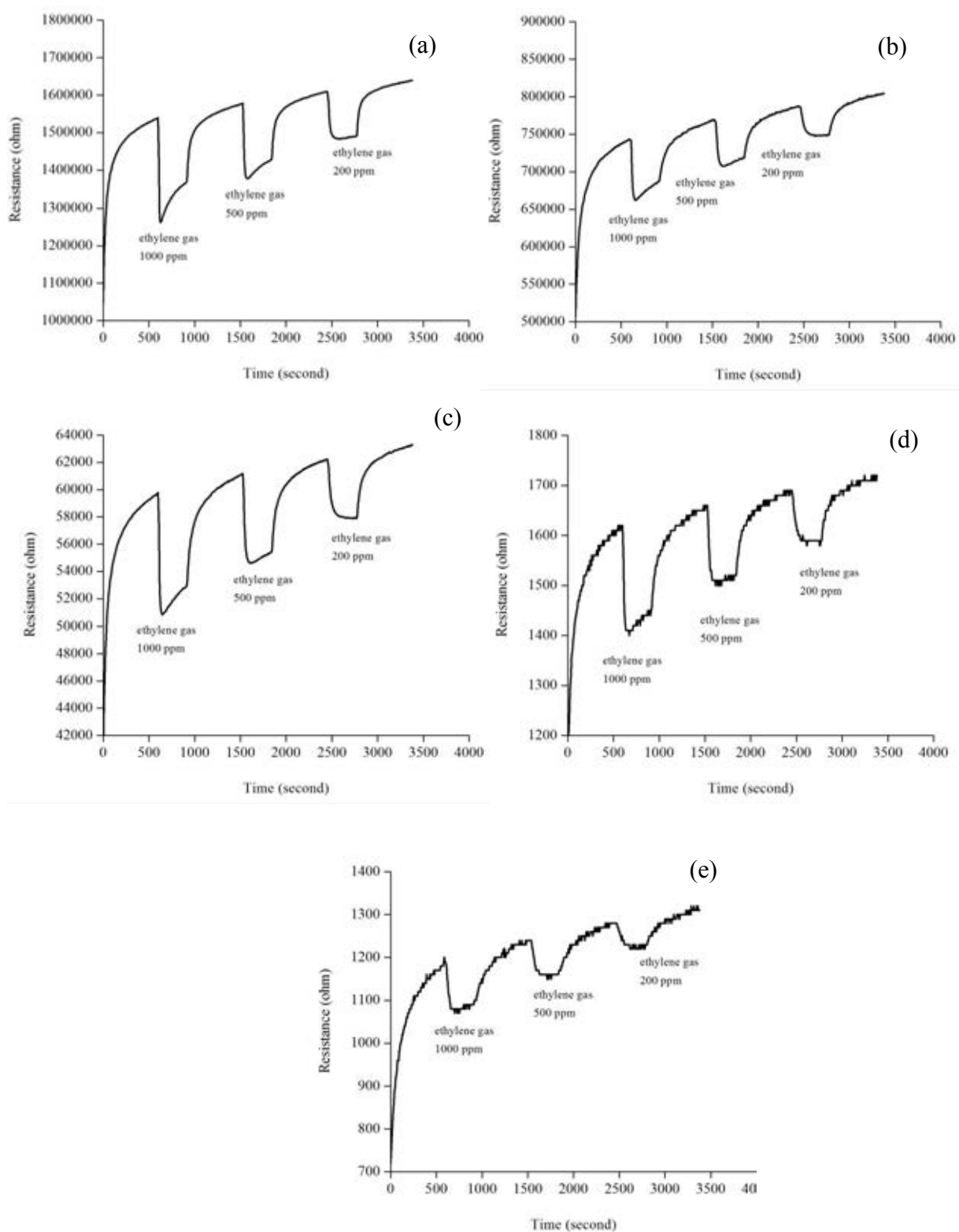


Figure 4.31 The resistance response behavior of PANi-H₃PO₄ derived from different acid doping concentrations after 1 month: a) 0.01 mol, b) 0.025 mol, c) 0.05 mol, d) 0.075 mol and e) 0.1 mol

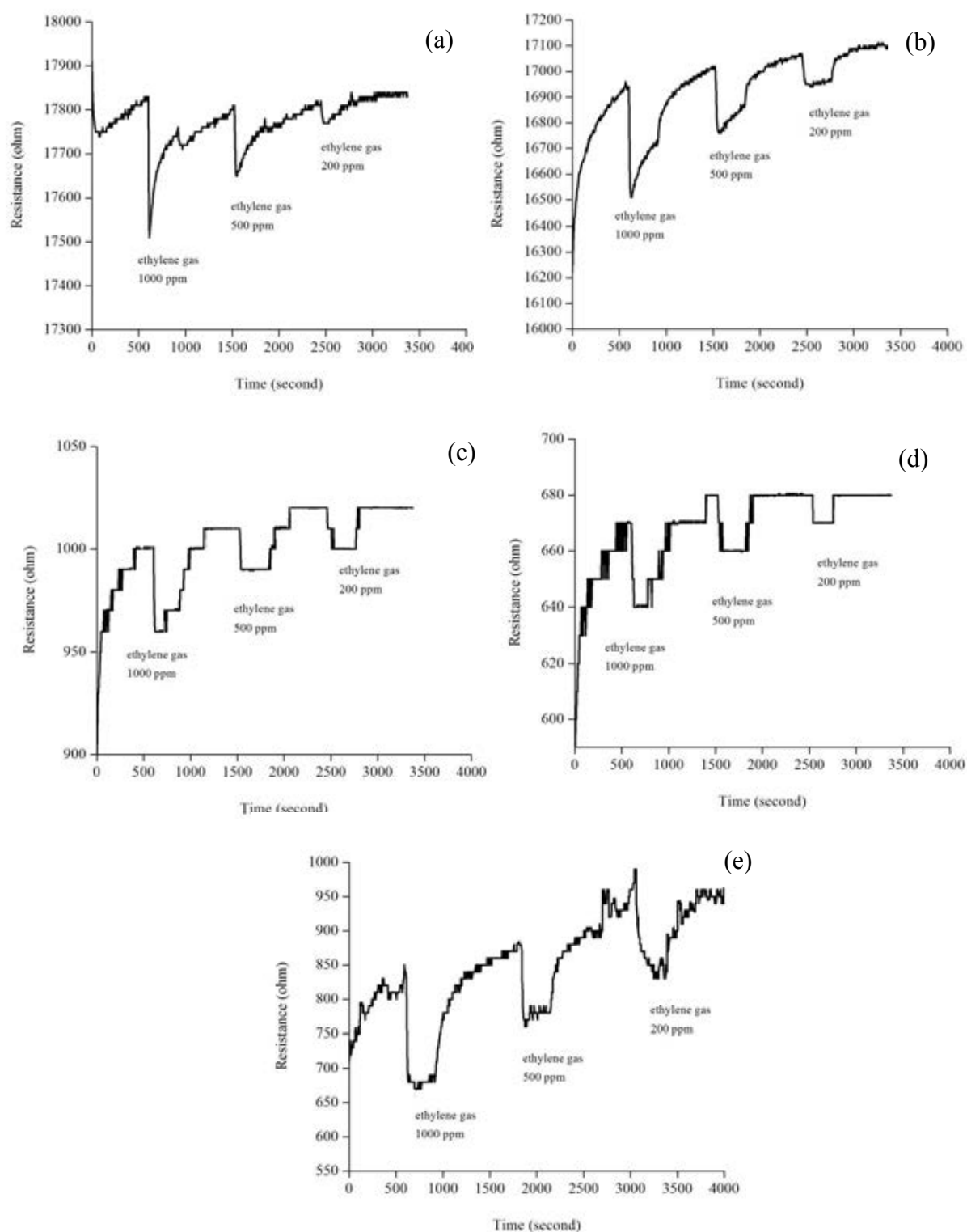


Figure 4.32 The resistance response behavior of PANi-DBSA derived from different acid doping concentrations after 1 month: a) 0.01 mol, b) 0.025 mol, c) 0.05 mol, d) 0.075 mol and e) 0.1 mol

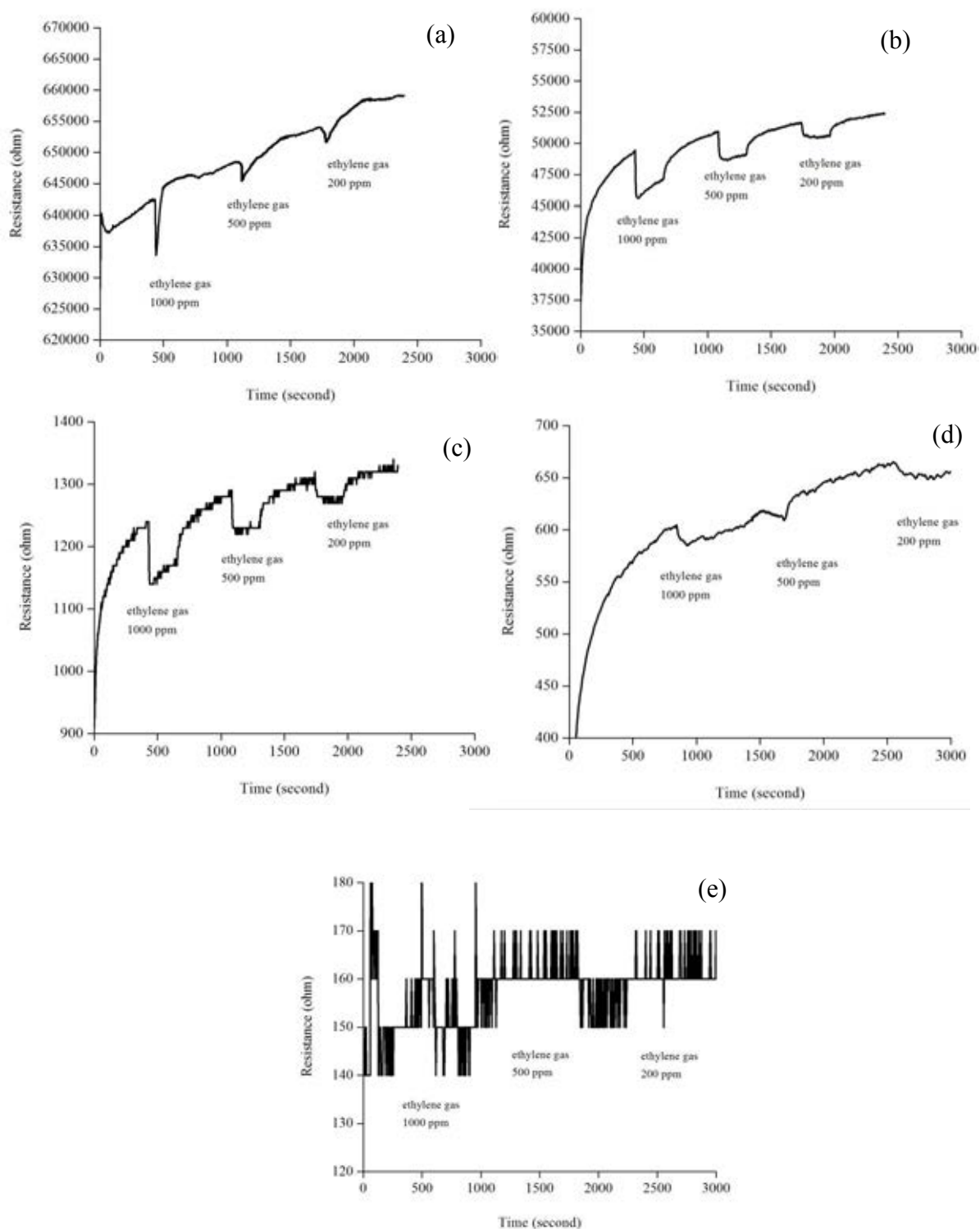


Figure 4.33 The resistance response behavior of PANi-TSA derived from different acid doping concentrations after 1 month: a) 0.01 mol, b) 0.025 mol c) 0.05 d) 0.075 mol and e) 0.1 mol

After three months of aging, all doped PANi sensors except PANi-DBSA sensor showed a good response to detect ethylene gas as lowest concentration as 10 ppm (as seen in Figure 4.34-4.36).

The different acid in term of acid type and concentration for doping PANi showed different in respond recovery behavior. For PANi-H₂SO₄, it exhibited good response to detect ethylene gas as lowest concentration as 10 ppm in all range of acid doping 0.01-0.01 mol. The PANi doped with H₃PO₄ lost its efficiency to detect ethylene gas after aging 3 month when the H₃PO₄ concentration was equal to or greater than 0.075 mol. The PANi-TSA in range of TSA doping 0.01-0.075 mol displayed good response to detect ethylene gas as lowest concentration as 10 ppm. But in case of PANi-DBSA, it lost its respond to detect ethylene gas after 3 months aging.

The resistance response data were converted into % sensitivity for comparing sensing properties. Considering at the first month of aging, in case of PANi doped with H₃PO₄, the increase of acid doping concentration led to a decrease in % sensitivity. But in case of PANi doped with H₂SO₄, DBSA, and TSA, the increase of acid doping concentration led to an increase in % sensitivity. The PANi-H₂SO₄ showed the highest sensitivity than the other acid doped PANi sensors. As shown in Figure 4.37 (a), the sensitivity of PANi doped with 0.1mol H₂SO₄ against ethylene gas at 1000, 500, and 200 ppm was about 63.31%, 47.22% and 24.51%, respectively. This result was supported as evidence by SEM analysis whereas the PANi-H₂SO₄ showed nano fibril morphology structure which can facilitate the absorption of ethylene gas on interdigitated substrate.

After three months aging, the PANi-H₂SO₄, PANi- H₃PO₄ and PANi-TSA were found to be increased sensing magnitude against ethylene gas at 200 ppm as seen in Figure 4.38. Similar to one month aging, in case of PANi doped with H₂SO₄ and TSA, the increase of acid doping led to increase in % sensitivity. Meanwhile, the PANi- H₃PO₄ showed a decrease in % sensitivity with increasing of acid concentration doping.

In addition, comparing the effect of acid type on ethylene gas sensing, the sensitivity against ethylene gas decreased in the order of H₂SO₄>H₃PO₄>TSA>DBSA. The sensing magnitude of PANi-H₂SO₄ at 0.1 M was improved sensing magnitudes of PANi from 24.5% to 35.54% for detection 200 ppm of ethylene gas after aging 3 month. The sensitivity of PANi doped with 0.1mol

H₂SO₄ against ethylene gas at 200, 100, 50, 20 and 10 ppm was about 35.54%, 26.55%, 14.70%, 5.71, and 2.94%, respectively.

Moreover, the sensitivity of PANi-H₂SO₄ after aging for 6 months was investigated as shown in Figure 4.39. The sensitivity values of PANi- H₂SO₄ against ethylene gas seem to be very close to its values of 3 months aging. It can be conclude that PANi-H₂SO₄ had highest sensing magnitude or sensitivity against ethylene gas, as well as, greatest stability upon 6 months for detection of ethylene gas.

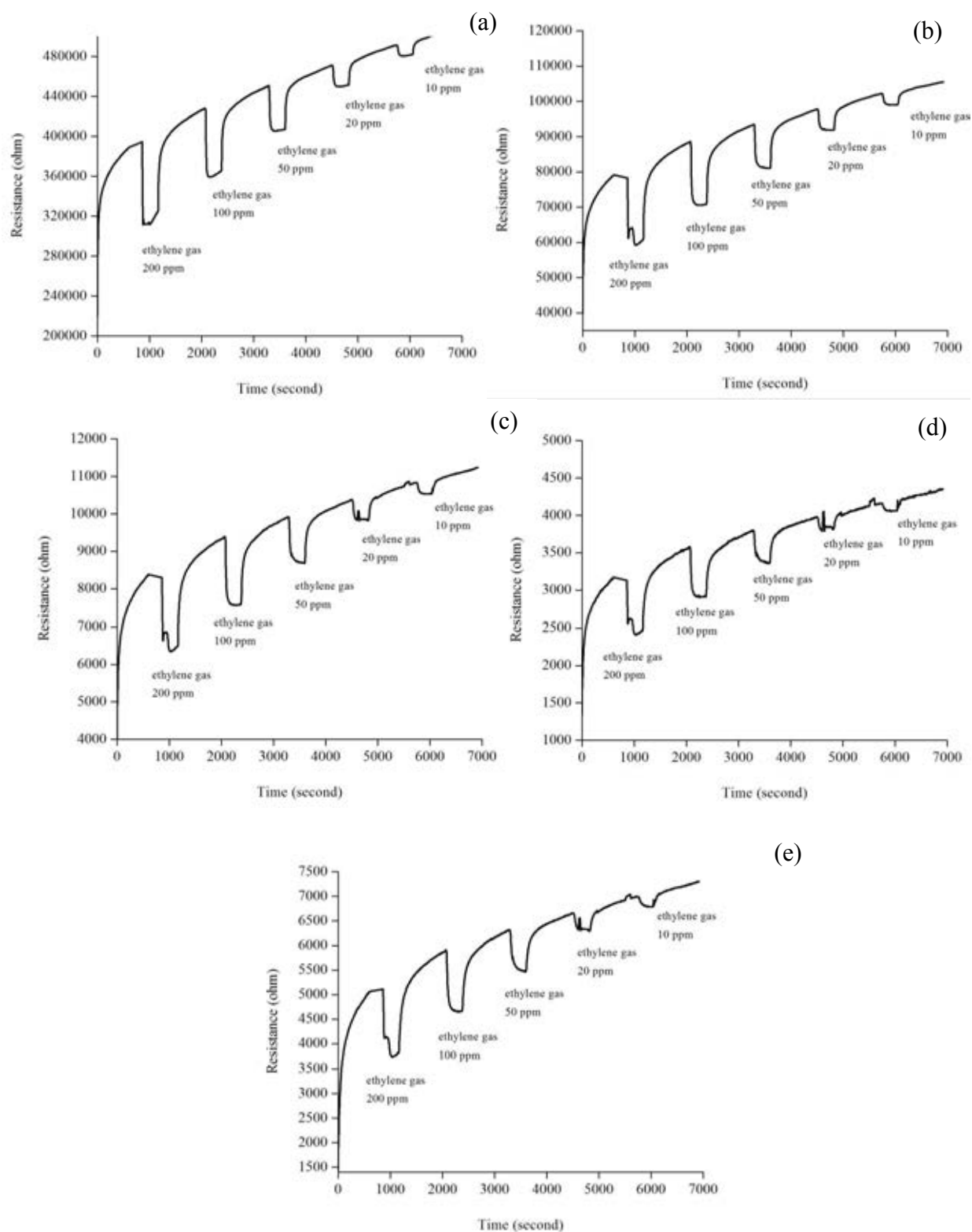


Figure 4.34 The resistance response behavior of PANi-H₂SO₄ derived from different acid doping concentrations after 3 months: a) 0.01 mol, b) 0.025 mol, c) 0.05 mol, d) 0.075 mol and e) 0.1 mol

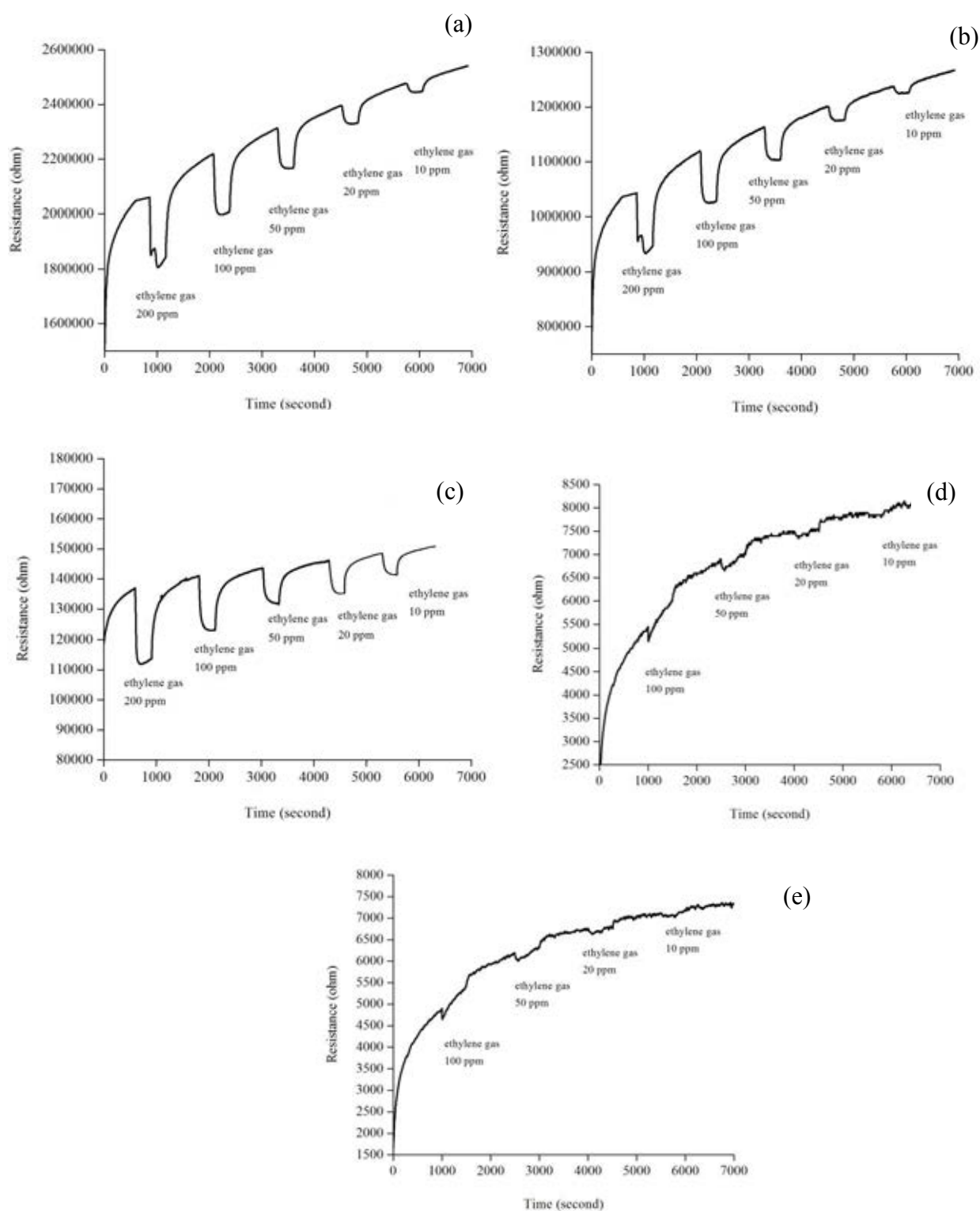


Figure 4.35 The resistance response behavior of PANi-H₃PO₄ derived from different acid doping concentrations after 3 months: a) 0.01 mol, b) 0.025 mol, c) 0.05 mol, d) 0.075 mole and e) 0.01 mol

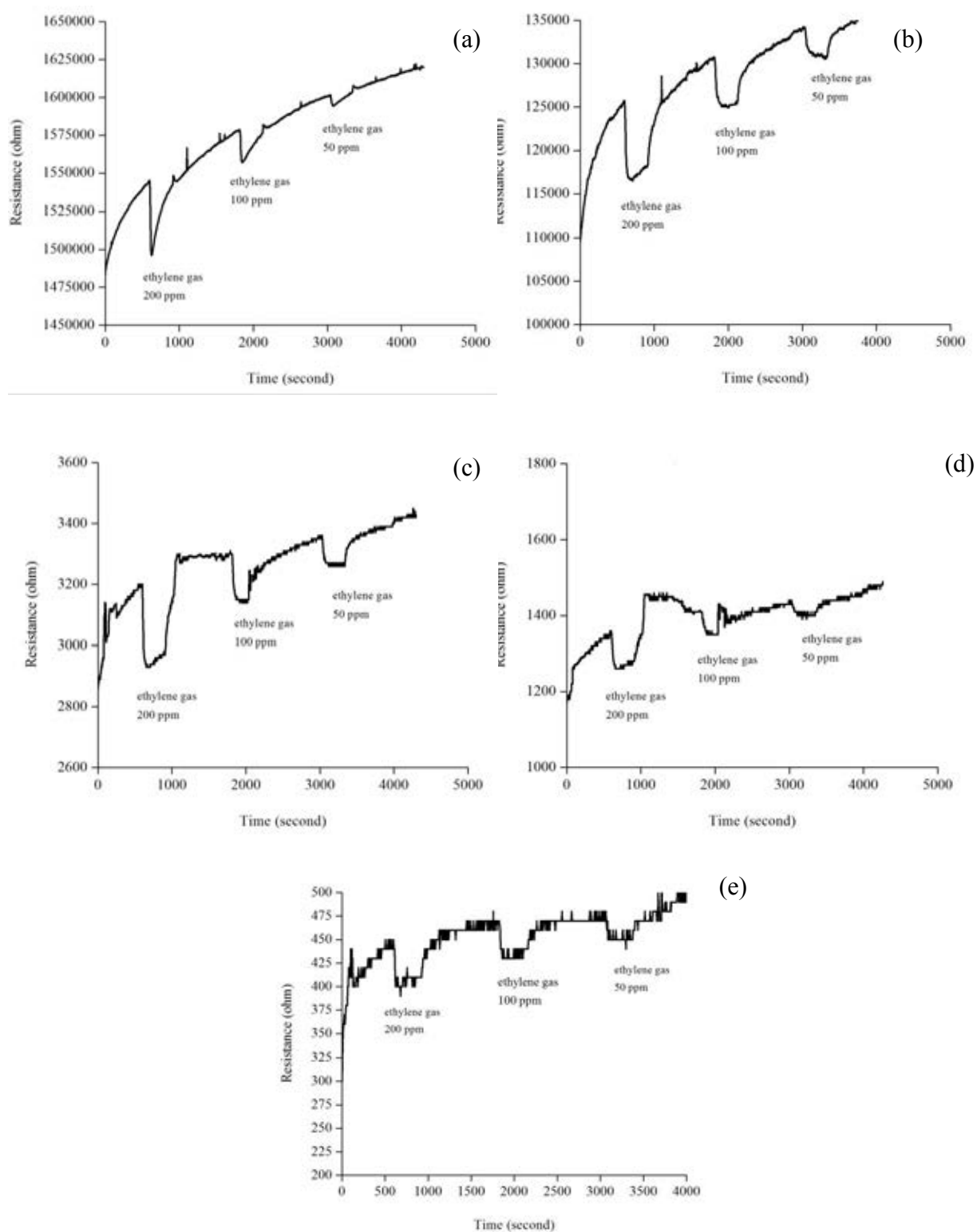


Figure 4.36 The resistance response behavior of PANi-TSA derived from different acid doping concentrations after 3 months: a) 0.01 mol, b) 0.025 mol, c) 0.05 mol d) 0.075 mol and e) 0.1 mol

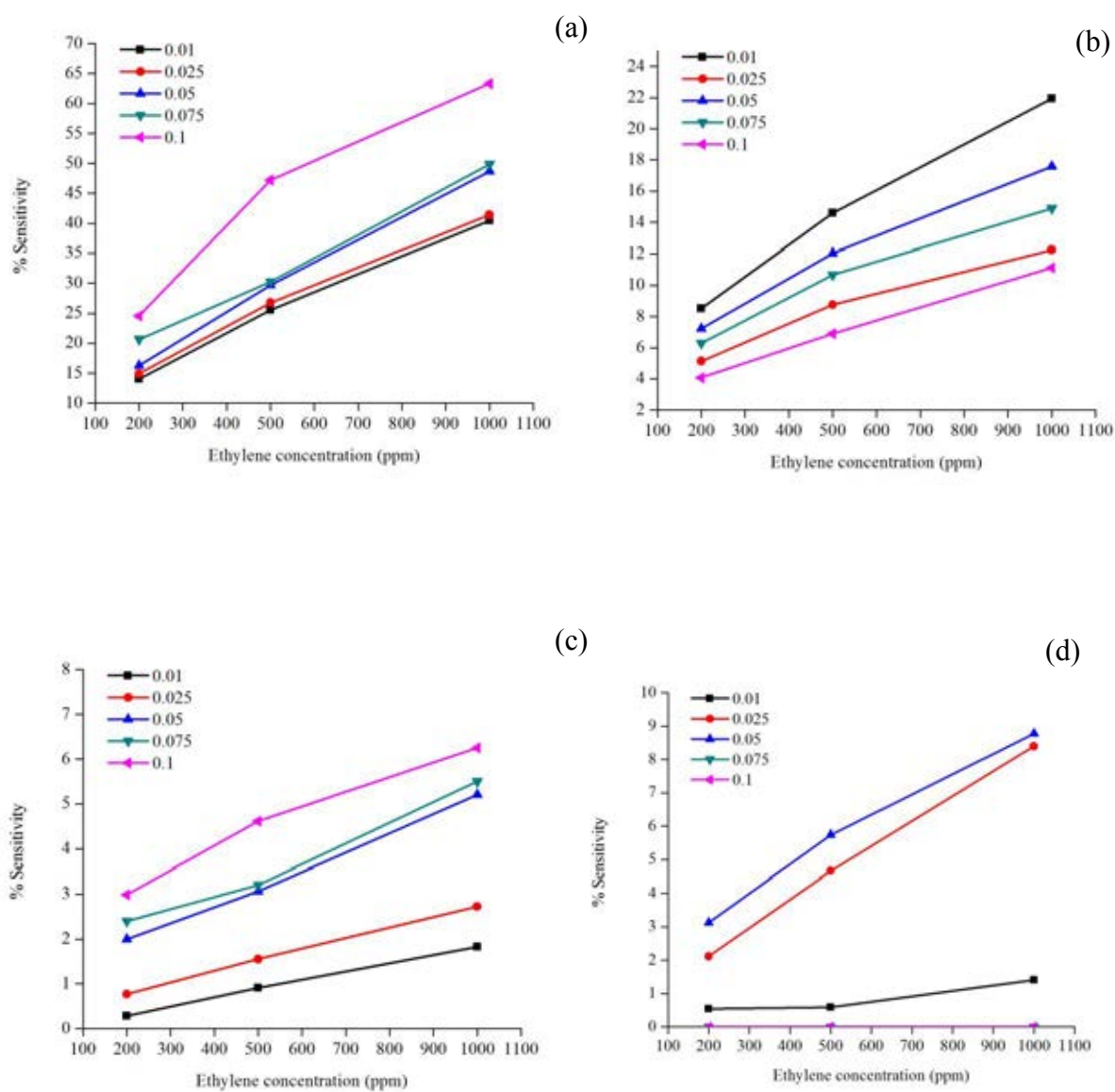


Figure 4.37 The sensing magnitude of the PANi in term of different acid dopings at various acid concentrations after 1 month: a) H₂SO₄, b) H₃PO₄, c) DBSA and d) TSA

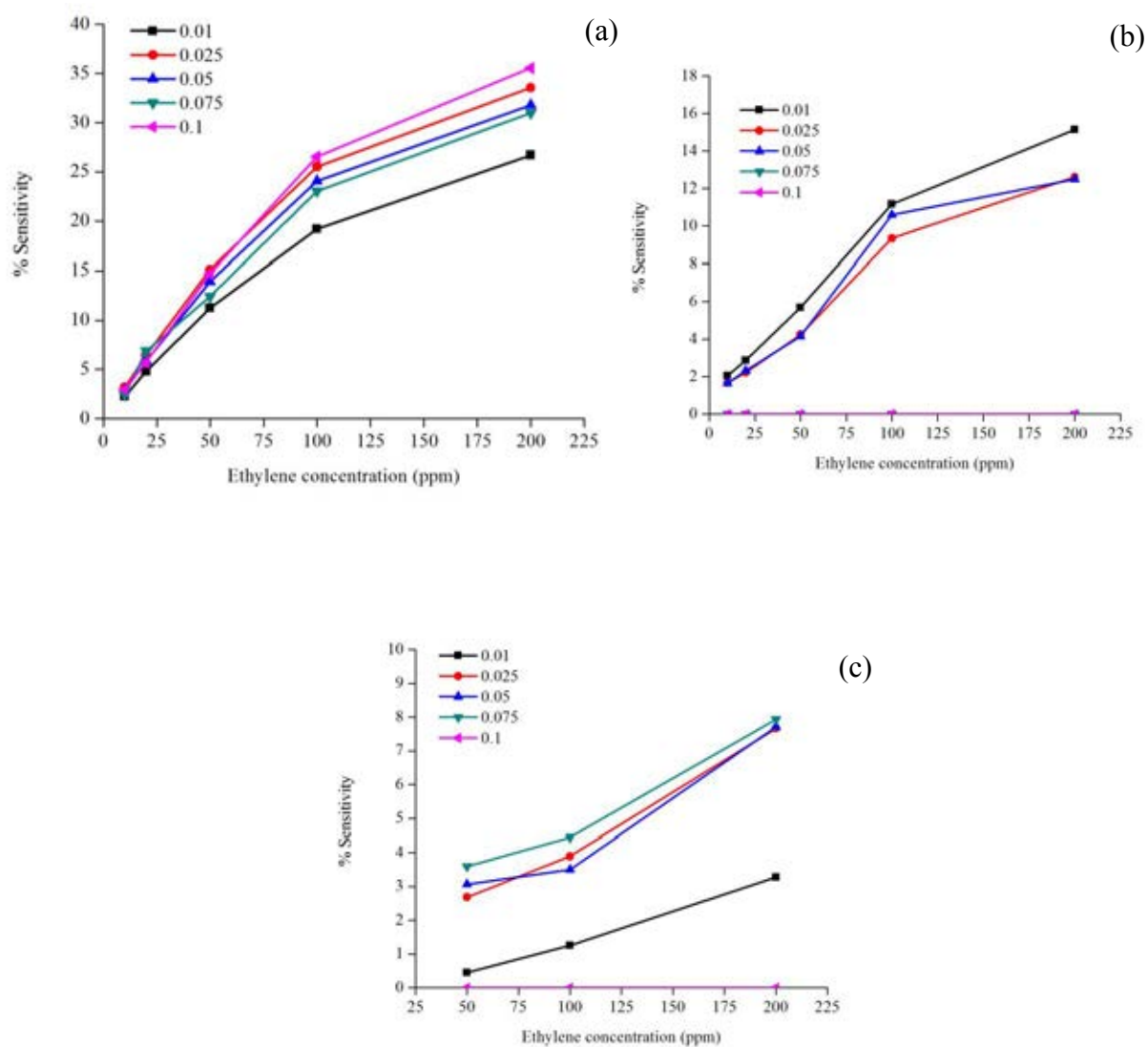


Figure 4.38 The sensing magnitude of PANi in term of different acid dopings at various acid concentrations after 3 months: a) H_2SO_4 , b) H_3PO_4 and c) TSA

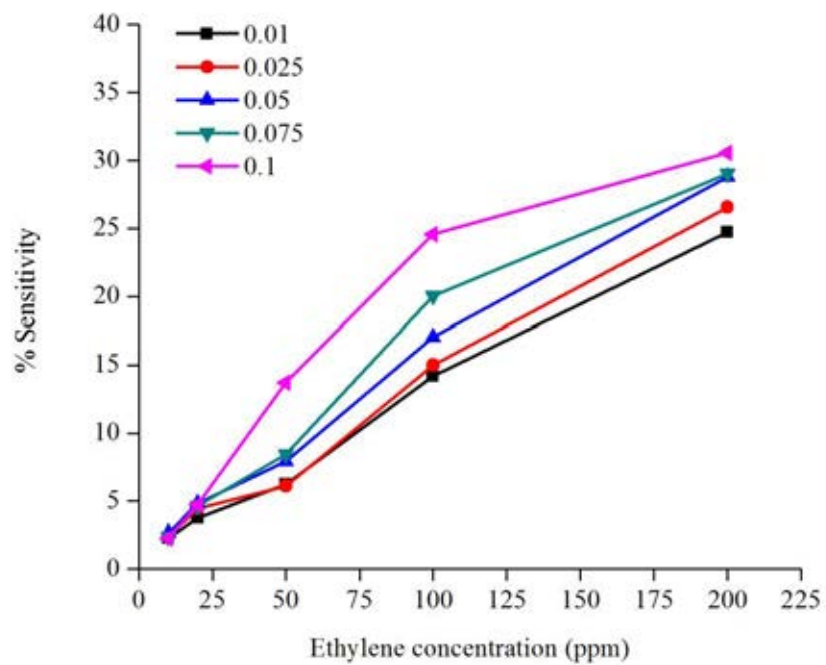


Figure 4.39 The sensing magnitude of the PANi-H₂SO₄ at different concentrations after 6 months

4.3 In-Situ Electrochemical Synthesis of Sensitive Layer of Polyaniline/Multiwall Carbon Nanotube Composite for ethylene gas detection

From the results in section 4.2, the PANi-H₂SO₄ revealed the highest sensitivity against ethylene gas detection as low as 10 ppm. However, in case of non-reactive volatile detection like ethylene gas, the lack of interfacial reaction between PANi and ethylene gas leads to limitation in their sensitivity performance.

In this section, the modification of PANi with multiwall carbon nanotube (MWCNT) was fabricated to improve sensing properties. Because of the high surface area of MWCNT and the functionalization of MWCNT with analyte-specific. A sensor for ethylene gas comprised of polyaniline/multiwall carbon nanotube (PANi/MWCNT) multilayer composite material was electrochemically synthesized onto a gold interdigitated substrate from aniline/MWCNT in acid aqueous solution. The effect of the MWCNT loadings (0, 0.2, 0.4, and 0.8 % wt) in the composite on the ethylene gas detection was investigated with different MWCNT loadings.

4.3.1 Electrochemical synthesis of PANi/MWCNT

Aniline with different percent loadings of 0, 0.2, 0.4, and 0.8 %w/w MWCNT were prepared by heat reflux at 12 hr. The electrolyte solution was prepared from the suspension solution of 0.1 M aniline/MWCNT in 1M aqueous sulfuric solution.

As presented in 4.1 section, the amount of deposited PANi films at 10 cyclic voltamogram scans of cycles revealed the optimum condition for detecting ethylene gas and then this condition was used in this section as well. Figure 4.40 shows cyclic voltammogram record during electro-polymerization ranging from -0.3-1.0 V with continuous scanning rate at 50 mVs⁻¹. This figure is represented for 0.2 % wt of MWCNT in 0.1 M aniline of 1M aqueous sulphuric acid as representative examples.

Under these conditions, the electro-polymerization was carried out from formation of radical cations at 0.2-0.3 V, proceeded by formation of head to tail dimer at 0.5 V, and then changed from emeraldine to pernigraniline structure at 0.8-1.0 V, respectively. In reverse direction, at -0.1-0.2 V the voltammogram revealed

reduction of polaron state as redox reactions of dimers, oligomers, and the degradation products such as *p*-aminophenol and quinoneimine. The increasing of their peak height increased with the number of potential cycle was an indicative of the deposition of conductive form of PANi [88].

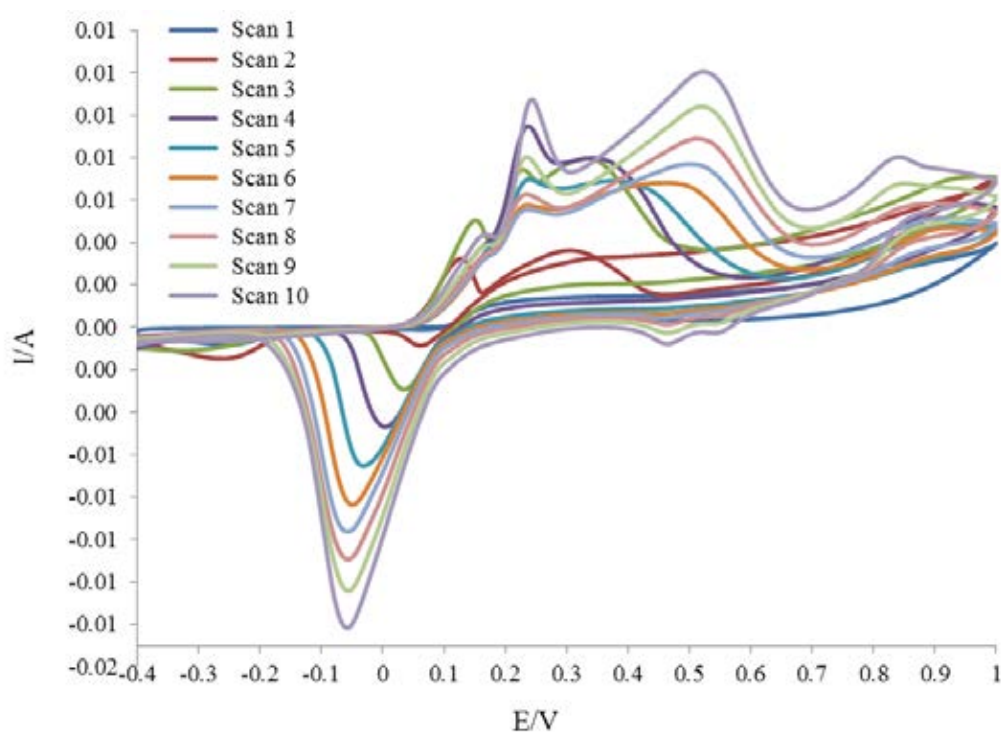


Fig. 4.40 The cyclic voltammogram of 0.2 % wt of MWCNT in 0.1 M aniline of 1M sulfuric acid at 50 mV/s

4.3.2 Raman characteristic of deposited PANi/MWCNT composites

The Raman spectra of MWCNT, PANi and, PANi/MWCNT composites containing 0.2 %wt MWCNT loading are shown in Figure 4.41. The raman spectrum of pure MWCNT showed two typical bands. The first peak at 1278 cm^{-1} corresponded to the D-band, which is attributed to the raman-allowed photon high-frequency mode of MWCNT, whereas the second one 1593 cm^{-1} was due to the G-band.

The raman spectrum of pure PANi showed three characteristic bands. The distinct peaks at 1162 , 1343 and 1497 cm^{-1} were the characteristic peaks of the C-H bending of the quinoid ring, -C-N- in benzenoid ring and -C=N- stretching in the quinoid and benzenoid ring.

For PANi/MWCNT composites, the raman spectrum showed two usual bands of MWCNT. The first peak at 1278 cm^{-1} corresponded to D-band; whereas the peak at 1593 cm^{-1} was due to G-band. This evidence suggested the existence of MWCNT in PANi. The other peaks spectra at 1162 , 1343 and 1497 cm^{-1} were obviously the characteristic peaks of the C-H bending of the quinoid ring, -C-N- and -C=N- stretching in the quinoid and benzenoid rings, respectively, of PANi molecule [95].

In addition, the spectrum of PANi/MWCNT revealed similar pattern with the spectrum of PANi but with a slight decrease in the intensity (of some peak in comparison with PANi). This evidence may be due to a site selective interaction between the quinoid ring of the doped PANi and MWCNT during electro-polymerization.

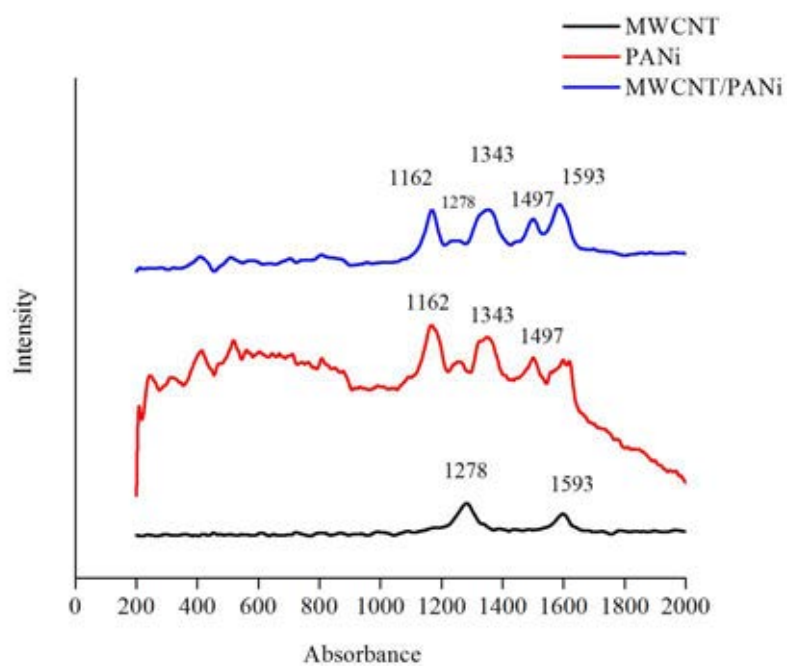


Figure 4.41. Raman spectra of the PANi, MWCNT and PANi/MWCNT at MWCNT loading at 0.8% wt.

4.3.3 Microstructure characterization of the deposited PANi/MWCNT

The SEM images of MWCNT, PANi and PANi/MWCNT composites with different MWCNT loadings of 0.2, 0.4 and 0.8 % wt are presented in Figure 4.42. The MWCNT revealed highly porous nanofibril structure in range of nanoscale with approximately 10 nm in diameter (as seen in figure 4.42(a)), while pure PANi film revealed highly porous nano fibril structure of PANi similar to MWCNT but with the shorter length of continuous nanofiber (as seen in figure 4.42(b)).

As shown in Figure 4.42(c), the PANi with 0.2 % wt MWCNT loading displayed porous nanofibril structure. The addition of 0.2 % wt MWCNT in PANi had not effect on morphology of PANi due to small content of MWCNT. However, this resultant can be expected that the MWCNT with 0.2 % wt can be interpreted into morphology of PANi by agglomeration into nanofiber structure. The agglomeration of PANi and MWCNT can be clearly observed with increasing MWCNT loading to 0.4 % wt as shown in Figure 4.42(d). This result correspond agreement with the work of Jing Zhang et.al, 2008 [96].

The introduction of 0.8% MWCNT in PANi had strong effect on morphology by changing in surface roughness of nanofiber. The increaing content of MWCNT in PANi led to increase the level of agglomeration of nanofibril structure of PANi as seen in Figure 4.42(e). This results may be due to formatted structure of long chain three-dimensional network of MWCNT created more active sites for condensation of nuclei during the chain growth.

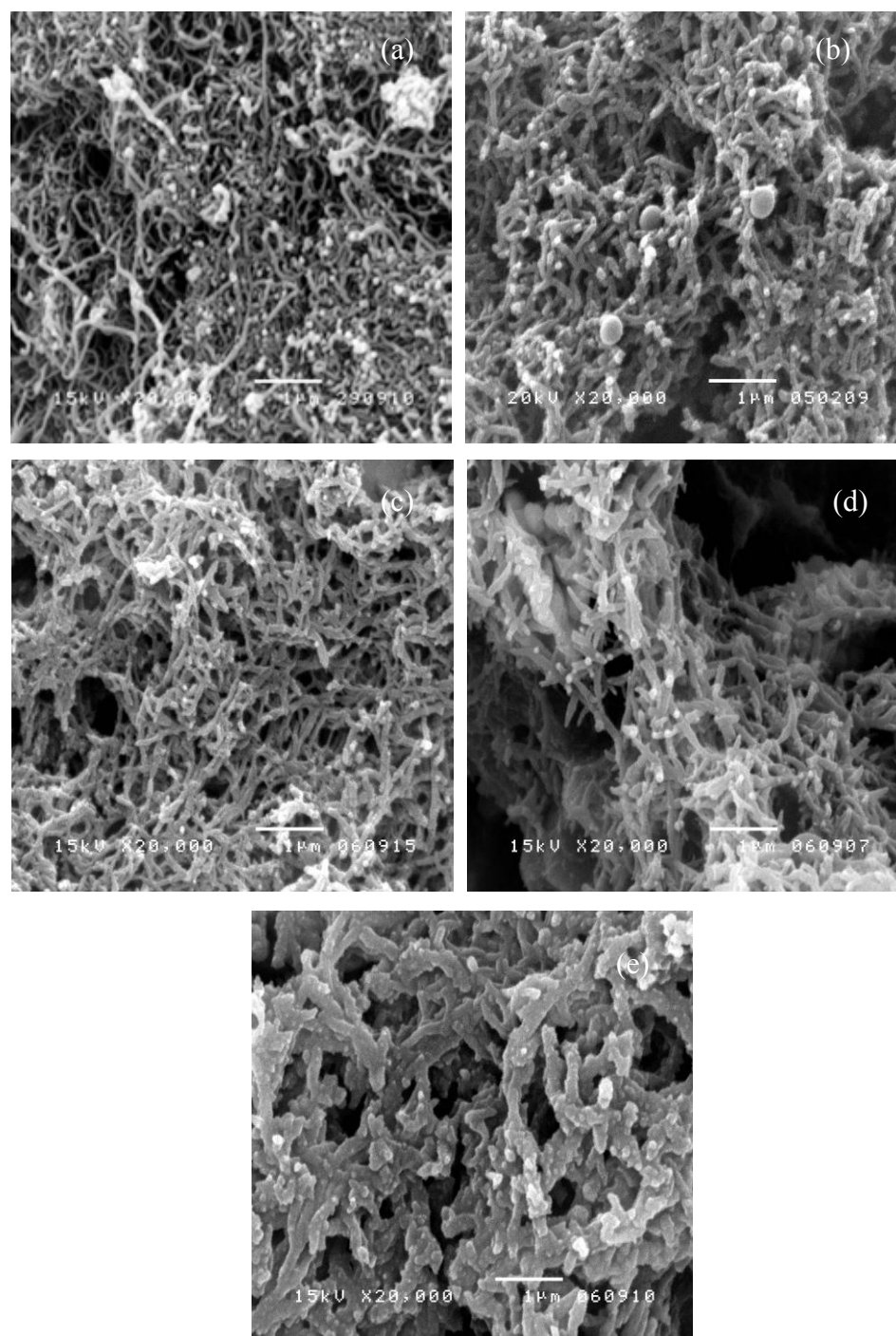


Figure 4.42 Representative SEM micrographs (20,000 x magnification) of the deposited PANi/MWCNT at different MWCNT loadings (a) pure MWCNT (b) PANi (c) 0.2%wt MWCNT/PANi (d) 0.4% wt MWCNT/PANi and (e) 0.8% wt MWCNT/PANi

4.3.4 Thermal behavior of PANi/MWCNT composites

Thermogravimetric analysis of neat PANi and PANi/MWCNT composites was investigated under O₂ atmosphere 10 °C min⁻¹ from 50 – 800 °C. The TGA thermograms of the neat PANi/MWCNT and PANi/MWCNT, derived from different MWCNT loadings of 0.2, 0.4 and 0.8 % wt are shown in Figure 4.43.

The neat PANi revealed a typical two-step weight loss. First step can be attributed to the loss of water molecules at temperature up to 100 °C. After the initial weight loss, the skeleton of polyaniline backbone started to oxidize and decompose at 180 °C. The neat PANi was completely oxidized at approximately 700 °C. This result correspond agreement with work of Fan Huang et. al., 2009 [97].

MWCNT started to oxidize at temperature 550 °C and it showed residual weight 10% of its original weight after 900 °C. In case of PANi/MWCNT, the first step of decomposition was also attributed to the loss of water molecules; while the second step revealed decomposition of the skeleton of polyaniline backbone and MWCNT. The PANi/MWCNT composite was completely oxidized at a similar temperature to neat PANi. However, comparing with PANi, PANi/MWCNT started to oxidize at a relatively higher temperature in term of the onset of oxidation temperature. The increasing MWCNT loading in PANi composite led to an increase in the onset of oxidation temperature at relative higher temperature due to higher thermal stability of MWCNT.

In addition, it clear that the onset oxidation temperature of MWCNT in PANi composite showed lower than on onset oxidation temperature of MWCNT pure. This result may be due to the oxidation transition of MWCNT overlapped with oxidation state of PANi.

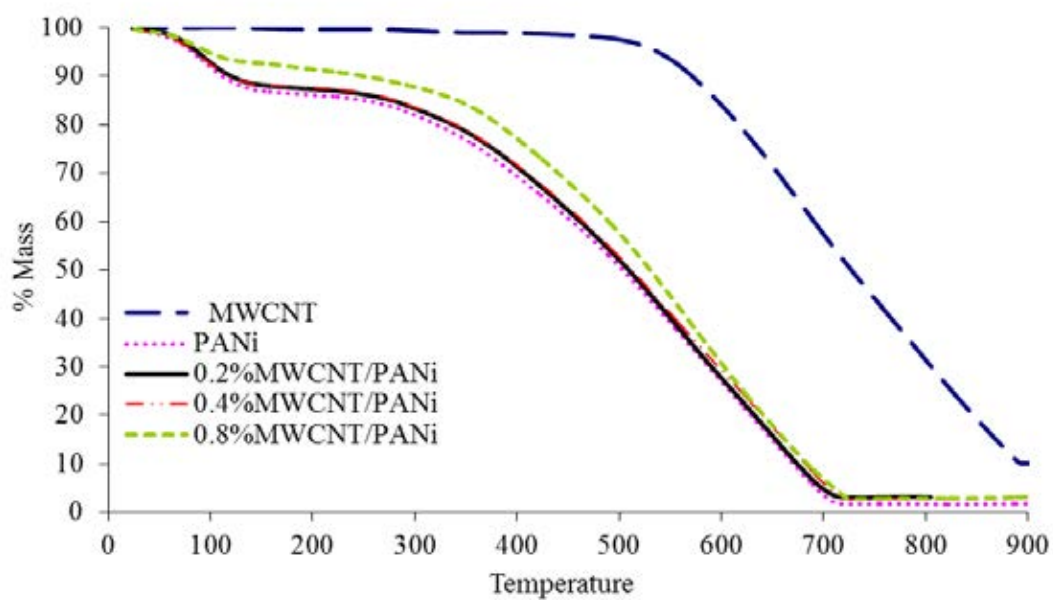


Figure 4.43 TGA thermograms of the MWCNT, PANi, and PANi/MWCNT composites at different MWCNT loadings

4.3.5 Ethylene gas detection of PANi/MWCNT composites via resistance measurement

The response–recovery characteristics of PANi with different MWCNT loadings against ethylene gas were revealed in Figure 4.44 (for 1 month aging) and Figure 4.45 (for 3 month aging). After being exposed to ethylene gas, the entire sensor responded to ethylene gas by undergoing a decrease in their resistance. This result was due to the diffusion of ethylene gas into the nanofibril structure of PANi-MWCNT and also attributed the expansion of compact form of PANi chain into linear form. After 3 month aging, it clearly observed that the addition of MWCNT in PANi can improve stability in detection of ethylene gas. As show in figure 4.45, the baseline of response-recovery characteristic of PANi-MWCNT promptly reached to steady-state during exposure to nitrogen gas and returned to its baseline when ethylene feed was discontinued.

For first month of aging, the sensing magnitude of pure PANi revealed higher sensitivity than PANi/MWCNT as seen in figure 4.46(a). The sensing magnitude of the PANi/ MWCNT decreased in the order of the MWCNT loadings, as pure PANi > 0.2% wt MWCNT/PANi > 0.4% wt MWCNT/PANi > 0.8% wt MWCNT/PANi. It clearly observed that, during 1 month aging, the introduction of MWCNT into PANi did not reveal significant to enhance sensing property against ethylene gas.

However, the sensitivity of all sensors was enhanced after 3 month aging. The pure PANi and PANi/MWCNT composites showed efficiency to detect ethylene gas as low as 10 ppm as seen in Figure 4.46 (b). The 0.2 %wt MWCNT/PANi showed higher sensitivity than pure PANi and exhibited the highest sensitivity against ethylene gas at 10 ppm by changing in sensing magnitude about 4.39%. The sensing magnitude of the MWCNT/PANi decreased in the order of the MWCNT loading, as 0.2% wt MWCNT/PANi> pure PANi > 0.4% wt MWCNT/PANi > 0.8% wt MWCNT/PANi.

In addition, the decrease in sensitivity of PANi with MWCNT loadings more than 0.2% can be explained as evidence support by SEM analysis, the increasing of MWCNT loadings in PANi more than 0.2% resulted to agglomerate PANi nanofibril. This result led to drop in ability of absorption and expansion of nanofibril structure of PANi.

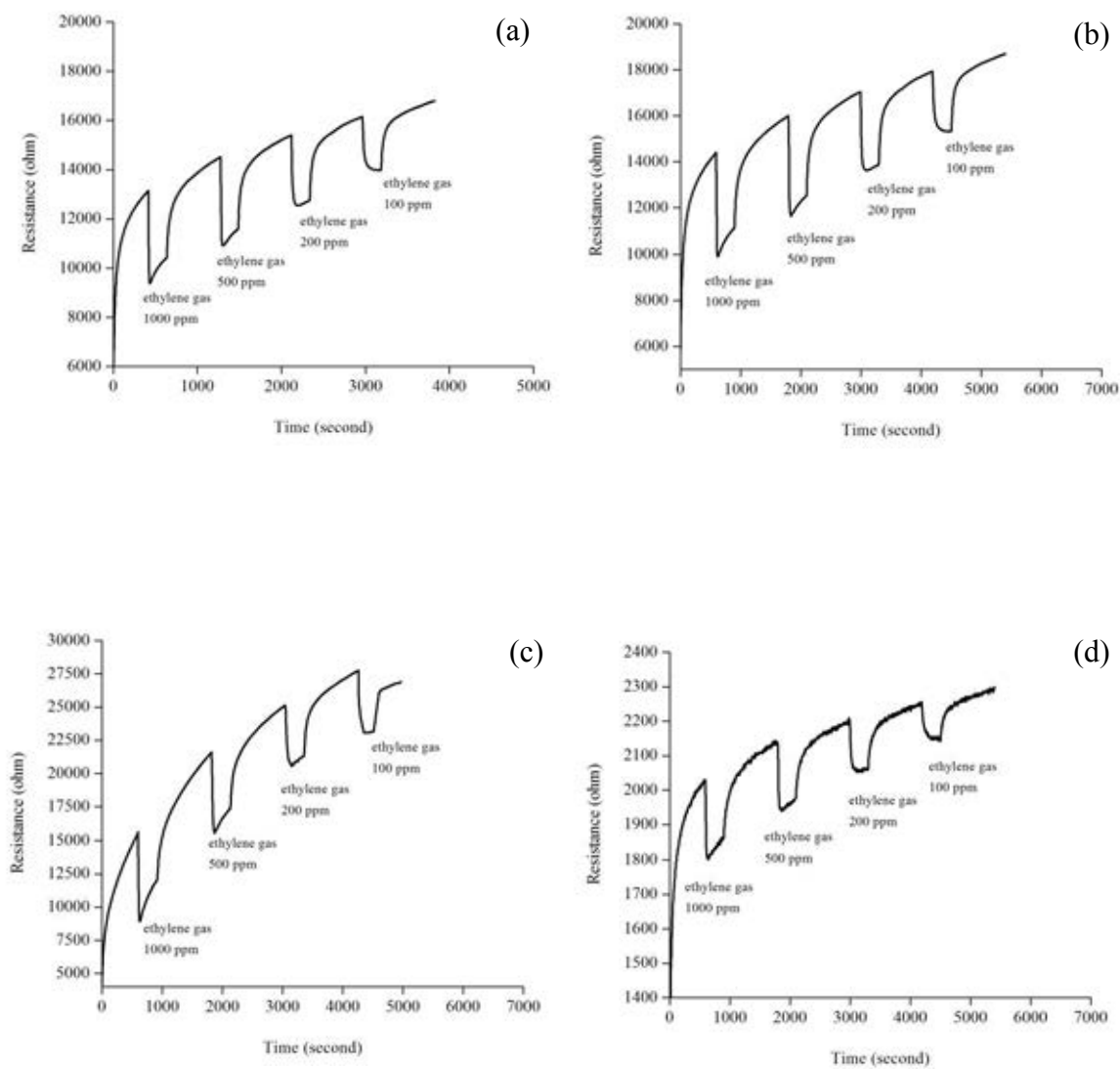


Figure 4.44 Response-recovery behavior of MWCNT/PANi at different MWCNT loadings after 1 month aging: (A) pure PANi , (B) 0.2% wt MWCNT/PANi, (C) 0.4% wt MWCNT/PANi and (D) 0.8% wt MWCNT/PANi

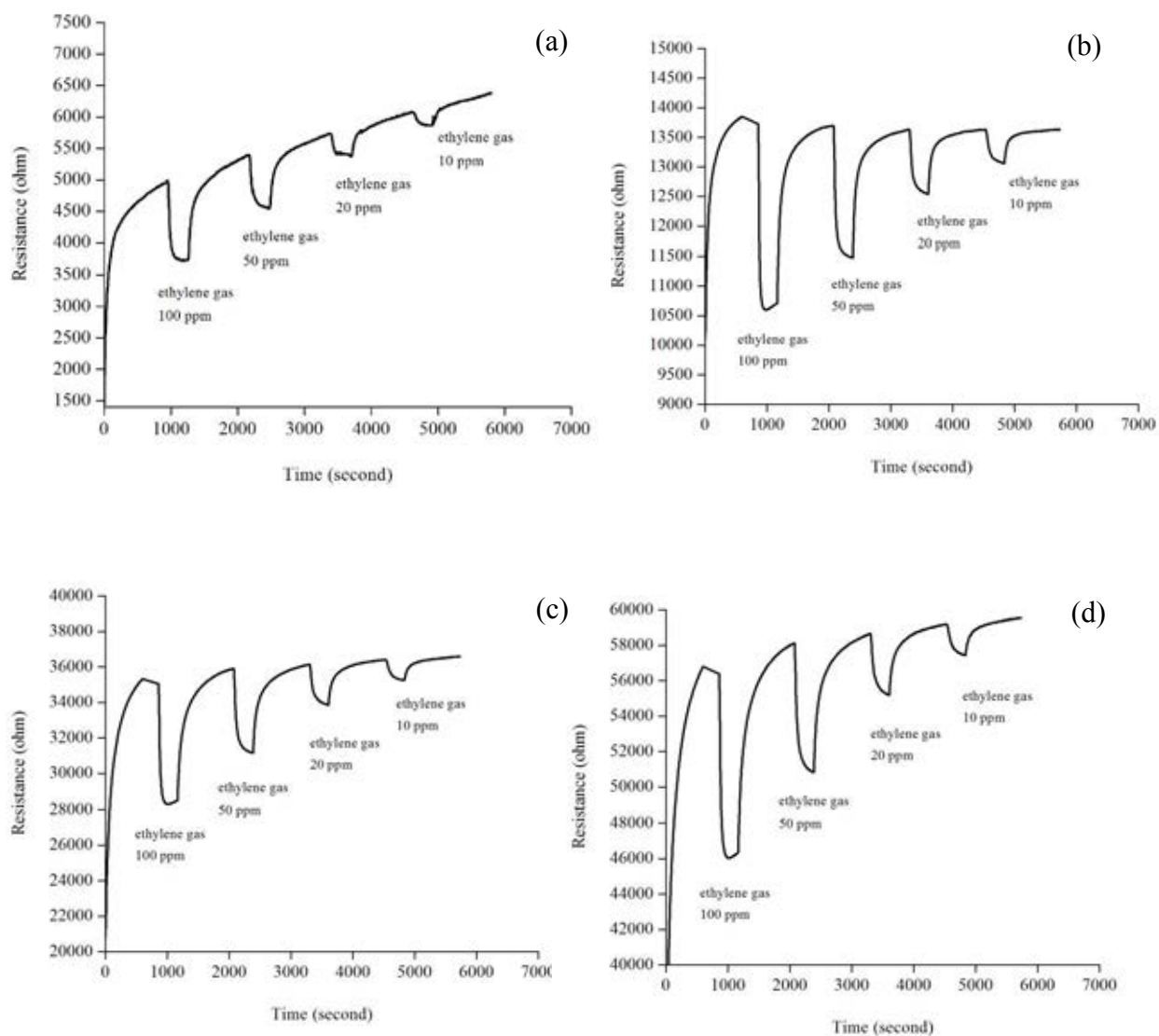
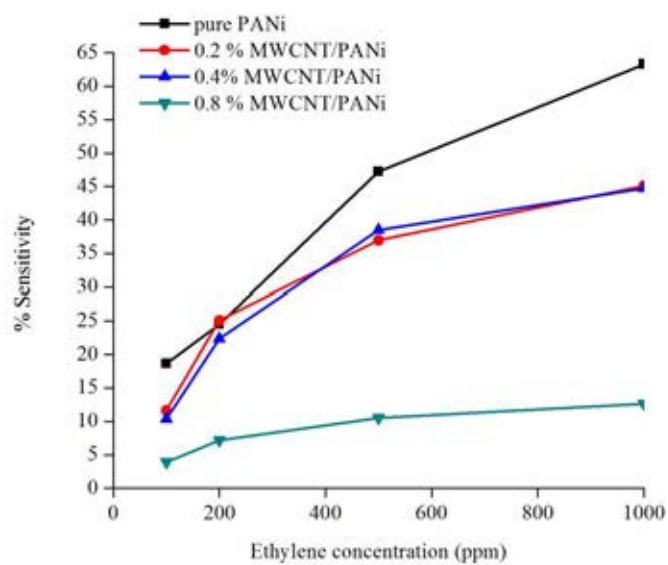
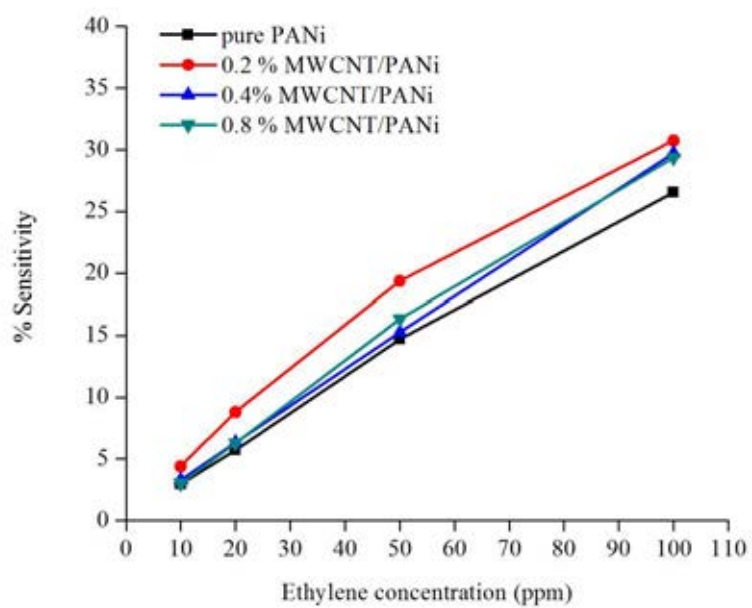


Figure 4.45 Response-recovery behavior of MWCNT/PANi at different MWCNT loadings after 3 month aging: (A) pure PANi , (B) 0.2% wt MWCNT/PANi, (C) 0.4% wt MWCNT/PANi and (D) 0.8% wt MWCNT/PANi



(a)



(b)

Figure 4.46 The sensitivity behavior of the PANi/MWCNT composites at different MWCNT loadings times after (a) 1 month and (b) 3 months aging.

4.4 In-situ electrochemical synthesis of novel sensitive layer of polyaniline/multiwall carbon nanotube/tin oxide hybrid materials for ethylene gas detection

In this section, a sensor for ethylene gas comprised of a polyaniline/multiwall carbon nanotube/tin oxide nanoparticle (PANi/MWCNT/SnO₂NP) multilayer composite material was successfully synthesized by electrophoretic deposition of SnO₂NPs onto a gold interdigitated substrate and then chronoamperometric deposition of the PANi/MWCNT film from an aniline/MWCNT solution. The effect of varying the SnO₂NP level in the composite on the subsequent ethylene gas detection ability was investigated for five different SnO₂NP loadings by varying the SnO₂NP deposition time (0, 60, 90, 120 and 150 sec). The details of each step are showed as follows:

4.4.1 Deposition of Tin oxide Nanoparticles onto the interdigitated gold

A colloidal suspension of 5% (w/v) SnO₂NPs in distilled water was prepared by sonification and the pH was adjusted to 2 with sulfuric acid. A gold pattern coated wire board, comprised of a 25 mm overlapping electrode length and 10 μm insulating gap, was used as the anode, whilst aluminum foil was used as the cathode. The electrophoretic deposition of SnO₂NPs was performed at 9 V with different deposition times (60, 90, 120 and 150 sec). Note that a 0 sec time refers to no SnO₂NP deposition stage. The lowest deposition time of SnO₂NPs (60 sec) was selected since this is the minimum deposition time required to yield a sufficient deposited coverage of SnO₂NPs to bridge the gaps between the conductive and the insulator gaps of the gold interdigitated substrate. Furthermore, the acidity of colloidal suspension was set at pH 2 with sulfuric acid in order to stabilize 5% (w/v) SnO₂NPs in colloidal suspension during their deposition [97].

4.4.1.1 Microstructure characterization of the deposited SnO₂NP layer

The SEM image of deposited SnO₂NPs at different deposited times (60, 90, 120 and 150 second) was showed in Figure 4.47. SEM analysis of the thin layer of deposited SnO₂NPs after different deposition times revealed a uniform distribution of the SnO₂NPs on the surface of the interdigitated gold for the different deposition times. The increasing of deposition time led to an increase in level of deposition of SnO₂NPs on substrate. No evidence of anisotropy was observed. All agglomerates of SnO₂NPs were in the nanoscale (100 - 200 nm diameter), implying that the SnO₂NPs were stable in colloidal suspension during the deposition.

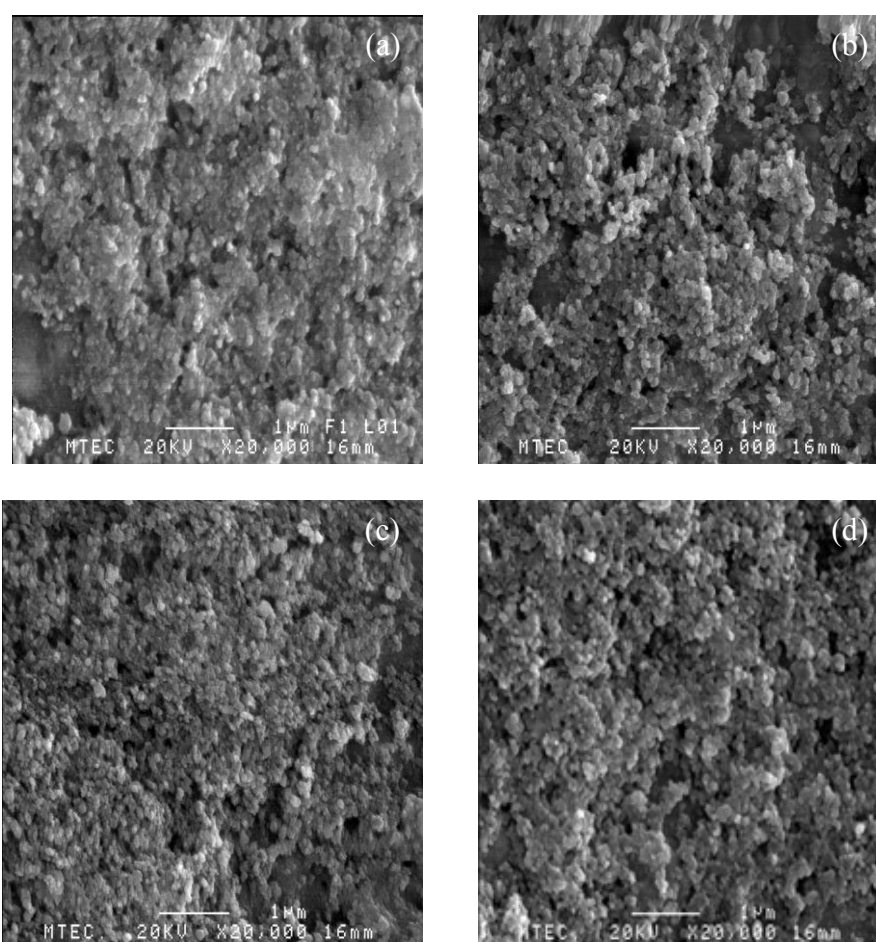
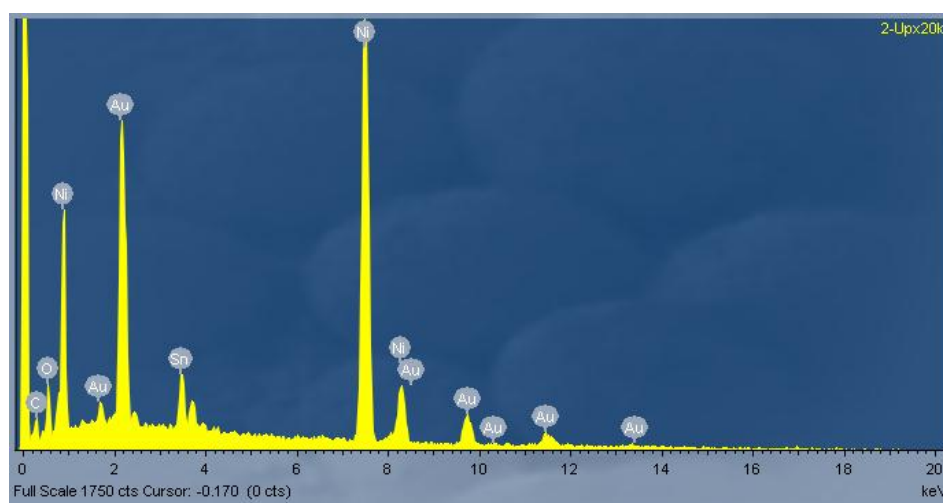


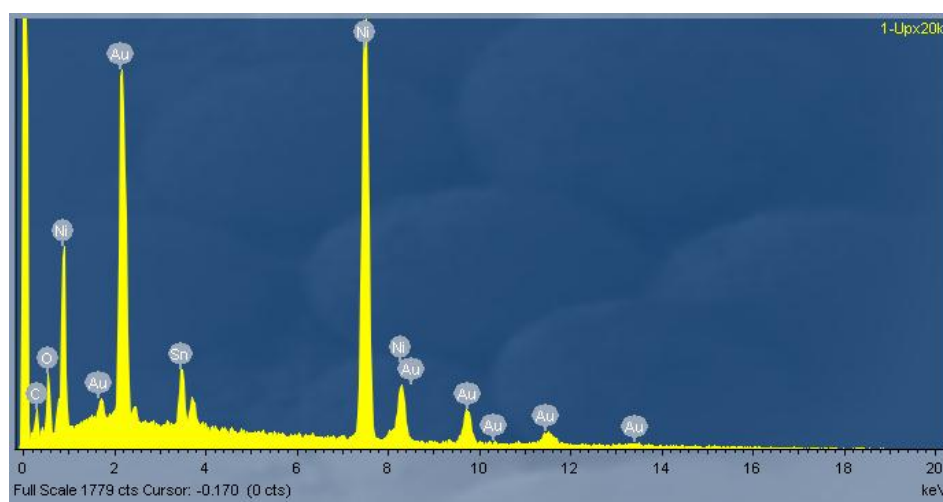
Figure 4.47 Representative SEM micrographs (20,000 x magnification) of the deposited SnO₂NP when deposited at 9 V for (a) 60 sec, (b) 90 sec, (c) 120 sec and (d) 150 second

4.4.1.2 Elemental analysis of the deposited SnO₂NP layer

The characteristic and level of SnO₂NPs coated onto the gold interdigitated substrate was determined by examination of the elemental distributions using SEM-EDS analysis. The Figure 4.48 shows characteristic signals from EDS analysis of SnO₂NPs coated for 60, 90, 120, and 150 second. The qualitatively elemental of EDS analysis exhibited two characteristic signals as the characteristic signals of SnO₂ at 0.6 and 3.4 KeV for the oxygen and tin atoms, respectively. This signal result correspond agreement with work of Haraiati T. 2009 [97]. Clearly, the amount of SnO₂NPs deposited increased with the increasing deposition time, where the intensity of the tin and oxygen signals increased with increasing deposition times from 60 to 150 second.

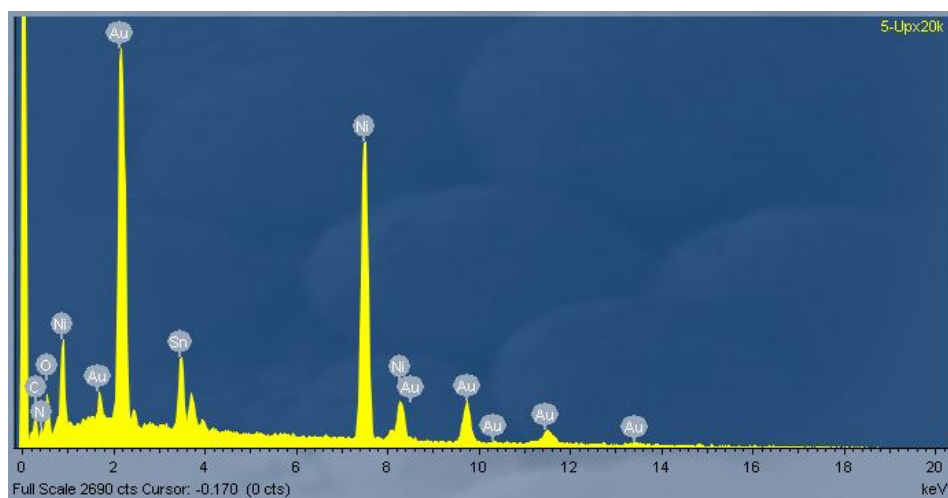


(a)

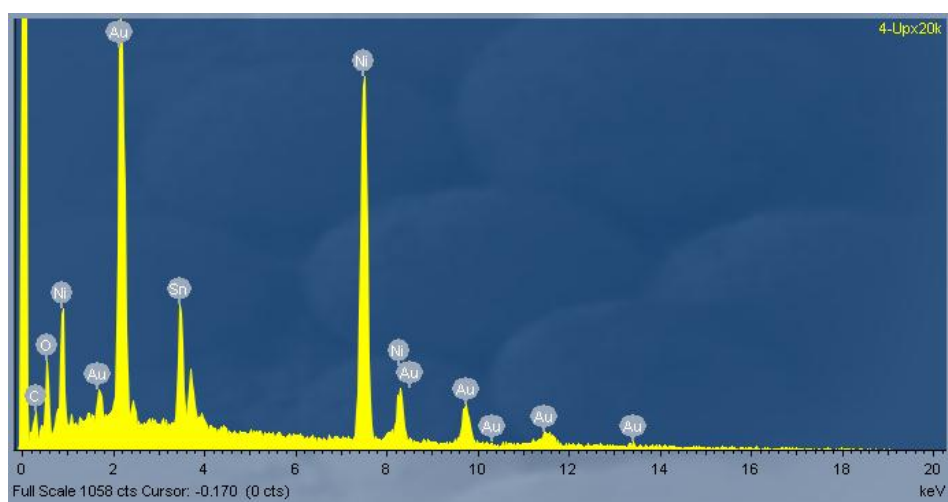


(b)

Figure 4.48 The elemental distributions of deposited SnO_2 NPs layer at different deposited times (a) 60 second, (b) 90 second, (c) 120 second, and (d) 150 second



(c)



(d)

Figure 4.48 (cont.) the elemental distributions of deposited SnO₂ nanoparticle layer at different deposited times (a) 60 second, (b) 90 second, (c) 120 second, and (d) 150 second

4.4.2 Deposition of nanofibers PANi/MWCNT on thin film of SnO₂ nanoparticle

To create second nanofibers PANi/MWCNT layer on thin film of SnO₂ NP, the nanofiber of PANi/MWCNT were deposited by electrochemistry method. The chronoamperometric deposition curve of 0.1 mol aniline/MWCNT in 25 ml of a 1.0 M H₂SO₄ solution is shown in Figure. 4.49, where the electrochemical polymerization of aniline mainly involves three stages of changes in the current density. The first stage is the induction period of aniline polymerization. During this period, the current density is significantly and rapidly decreased, and no PANi was found at the electrode. During the second stage the current density increased rapidly and the aniline was polymerized and started to deposit onto the layer of SnO₂NPs at the anode. Finally, in the last stage, the growth polymerization of PANi/MWCNT revealed a constant current density.

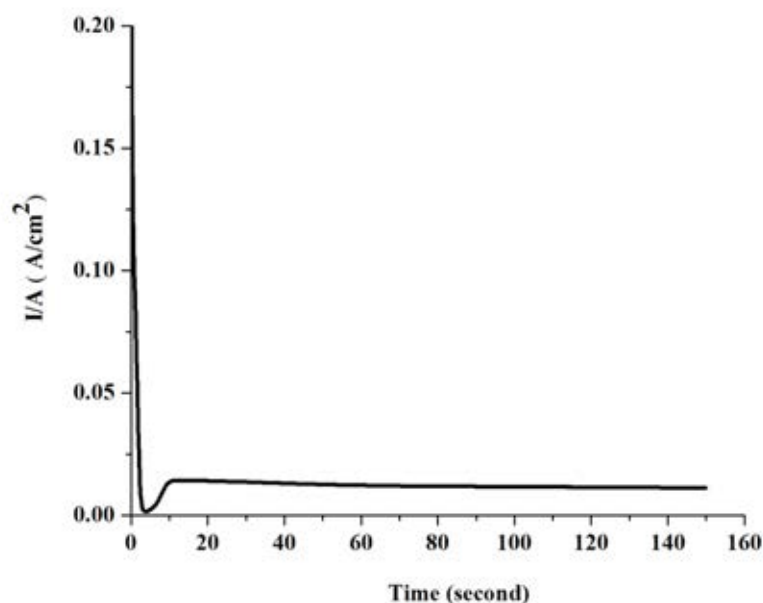


Figure 4.49 Chronoamperometric deposition curve of a 0.1 mol aniline/MWCNT in 1.0 M H₂SO₄ solution onto the SnO₂NP layer of a gold interdigitated anode

4.4.2.1 Microstructure characterization of the deposited PANi/MWCNT layer

A second layer of PANi/MWCNT was deposited on top of the SnO₂NP layer by chronoamperometric deposition. The SEM image of deposited PANi/MWCNT at different deposition times was showed in Figure 4.50. The obtained PANi/MWCNT layer showed bulk surface roughness nanofibril PANi/MWCNT after deposition PANi/MWCNT for 90 second as displayed in Figure 4.50(a). SEM analysis of the resultant PANi/MWCNT layer reveals that after deposition for 120 and 150 second, the obtained PANi/MWCNT layer shows a formatted structure of a three-dimensional nanofibril network as illustrated in Figure 4.50(b) and (c). This nanoporous structure can act as a support for gas absorption. Meanwhile, after deposition for 160 second, the obtained PANi/MWCNT layer showed agglomeration of nanofibril PANi/MWCNT as presented in Figure 4.50(d). It can be concluded that nanoporous structure of PANi/MWCNT can be obtained when the deposition time was varied between 120-150 second.

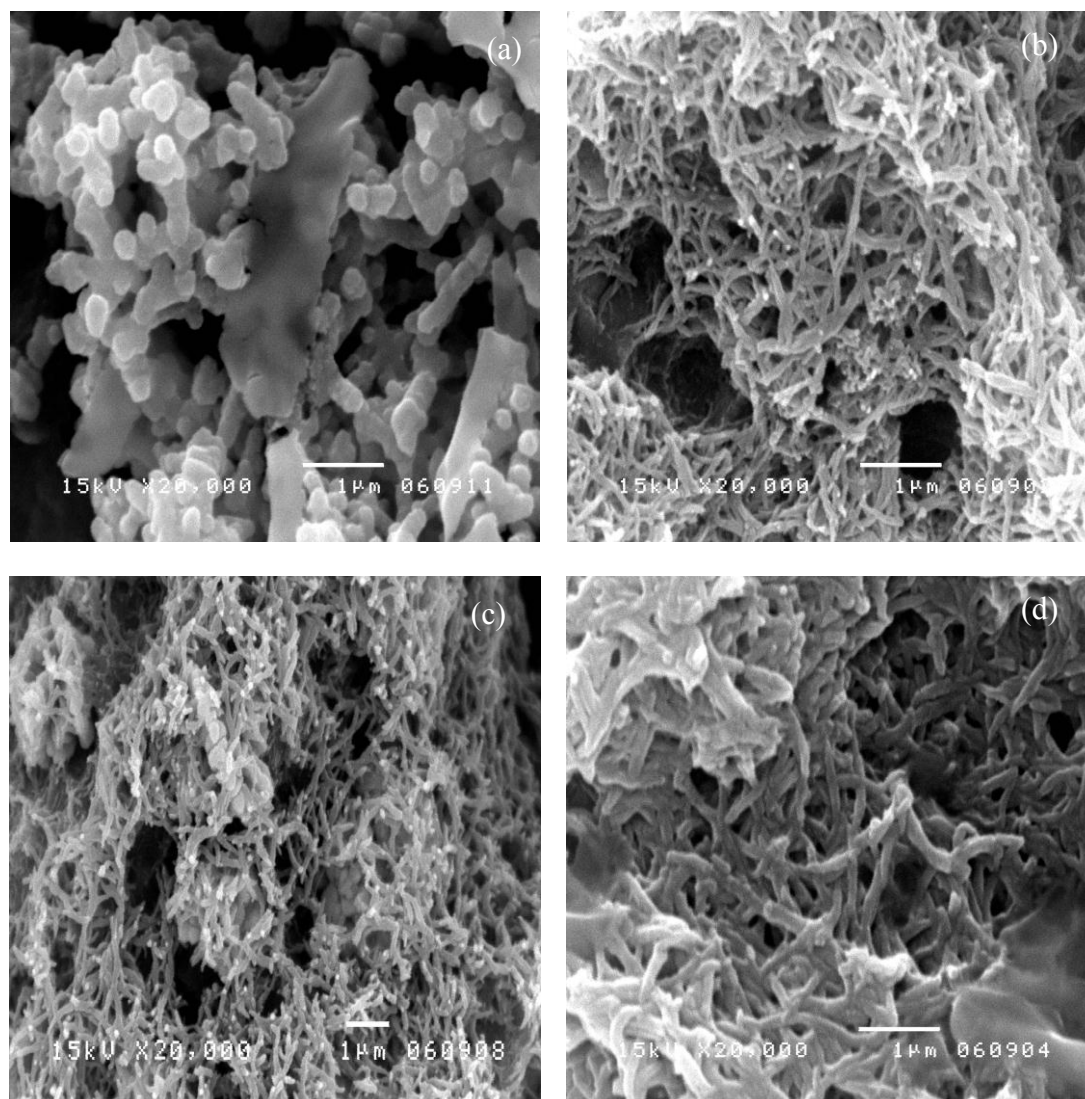


Figure 4.50 Representative SEM micrographs (20,000 x magnification) of the deposited PANi/MWCNT coatings when deposited at 1 V for (a) 90 second, (b) 120 second, (c) 150 second, and (d) 160 second

4.4.2.2 Raman characteristic of PANi/MWCNT and PANi/MWCNT/SnO₂ nanoparticle

The Raman spectra of the PANi/MWCNT and, for the PANi/MWCNT/SnO₂NP composites that are derived from a 90 sec SnO₂NP deposition time, are shown in figure 4.51. The Raman spectrum of PANi/MWCNT showed two usual bands of MWCNT characteristic. The first peak at 1351 cm⁻¹ corresponded to the D-band, which is attributed to the raman-allowed photon high-frequency mode of MWCNT, whereas that at 1593 cm⁻¹ was due to the G-band. This evidence suggested the existence of MWCNT. The raman spectra at 1162, 1343 and 1497 cm⁻¹ were the characteristic peaks of the C-H bending of the quinoid ring, –C–N– in benzenoid ring and –C=N– stretching in the quinoid and rings.[95].

Additionally, the PANi/MWCNT/SnO₂NP composite revealed broadly similar spectrum patterns as that for PANi/MWCNT. Note that although this figure shows the PANi/MWCNT/SnO₂NP composite that is derived from a 90 sec SnO₂NP deposition time; this is representative of the other composites derived from the other deposition times. The spectrum showed appearance of a broad peak at 431 cm⁻¹ was corresponded to the S2 band of SnO₂, while the peak at 767 cm⁻¹ was due to B2g mode of SnO₂. This resultant is similar to the previous work of Haraiati T. 2009 [97].

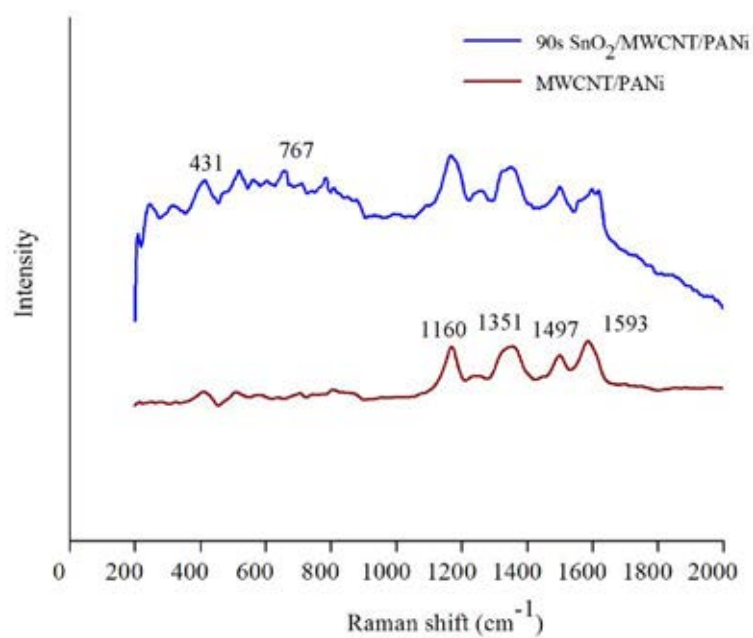


Figure 4.51 Raman spectra of the PANi/MWCNT and the PANi/MWCNT/SnO₂NP composite derived from a SnO₂NP deposition time of 90 second

4.4.2.3 Thermal behavior of PANi/MWCNT and PANi/MWCNT/SnO₂ nanoparticle

Thermogravimetric analysis of PANi/MWCNT and PANi/MWCNT/SnO₂ were investigated under O₂ atmosphere at 10 °C min⁻¹ from 50 – 800 °C. The TGA thermograms of the PANi/MWCNT and PANi/MWCNT/SnO₂, derived from SnO₂NP deposition times of 120 and 150 second as representative examples, are shown in Figure 4.52.

The PANi/MWCNT composite revealed a typical two-step weight loss. The first stage of decomposition, at a temperature of up to 100 °C, is attributed to the loss of water molecules. The second step, at approximately 180 °C upwards, corresponded to the decomposition temperature of the polyaniline backbone and MWCNT. The PANi/MWCNT was almost completely oxidized at approximately 700 °C. In the case of the various PANi/MWCNT/SnO₂NP composites, they exhibited similar thermograms to that of the PANi/MWCNT. Its first step was also assigned to the loss of water molecules at 100 °C. Similarly, the skeleton of polyaniline and MWCNT backbone started to oxidize and decompose at 180 °C. However, compared with that for PANi/MWCNT, the PANi/MWCNT/SnO₂NP composites started to oxidize at a relatively higher temperature in terms of the onset of the oxidation temperature and this increased slightly with the comparatively longer SnO₂NP deposition times. Moreover, the PANi/MWCNT/SnO₂ composites also showed a slightly higher percent weight residue than the PANi/MWCNT, which would be due to the high thermal stability of the SnO₂NPs in the composite.

For shorter SnO₂NPs deposition times, (i.e., 60 and 90 second) PANi/MWCNT/ SnO₂NPs showed similar thermal behavior to that of the PANi/MWCNT. No significant differences from the effect of SnO₂ NPs in these TGA thermograms was observed probably due to the low amount SnO₂NPs in the composite.

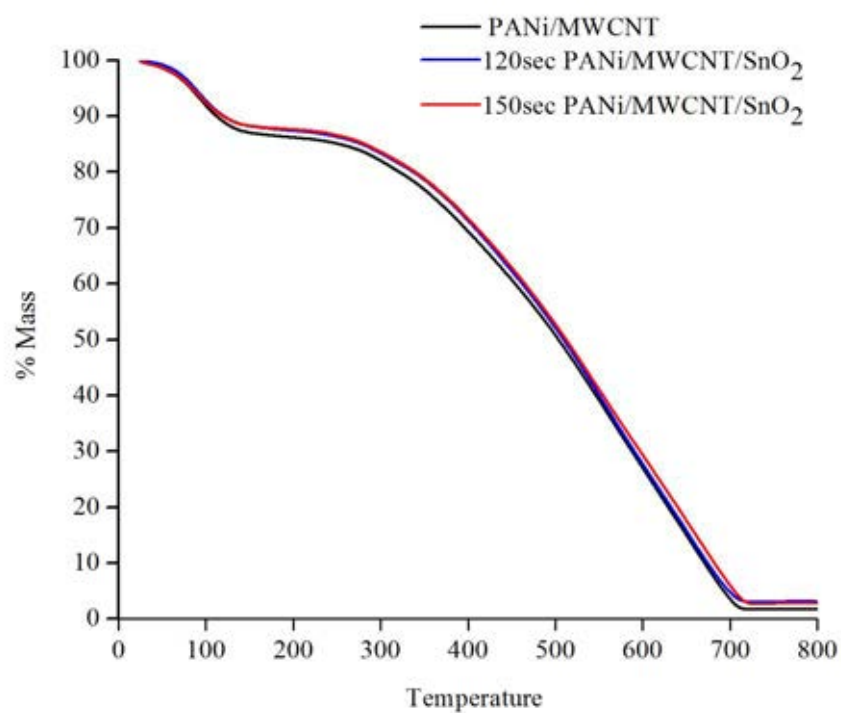


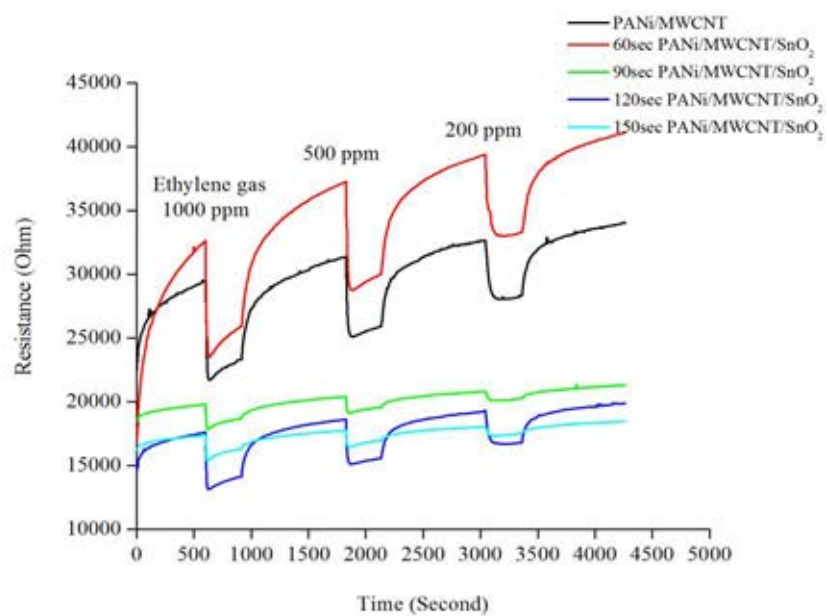
Figure 4.52 TGA thermograms of the PANi/MWCNT and PANi/MWCNT/SnO₂NP composite derived from SnO₂NP deposition times of 120 and 150 second

4.4.3 Ethylene gas detection via resistance measurement of PANi/MWCNT and PANi/MWCNT/SnO₂ nanoparticle

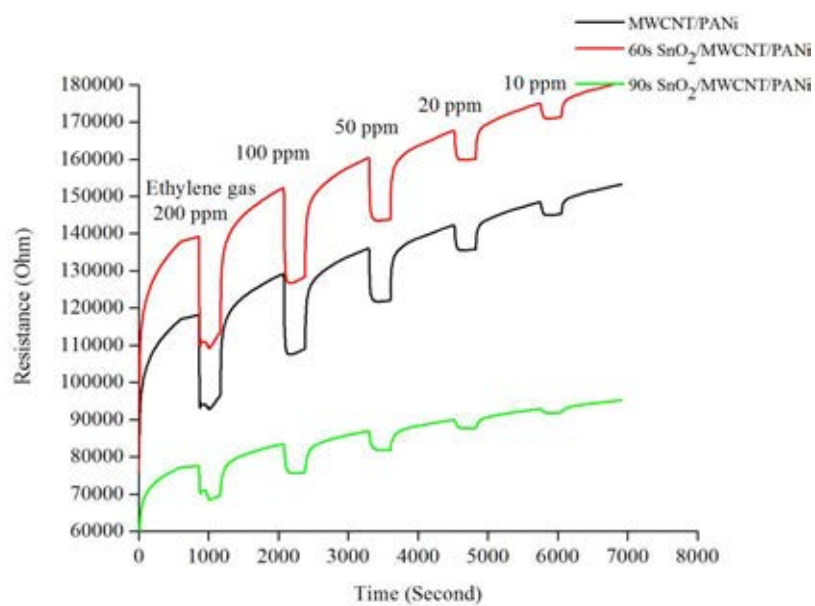
The response–recovery characteristics of the PANi/MWCNT/SnO₂NPs composites with different SnO₂NPs loadings (that is derived from different SnO₂NP deposition times) at different ethylene gas concentration are shown as in figure 4.53(a) for 1 month aging and 4.53(b) for 3 month aging. The sensing magnitudes of PANi/MWCNT/SnO₂NPs with different SnO₂NPs loadings at different ethylene gas concentration are presented in Figure 4.54(a) for 1 month and 4.54(b) for 3 month aging.

The respond behaviour after being exposed to ethylene gas, the entire sensor responded by a decrease in its resistance as shown in Figure 4.53. This is due to the nanofibril structure of PANi-MWCNT, which subserves to the diffusion of ethylene gas and is also attributed to the ease of expansion of the compact form of the PANi-MWCNT chain [x]. For the first month of aging, the sensing magnitude of the SnO₂NP/ PANi/MWCNT composite derived from a 60 sec SnO₂NP deposition time displayed the highest sensitivity, and this decreased for the composites, in the order of the SnO₂NP deposition time, as 60 sec > 0 sec (no SnO₂NP) > 90 sec > 120 sec > 150 sec (Figure 4.54(a)). The effect of the addition of SnO₂NPs into the PANi/MWCNT for ethylene gas detection is still unresolved.

Moreover, after three months aging, the PANi/MWCNT/SnO₂NP composites showed a substantial increase in their sensing magnitude against ethylene gas and can detect ethylene gas at levels as low as 10 ppm in the case of the composites with a SnO₂NP deposition time of 0, 60, and 90 sec (Figure 4.54(b)). The PANi/MWCNT/ SnO₂NP composite derived from a SnO₂NP deposition time of 60 sec exhibited the highest sensitivity for the detection of ethylene gas at 10 ppm, with a change in the sensing magnitude of about 2.42%, followed by the PANi/MWCNT, with that for the PANi/MWCNT/SnO₂NP composite derived from a 90 sec SnO₂ deposition time being significantly lower.

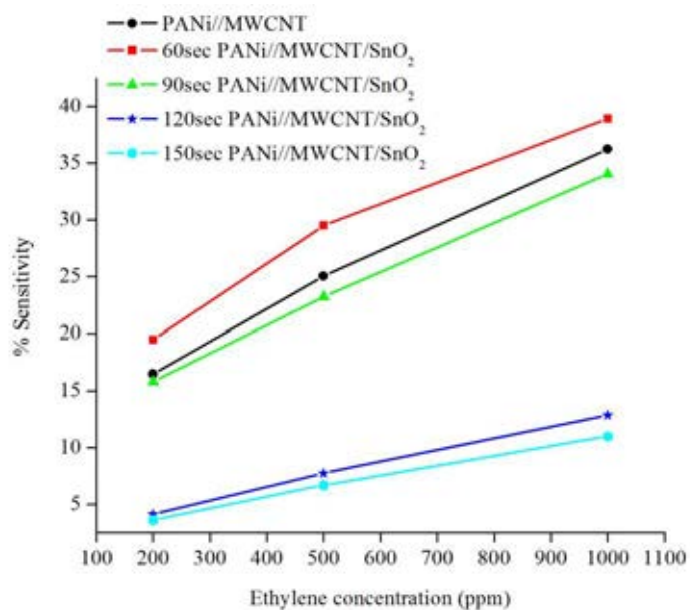


(a)

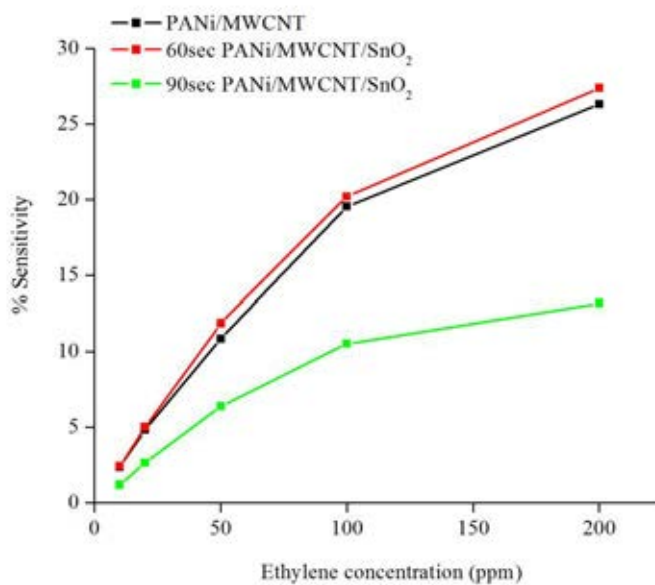


(b)

Figure 4.53 The resistance response of PANi/MWCNT/SnO₂NP composites derived from different SnO₂NP deposition times after (a) 1 month and (b) 3 months ageing



(a)



(b)

Figure 4.54 The sensitivity behavior of the PANi/MWCNT/SnO₂NP composites derived from different SnO₂NP deposition times after (a) 1 month and (b) 3 months aging

CHAPTER V

CONCLUSIONS

The ethylene gas detection based on polyaniline (PANi) and/or PANi composites was successfully fabricated on interdigitated gold substrate by electrochemistry method. The four step methods were used to develop polyaniline and/or PANi composites sensor for gas ethylene detection. All of the result products were characterized. All of the possible variables were explored for enhancing ethylene gas sensing include of the effect of amount deposited polyaniline, the effect of acid dopant, the effect of multiwall carbon nanotube and the effect of tin oxide nanoparticle. The results are summarized as follows.

In first step, the sensitive layer PANi was achieved by cyclic voltammetry method.

- The optimum conditions was carried out by cyclic voltammetry method under applying continuous potential cycle ranging from -0.3-1 V with scanning rate 10 mV/s was 10 scan of cyclic voltammetry. The resulting product is PANi with sulfonate ion.
- The PANi with sulfonate ion exhibited evidence of polymerization as the presence of eight important transmittance bands at 1556 cm^{-1} (C=N of quinoid ring), 1470 cm^{-1} (C-H stretching of benzoid ring), 1303 cm^{-1} (C-N stretching), 1237 cm^{-1} (C-N stretching), 1135 cm^{-1} (C-H stretching of quinoid ring), 800 cm^{-1} (C-H bending of benzoid), 878 cm^{-1} (C-H bending of benzoid), and 1078 cm^{-1} (SO_4^{2-} group).
- SEM micrographs of PANi revealed structure development from bulk film to nano fibril/micro bead film as increasing amount of deposited PANi by increasing number of cyclic voltammetry from 5 to 25 scans of cyclic voltammetry. The nano fibril structure of PANi film was successfully obtained under applying continuous potential cycle ranging from -0.3-1 V with a scanning rate of 10 mV/s at 10 scan of cyclic voltammetry.

- The PANi film responded ethylene gas by undergoing a decrease in its resistance response and sensed against ethylene gas with almost linear dependence of the signal on ethylene concentration in the parts per million ranges. The deposit PANi at 10 scan of cyclic voltammetry exhibited the highest sensitivity for detection ethylene gas at 200 ppm with a change in the sensing magnitude of about 10.79 % and this sensitivity decreased in the order of deposited PANi as the number of cyclic voltammetry as 10 CV > 15 CV > 20 CV > 25 CV > 5 CV.

In second step, the sensitive layer PANi was improved ethylene sensing property by acid doping process.

- Based on UV-VIS spectroscopy technique, the degree protonation of acid dopant on PANi was investigated. The result showed that a higher acid concentration dopant of PANi gave a higher bipolaron/polaron state.
- The PANi with different acid dopants exhibited evidence of acid dopant by the characteristic peaks of acid anion, depending on each type of acid dopant. PANi dope with HCl, H₂SO₄, H₃PO₄, TSA and DBSA exhibited the characteristic peak of Cl⁻, SO₄²⁻, vibration mode of P=O, sulphinic ester anion and sulphoxide anion at 1120, 979, 1108, 1033 and 1006 cm⁻¹.
- The thermal stability of polyaniline was strongly dependent upon on the counter ions of acid dopant. PANi-H₃PO₄ exhibited the highest thermal stability and displayed significant weight losses of dopant and polyaniline skeletal at about 200-600 °C. PANi-H₂SO₄ displayed two steps weight loss at 168 and 400 °C which were attributed to the degradation of acid dopant and PANi skeletal, respectively. PANi-HCl displayed two step weight losses of dopant at 180-300°C and skeletal of polyaniline at 350°C. PANi-DBSA and PANi-TSA showed step weight loss of acid dopant at approximately 250 °C.
- Different acid dopants had effect on the morphology of polyaniline. The using of phosphoric and sulfuric acid did not affect on morphology of PANi nano fibril. However, using of HCl, TSA, and DBSA as acid dopant at high

concentration (more than 0.05 mole) showed different morphology because of an agglomeration of acid anion into morphology of PANi in which its dimension was increased with increasing of acid anion concentration.

- Comparing the effects of different acid dopant on ethylene gas detection, the PANi doped with H₂SO₄ sensor revealed the highest sensitivity against ethylene gas and decreased in order of PANi-H₂SO₄>PANi-H₃PO₄>PANi-TSA>PANi-DBSA. After three months aging, polyaniline doped with sulfuric acid at 0.1 M showed the highest sensitivity against ethylene gas detection. (Increase sensitivity from 5.68% to 24% for 200 ppm ethylene gas and respond ethylene gas at 10 ppm with 2.94 % sensitivity).

In third step, composited sensor modified functional polyaniline-multiwall carbon nanotubes (PANi/MWCNT) were achieved.

- PANi/MWCNT sensitive layer was successfully fabricated by electro-polymerization the suspension solution of 0.1 M aniline/MWCT in 1M sulfuric solution with cyclic voltammetry under applying continuous potential cycle in ranging from -0.3-1 V with a scanning rate of 10 mV/s.
- The raman spectroscopy confirmed the existence of two usual bands of multiwall carbon nanotube in PANi/MWCNT composite by appearance of characteristic peaks at 1278 and 1593 cm⁻¹ which were corresponded to D-band and G-band, respectively.
- As evidence by SEM image, the introduction of MWCNT into PANi led to increase three-dimensional network of nanofibril morphology of polyaniline in which its dimension was increased with an increasing of % MWCNT loading. This result was due to formatted structure of MWCNT which created more active sites for condensation of nuclei during the chain growth.
- The introduction of MWCNT in PANi attributed to an increase in thermal stability and onset of oxidation temperature with % MWCNT loading. PANi/MWCNT composited displayed two significant weight losses at about

100 °C and 150 °C which are corresponding to the decomposition of water molecule and skeletal of polyaniline/multiwall carbon nanotube, respectively.

- The addition MWCNT in PANi did not showed efficiency to increase sensitivity against ethylene gas in first month aging. However, after three month aging, the 0.2 % wt. multiwall carbon nanotube/polyaniline showed the highest sensitivity but its sensitivity against ethylene gas decreased with increasing of multiwall carbon nanotube loading. (Sensitivity increased from 2.94% (PANi) to 4.39% (PANi/MWCNT) for detection 10 ppm of ethylene gas.)

In forth step, a hybrid modified functional polyaniline-multiwall carbon nanotube and tin oxide nanoparticles (PANi/MWCNT/SnO₂) were achieved.

- PANi/MWCNT/ SnO₂NPs comprised of a multilayer composite material was successfully synthesized by electrophoretic deposition of tin oxide nanoparticle onto a gold interdigitated substrate and then chronoamperometric deposition of the PANi/MWCNT film from an aniline/MWCNT solution.
- SEM analysis showed uniform distribution of the SnO₂NPs on the surface of the interdigitated gold with different deposition time and the level of deposition of the SnO₂NPs increased with an increasing of deposition time.
- The three-dimensional nanofibril network of PANi/MWCNT nanotube layer was successfully carried out by chronoamperometric deposition at 1 V with deposition time in the range of 120-150 second.
- As evidence of raman spectroscopy, the presence of MWCNT in PANi composite was confirmed at 1351 (D-band) and 1593 cm⁻¹ (G-band). Meanwhile, the presence of SnO₂NPs in PANi was confirmed at 431 cm⁻¹ (S2 band) and 767 cm⁻¹ (B2g mode of SnO₂).

- PANi/MWCNT/SnO₂ NPs composites displayed oxidize and decompose of polyaniline/multiwall carbon nanotube at 180 °C. The introduction SnO₂ NPs in PANi/MWCNT attributed to an increase in thermal stability and onset of oxidation temperature with % SnO₂ NPs loading.
- The addition SnO₂ NPs in PANi/MWCNT did not show efficiency to increase sensitivity against ethylene gas in first month aging. After three months aging, the addition SnO₂ NPs at deposition time 60 second in the PANi/MWCNT composites exhibited the sensitivity against ethylene gas at 10 ppm (with sensitivity 2.4%, nearly same PANi/MWCNT) and its sensitivity decreased with increasing SnO₂ NPs.

References

- [1.] Coombe, B. G., Research on Development and Ripening of the Grape Berry Am J Enol Vitic 43 (1992):101-110.
- [2.] Hua, B., Gaoquan S., Gas Sensors Based on Conducting Polymers. Sensors 7 (2007): 267-307.
- [3.] Jiaying, H., Syntheses and applications of conducting polymer polyaniline nanofibers. Pure Appl. Chem. 78 (2006): 15–27.
- [4.] Jens, R., Parisi, J. R., Derck, S., Electrochemical growth of gas-sensitive polyaniline thin films across an insulating gap. Thin Solid Films 466 (2004): 320-325.
- [5.] Agbor, N. E., Petty, M. C. Monkman, A. P., Polyaniline thin film for gas sensing. Sensors and Actuators B 28 (1995):173-179.
- [6.] Manoj, K. R., Yavuz, O. Z. Y., Lahsangah V., Aldissi, M., CO gas sensing from ultrathin nano- composite conducting polymer film. Sensors and Actuators B 106 (2005):750–757.
- [7.] Shanzuo J., Yang, L., Mujie, Y., Gas sensing properties of a composite composed of electrospun poly(methyl methacrylate) nanofibers and in situ polymerized polyaniline. Sensors and Actuators B 133(2008):644-649.
- [8.] Shabnam, V., Jiaying, H., Richard, B, K., Bruce H. W., Polyaniline Nanofiber Gas Sensors: Examination of Response Mechanisms. Nano Lett. 4(2004):491-496.
- [9.] Campos M., Bulhoões, L. O. S., Cleber, A. L., Gas-sensitive characteristics of metal /semiconductor polymer Schottky device. Sensors and Actuators (2000) 87:67–71.
- [10.] Anjali, A. A., Milind, V. K., Polyaniline and its substituted derivatives as sensor for aliphatic alcohols. Sensors and Actuators B 67(2000): pp.173-177.
- [11.] Haibin, Z., Jixiao, W., Zhi, W., Fengbao, Z., Shichang, W., Electrodeposition of polyaniline nanostructures: A lamellar structure. Synthetic Metals 159(2009): 277-281.

- [12.] Dominique, N. F., Poncin, E., Polyaniline as a new sensitive layer for gas sensors. Analytica Chimica Acta (2003) 475: 1–15.
- [13.] Ulmann, M., Kostecki, R., Augustynski J., Strike, D.J., Koudelka-Hep, M., Modification des polymères conducteurs avec de petites particules métalliques. Chimia 46 (1992) 138–140.
- [14.] Qifei, C., Kai, Z., Xing, C., Minqiang, L. Jinhui, L., Preparation of gold/polyaniline/multiwall carbon nanotube nanocomposites and application in ammonia gas detection. J Mater Sci 43(2008):5861–5866.
- [15.] Wikimedia Foundation, Inc. Ethylene. Wikipedia [online]. 2005. Available from: <http://en.wikipedia.org/wiki/Ethylene> [2011, May]
- [16.] Farlex, Inc. Ethylene. The free dictionary [online].2005 Available from: [http://encyclopedia2.thefreedictionary.com/Ethylene+\(plant+hormone\)](http://encyclopedia2.thefreedictionary.com/Ethylene+(plant+hormone)) [2011, May]
- [17.] Wikimedia Foundation, Inc. Ethylene gas. Wikipedia [online]. 2005. Available from: <http://en.wikipedia.org/wiki/Ethylene> [2011, May]
- [18.] Yang, S. F., Hoffman, N. E., Ethylene biosynthesis and its regulation in higher plants. Ann. Rev. Plant Physiol 35(1984): 155–89.
- [19.] Pheltelket, B. K. Ripeness. nepostharvest [Online]. 2008 Available from: <http://nepostharvest.com/ripening.htm#controlledatmosphereripening> [2011, May]
- [20.] Stanley, P. B., Ethylene, Plant Senescence and Abscission. Plant Physiol 43 (1968):1503-1511.
- [21.] Heeger, A.J., Synth. Met. 125 (2002):23–42.
- [22.] MacDiarmid, A.G., Synth. Met. 125 (2002):11–22.
- [23.] Sambhu, B., Dipak, K., Nikhil, K. S., Joong, H. L., Progress in Polymer Science 34 (2009):783–810.
- [24.] Unsworth, J., Lunn, B. A., Innis, P. C., Jin, Z. Kaynak, A., Booth, N.G., Technical review: conducting polymer electronics. J Intel Mat Syst Str 3 (1992):380–95.
- [25.] Shirakawa, L. H., MacDiarmid, A.G, Chiang, C.K., Heeger, A.J., Synthesis of electrically conducting organic polymers: halogen derivatives of polyacetylene, (CH)_x. J Chem Soc Chem Commun (1977):578–580.

- [26.] Wikimedia Foundation, Inc. Band gap Energy. Wikipedia [online]. 2005. Available from: http://en.wikipedia.org/wiki/Band_gap [May, 2011]
- [27.] Colin P. Conductive polymer . Ntlworld[Online]. 1996. Available from: <http://homepage.ntlworld.com/colin.pratt/cpoly.pdf> [May,2011]
- [28.] Dominique, N.D., Fabienne, P.E., Polyaniline as a new sensitive layer for gas sensors Analytica Chimica Acta 475 (2003): 1–15.
- [29.] Rao, P. S., Sathyanarayana, D. N., Jeevananda, T., In Advanced Functional Molecules and Polymers, Nalwa, H. S. (ed.), Gordon B., 79. Tokyo: Vol.3, 2001.
- [30.] Heeger, A. J. Angew Chem. Int. Ed. 40(2001):2591.
- [31.] Oltorf, P. Conductive polymer . fortunecity.com [online].2000. Available from: <http://meltingpot.fortunecity.com/oltorf/601/introduction.html> [May, 2011]
- [32.] Stafstrom, S., Bredas, J.L., Polaron lattice in highly conducting polyaniline: Theoretical and optical studies. physical review letters 59 13 (1987) : 1464-1467.
- [33.] Zhang, X. et al., Synthetic Metals 145 (2004):23–29.
- [34.] Yan, X.B. et al., Sensors and Actuators B 123 (2007):107–113.
- [35.] Zhixiang, W. et al., Langmuir 18 3 (2002).
- [36.] Jiaying, H., Richard, B. K., A general chemical route to polyaniline nanofibers. J. AM. CHEM. SOC. 126 (2004):181-185.
- [37.] Agbor, N E., Petty, M. C. Monkman, A.P., Polyaniline thin film for gas sensing. Sensors and Actuators B 28(1995):173-179.
- [38.] Shabnam, V., Jiaying, H., Richard, B. K., Bruce, H. W., Polyaniline Nanofiber Gas Sensors: Examination of Response Mechanisms. Nano Lett. 4 (2004): 491-496.
- [39.] Manoj, K. R., Yavuz, O. Z. Y., Lahsangah, V., Aldissi, M., CO gas sensing from ultrathin nano- composite conducting polymer film. Sensors and Actuators B 106 (2005): pp. 750–757.
- [40.] Jens, R., Parisi, J. R., Derck, S., Electrochemical growth of gas-sensitive polyaniline thin films across an insulating gap. Thin Solid Films 466 (2004):320-325.
- [41.] Wikimedia Foundation, Inc. Electrochemistry. Wikipedia [online]. 2005. Available from: <http://en.wikipedia.org/wiki/Electrochemistry> [May, 2011]

- Sawyer, D.T., Sobkowiak, A., Roberts, J.L.Jr., Electrochemistry for chemists 2nd ed. New York: John Wiley & Sons, Inc., 1995.
- [42.] Monk, P. M.S., Fundamentals of Electroanalytical chemistry New York: John Wiley & Sons, New York, Inc., 2001.
- [43.] Lakshmi, A. K. Electrochemical cell. Ustudy of MSPVL Polytechnic College [Online]. 2008. Available from: <http://www.ustudy.in/node/3217> [May, 2011]
- [44.] Koti, P. Potentiometry. Medical chemistry Note[Online].2008. Available from: http://tera.chem.ut.ee/~koit/arstpr/pot_en.pdf [May, 2011]
- [45.] Bard, A. J., Faulkner, L. R., Electrochemical methods : fundamentals and applications New York: John Wiley & Sons, New York, Inc., 1980.
- [46.] Chang, T. Cyclic voltammetry. University of Cambridge[Online].2005. Available from: <http://www.cheng.cam.ac.uk/research/groups/electrochem/teaching.html> [May, 2011]
- [47.] Skoog, D.A. and Leary, J.J., Principles of Instrumental Analysis 4th Ed. New York: Harcourt Brace College Publishers, 1992.
- [48.] Eggins., Brain Biosensors: An introduction New York: John Wiley & Sons, Inc., 1996.
- [49.] Wikimedia Foundation, Inc. Nernst equation . Wikipedia [online]. 2004. Available from: http://en.wikipedia.org/wiki/Nernst_equation [May, 2011]
- [50.] Andrienk, K. cyclic voltammetry. Journal club[Online].2004. Available from: http://www.mpipmainz.mpg.de/~andrienk/journal_club/cyclic_voltammetry.pdf [May, 2011]
- [51.] Douglas C., Joel, D. and Martin, L., Chem. Mater. 7(1995): 1504-1509.
- [52.] Haibin, Z., Jixiao, W., Zhi, W., Fengbao, Z., Shichang, W., Electrodeposition of polyaniline nanostructures : A lamellar structure. Synthetic metals 159 (2009): 227-281.
- [53.] Dominique, N. F., Poncin, E., Analytica Chimica Acta 475(2003):1–15.
- [54.] Jens, R., Jürgen, P., Derck, S., Electrochemical growth of gas-sensitive polyaniline thin films across an insulating gap. Thin Solid Films 466 (2004):320– 325.

- [55.] Hussain, A. M., Kumar, A., Electrochemical synthesis and characterization of chloride doped polyaniline. Bull. Mater. Sci. 26 3 (2003): 329–334.
- [56.] Ulrich, L., Nataliya, V. R., Vladimir, M. M., Conducting polymers in chemical sensors and arrays. Analytica chimica acta 6 14 (2008):1–26.
- [57.] Anjali, A. A., Milind, V. K., Polyaniline and its substituted derivatives as sensor for aliphatic alcohols. Sensors and Actuators B 67 (2000):173-177.
- [58.] Shanzuo, J., Yang. L., Mujie. Y., Gas sensing properties of a composite composed of electrospun poly(methyl methacrylate) nanofibers and in situ polymerized polyaniline. Sensors and Actuators B 133(2008): 644-649.
- [59.] Shabnam, V., Richard, B., Bruce, H. W., Hydrogen sensor based on conductivity changes in polyaniline nanofibers. J. Phys. Chem. B 110(2006): 22266-22270.
- [60.] Xiaoxia, J., Lei, Y., Xiangqun, Z., Enhancing the sensitivity of ionic liquid sensors for methane detection with polyaniline template. Sensors and Actuators B 133(2008):526–532.
- [61.] Mangu, R., Rajaputra, S. Singh, V.P., MWCNT-polymer composites as highly sensitive and selective room temperature gas sensors. Nanotechnology 21 (2011): 22.
- [62.] Wikimedia Foundation, Inc. Multi wall carbon nanotube. Wikipedia [online]. 2004. Available from: http://en.wikipedia.org/wiki/Carbon_nanotube [May, 2011]
- [63.] Netsons, D. E., Drupal I. Multi wall carbon nanotube. Mavimo[Online]. 2000. Available from: <http://mavimo.org/chimica/nanotube> [May, 2011]
- [64.] Woo, S. C., Seung, i. M., Yang, D. L., Yun, H. L., Jung, H. P., Byeong, K. J., Electron Device Letters. 26 7:498-500.
- [65.] Ting, Z., Syed, M., Nosang, V. M. Deshusses, M. A., Recent progress in carbon nanotube-based gas sensors. Nanotechnology 19(2008):33.
- [66.] Liping, Z., Mansoo, C., Hyun-Su, K., Seong-Hyeon, H., The effect of multiwalled carbon nanotube doping on the CO gas sensitivity of SnO₂-based nanomaterials. Nanotechnology 18 (2007): 44.

- [67.] Abdullah, H.Z., Taib, H., Serrell, C.C., Coating Methods for Self-Cleaning Thick Films of Titania. Advances in applied Ceramics 106 [1/2] (2007): 105-112.
- [68.] Gaver, C.C., in Kroschwitz J.i., Howe-Grant M. (Eds.), Kirk-Othmer Encyclopedia of Chemical Technology. vol. 4. USA: John Wiley & Sons: 2001:105-122.
- [69.] Hahn, S., SnO₂ thick film sensors at the ultimate limits. Ph.D. Thesis University Tübingen, 2002.
- [70.] Heiland, G., Homogeneous semiconducting gas sensor. Sensors and Actuators 2(1982):343- 361
- [71.] Lalauze, R., Pijolat, C., A new approach to selective detection of gas by an SnO₂ solid-state sensor. Sensors and Actuators A 5 (1984):55-63
- [72.] Windischmann, H., Mark P., J. Electro. Chem. 26 (4) (1979):627-633.
- [73.] Lar, B. How sensor work. biosystems application note [Online]. 2000. Available from: http://www.brandtinst.com/biosystems/appnotes/Downloads/7.%20How_Electrochemical_Sensors_Work.pdf [May, 2011]
- [74.] Toshiwal Sensors Pvt. Ltd. Gas sensor. Tsdpl [Online]. 2005. Available from: <http://www.tsdpl.com/TGS-2000.htm> [May, 2011]
- [75.] Weh, T., Fleischer, M., Meixner, H., Optimization of physical filtering for selective high temperature H₂ sensors. Sensors and Actuators B 68 (2000):146–150.
- [76.] Wikimedia Foundation, Inc. Electrophoretic deposition. Wikipedia [online]. 2004. Available from: http://en.wikipedia.org/wiki/Electrophoretic_deposition [May, 2011]
- [77.] Boccaccini, A.R., Zhitomirsky, I. Application of electrophoretic and electrolytic deposition techniques in ceramics processing. Current Opinion in Solid State and Materials Science 6 [3] (2006):251-260.
- [78.] Zhitomirsky, I., Cathodic electrodeposition of ceramic and organoceramic materials Fundamental aspects. Advances in Colloid and Interface Science 97 [1-3] (2002):277-315.
- [79.] Sarkar, P., Nicholson, P.S., Electrophoretic Deposition (EPD): Mechanisms, Kinetics, and Application to Ceramics. Journal of the American Ceramic Society 79[8] (1996):1987-2002

- [80.] Heavens, S.N., Electrophoretic Deposition as a Processing Route for Ceramics, Advanced Ceramic Processing and Technology pp. 255-279. New Jersey: William Andrews Publishing/Noyes, 1990.
- [81.] Besra, L., Liu, M. A., review on fundamentals and applications of electrophoretic deposition (EPD). Progress in materials Science 52[1] (2007):1-62
- Bergstrom, L., Colloid Processing of Ceramics, Handbook of Applied Surface and Colloid Chemistry pp. 201-218. England: John Wiley & Sons Ltd., West Sussex, 2001.
- [82.] Van der Biest, O.O., Vandepere, L.J., Electrophoretic Deposition of Materials. Annual Review of Materials Science 29[1] (1999):327-325.
- [83.] Cao, G., Nanostructures & Nanomaterials – Synthesis, Properties & Applications, Imperial College Press, London, UK, (2004).
- [84.] Lewis, J.A., Colloidal Processing of Ceramics, Journal of the American Ceramic Society 83[10] (2000): 2341-2359.
- [85.] Sarkar, P., Nicholso, P. S., electrophoretic Deposition (EPD): Mechanisms, Kinetics, and Application to Ceramics. Journal of the American Ceramic Society 79[8] (1996): 1987–2002.
- [86.] Dao-jun, G., Hu-lin, Li., Well-dispersed multi-walled carbon nanotube/polyaniline composite films Journal of Solid State Electrochemistry 9 [6]: 445-449.
- [87.] Genies, E. M., Syed, A.A., Tsintavis, C., Electrochemical Study of Polyaniline In Aqueous And Organic Medium. Redox and Kinetic Properties. Molecular Crystals and Liquid Crystals. 1211-4 (1985):181-186.
- [88.] Chen, S.A., Lin, L.C., Polyaniline Doped by the new class of dopant, ionic salt: Structure and properties. Macromolecules, 28(1995):1239-1245.
- [89.] Milton, A.J., Monkmon, A.P.A., Comparative study of polyaniline films using thermal analyses and IR spectroscopy. Journal of Physical D: Apply Physics, 26 (1993):1468-1474.
- [90.] John,A.D., Lange' s Handbook of chemistry. 13th ed. New York: McGraw-Hill Book Company, 1987.
- [91.] Koenig, J. L., Spectroscopy of polymers. 2nd ed. Amsterdam: Elsevier, 1999.

- [92.] Pavia, D. L, Lampman G. M., Kriz G S., Introduction to spectroscopy 3rd ed. Fort Worth: Harcourt College Publishers, 2001.
- [93.] Lili, D., Xingwu, W. Gregory, R. V., Thermal properties of chemically synthesized polyaniline (EB) powder. Synthetic Metals, 104 2 (1999):73-78.
- [94.] Fan, H., Estelle, V., Chen, De., In situ polymerization and characterizations of polyaniline on MWCNT powders. Catalysis Today, 150 (2010):71–76.
- [95.] Jing, Z., Ling-Bin, K., Bin, W., Yong-Chun, L., Long, K., In-situ electrochemical polymerization of multi-walled carbon nanotube/polyaniline composite films for electrochemical supercapacitors. Synthetic Metals, 159 3-4, (2009): 260-266.
- [96.] Haraiati, T., 2009. Synthesis and electrophoretic deposition of tin oxide (SnO₂). Ph.d. Material Science and Engineering. Faculty of Science University of New South Wales.

Appendices

Appendix A

TableA1 Result of deposited PANi at various number of cyclic voltammetry

Batch	Weight Before	Weight After	%Weight Increase
102	1.4233	1.4244	0.077285182
103	1.427	1.428	0.070077085
104	1.5723	1.5735	0.076321313
105	1.4485	1.4494	0.062133241
151	1.5414	1.5424	0.064876087
152	1.5496	1.5525	0.18714507
153	1.6285	1.6298	0.079828063
154	1.464	1.4635	-0.034153005
155	1.5449	1.5464	0.097093663
201	1.5347	1.5368	0.136834561
202	1.5357	1.5373	0.104187016
203	1.4633	1.4654	0.143511242
204	1.5412	1.5428	0.103815209
251	1.477	1.4761	-0.060934326
252	1.5826	1.5817	-0.056868444
253	1.5821	1.5848	0.17065925
254	1.5686	1.5709	0.146627566

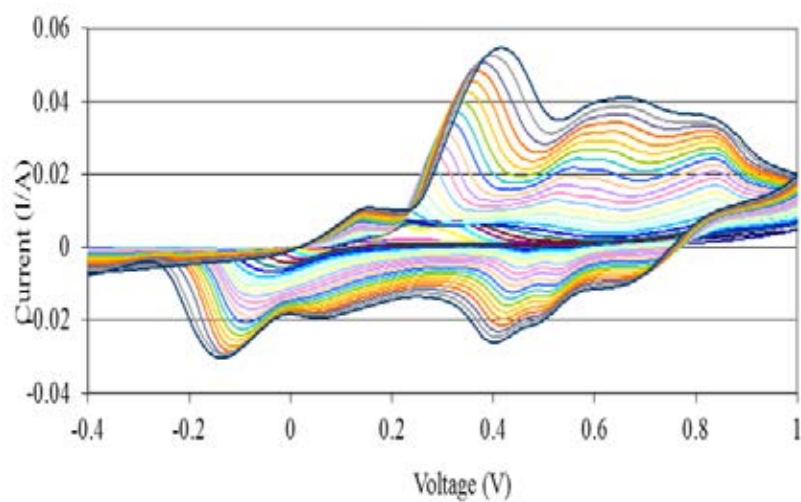


Figure A1 Cyclic voltammograms of polyaniline film growth at varying 1 to 25 of number of scan with a scanning rates of 50 mV/Sec

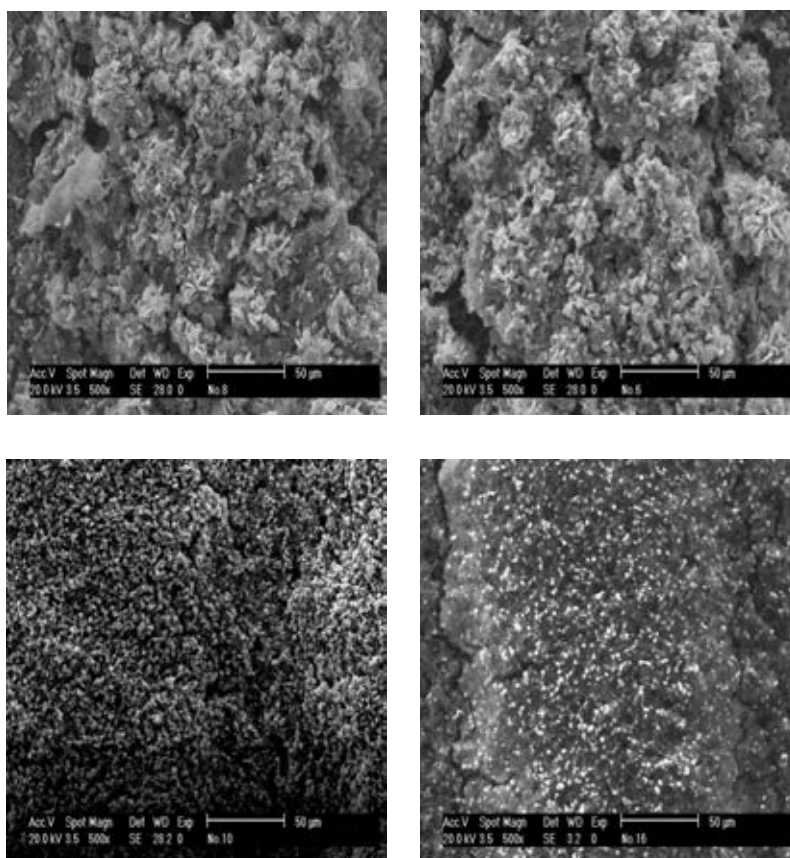


Figure A2 SEM images of PANi prepared by cyclic voltammetry on interdigitated gold substrate at different numbers scan of cyclic voltammetry: (a) 8 scans (b) 9 scans (c) 10 scans (d) 15 scans

TableA2 Sensitivity of PANi against ethylene gas at different amount of PANi after 1 month (different cyclic voltammetry(CV))

No. of scan CV \ Ethylene gas	10 cv	15 cv	20 cv	25 cv
1000 ppm	27.07401	23.04112	16.93532	5.28169
500 ppm	17.74421	16.85546	12.89314	4.55293
200 ppm	10.79256	10.77246	8.41924	4.45765

TableA3 Sensitivity of PANi against ethylene gas at different H₂SO₄ concentration after 1 month

H ₂ SO ₄ Conc. \ Ethylene gas	0.01	0.025	0.05	0.075	0.1
1000 ppm	21.94146	12.25439	17.58458	14.89362	11.11111
500 ppm	14.59574	8.76149	12.04908	10.66667	6.89655
200 ppm	8.52008	5.13314	7.23639	6.28931	4.06504

TableA4 Sensitivity of PANi against ethylene gas at different H₃PO₄ concentration after 1 month

H ₃ PO ₄ Conc. \ Ethylene gas	0.01 mole	0.025 mole	0.05 mole	0.075 mole	0.1 mole
1000 ppm	40.46193	41.41747	48.67725	49.90837	63.31084
500 ppm	25.55556	26.73428	29.66292	30.23882	47.22605
200 ppm	13.99043	14.91369	16.27451	20.6431	24.51213

TableA5 Sensitivity of PANi against ethylene gas at different TSA after 1 month

TSA Conc. \ Ethylene gas	0.01 mole	0.025 mole	0.05 mole	0.075 mole	0.1 mole
1000 ppm	1.4014	8.39544	8.77193	0	0
500 ppm	0.5901	4.66311	5.7377	0	0
200 ppm	0.5369	2.11462	3.125	0	0

TableA6 Sensitivity of PANi against ethylene gas at different DBSA concentration after 1 month

DBSA Conc. / Ethylene gas	0.01 mole	0.025 mole	0.05 mole	0.075 mole	0.1 mole
1000 ppm	1.82753	2.72562	5.20833	5.5	6.25
500 ppm	0.90652	1.55131	3.06122	3.2	4.61538
200 ppm	0.28137	0.76741	2	2.4	2.98507

TableA7 Sensitivity of PANi against ethylene gas at different H₃PO₄ concentration after 3 month

H ₃ PO ₄ Conc. / Ethylene gas	0.01	0.025	0.05	0.075	0.1
200 ppm	15.15178	12.60904	12.47653	0	0
100 ppm	11.16866	9.34419	10.58621	0	0
50 ppm	5.68901	4.24266	4.15653	0	0
20 ppm	2.87909	2.21721	2.3104	0	0
10 ppm	2.04456	1.66608	1.649	0	0

TableA8 Sensitivity of PANi against ethylene gas at different H₂SO₄ concentration after 3 month

H ₂ SO ₄ Conc. / Ethylene gas	0.01	0.025	0.05	0.075	0.1
200 ppm	26.69408	33.55818	31.76101	30.99174	35.54377
100 ppm	19.20657	25.52438	24.04227	23.02405	26.55246
50 ppm	11.2323	15.11084	13.89208	12.42604	14.70054
20 ppm	4.75661	6.44178	5.8104	6.86016	5.71429
10 ppm	2.2662	3.1597	2.849	2.46305	2.94118

TableA8 Sensitivity of PANi against ethylene gas at different TSA concentration after 3 month

TSA Conc. Ethylene gas	0.01	0.025	0.05	0.075	0.1
200 ppm	3.27828	7.66333	7.71502	7.93651	0
100 ppm	1.25499	3.89444	3.50318	4.44444	0
50 ppm	0.44593	2.6841	3.06748	3.59712	0
20 ppm	0	0	0	0	0
10 ppm	0	0	0	0	0

Table A9 The sensing magnitude of the PANi-H₂SO₄ at different concentrations after 6 months

H ₂ SO ₄ Conc. Ethylene gas	0.01	0.025	0.05	0.075	0.1
200 ppm	24.69408	26.55818	28.76101	28.99174	30.54377
100 ppm	14.20657	15	17.04227	20.02405	24.55246
50 ppm	6.2323	6.11084	7.89208	8.42604	13.70054
20 ppm	3.75661	4.44178	4.8104	4.66016	4.71429
10 ppm	2.2662	2.3597	2.649	2.36305	2.24118

Table A10 The sensing magnitude of the PANi-MWCNT at different MWCNT loading after 1 months

Sensor Ethylene gas	pure PANi	0.2 % MWCNT /PANi	0.4% MWCNT /PANi	0.8 % MWCNT /PANi
1000	63.31084	45.10733	44.70514	12.65963
500	47.22605	36.93439	38.46129	10.52089
200	24.51213	25.07338	22.33873	7.16025
100	18.67	11.62229	10.33521	3.91974

Table A11 The sensing magnitude of the PANi-MWCNT at different MWCNT loading after 3 months

Sensor	pure PANi	0.2 % MWCNT /PANi	0.4%MWCNT /PANi	0.8 % MWCNT /PANi
Ethylene gas				
100	26.55246	30.73156	29.70734	29.33627
50	14.70054	19.36302	15.2653	16.34129
20	5.71429	8.78531	6.32377	6.2886
10	2.94118	4.39187	3.28369	3.03175

Table A12 The sensing magnitude of the PANi-MWCNT-SnO₂ at different concentrations after 1 months

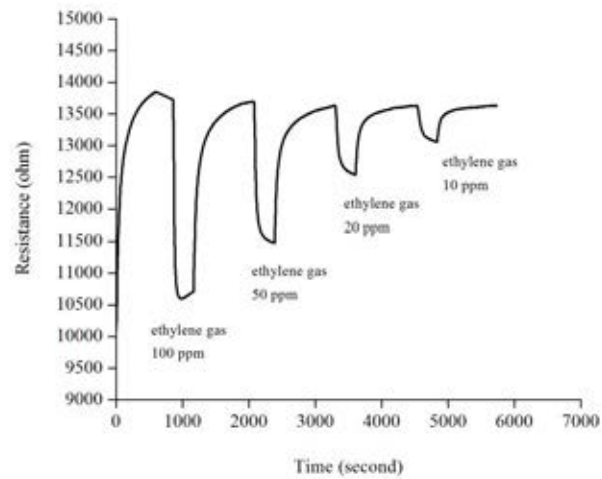
Sensor	MWCNT/P ANi	MWCNT/PANi/ 60Sec SnO ₂	MWCNT/PANi/ 90Sec SnO ₂	MWCNT/ PANi/120 Sec SnO ₂	MWCNT/PA Ni/150Sec SnO ₂
Ethylene gas					
1000	36.21809	38.89887	34.04417	12.85267	10.98901
500	25.02637	29.50053	23.24503	7.73557	6.6912
200	16.48024	19.47073	15.82734	4.11192	3.62507

Table A13 The sensing magnitude of the PANi-MWCNT-SnO₂ at different concentrations after 3 months

Sensor	MWCNT/PANi	MWCNT/PANi/60Sec SnO ₂	MWCNT/PANi/90Sec SnO ₂
Ethylene gas			
200	26.332	27.39787	13.18302
100	19.5601	20.22105	10.52203
50	10.84751	11.87817	6.37822
20	4.8311	5.01845	2.64419
10	2.38193	2.42002	1.19184

Appendix B

1) Determination of % Sensitivity



% sensitivity at ethylene gas 100 ppm

$$\begin{aligned}
 &= \frac{R_{\text{in nitrogen}} - R_{\text{in ethylene}}}{R_{\text{in ethylene}}} \times 100 \\
 &= \frac{(3507095 - 2831900)}{2831900} \\
 &= 23.84 \%
 \end{aligned}$$

Biography

Mr. Prasit Pattanauwat was born on August 13, 1980 in Bangkok, Thailand. He received his Bachelor degree of Engineering majoring in peterochemical and polymeric material of Engineering and Industrial Technology at Silpakorn University in 2002. After that, he received his master degree of Applied Polymer Science and Textile Technology at Department of Materials Science, Faculty of Science, Chulalongkorn University in September 2004.

In 2005, he worked on production engineering in field of biaxially-oriented polyethylene terephthalate film at A.J.PLAST Corporation Ltd.

In 2006, he worked on research and development in field of urea-formaldehyde resin at Thai Corporation Ltd.

In 2007, he pursued his Doctor of Philosophy at Department of Material Science, Faculty of Science Chulalongkorn University, and obtained his Doctor of Philosophy in Material Science in September 2011.

Publications

International Journals

1. Pattanauwat P, Aht-Ong D., Electrochemical Synthesis of Polyaniline as Ethylene Gas Sensor. Advanced Materials Research. 93-94 (2010): 459-462.
2. Pattanauwat P, Aht-Ong D., Electrochemical Synthesis of Sensitive Layer of Polyaniline: Effects of Acid Doping on Ethylene Gas Sensing Materials Science Forum. 654-656 (2010): 2285-2288.
3. Pattanauwat P, Aht-Ong D., Electrochemical Synthesis of Sensitive Layer of Polyaniline/Multi Wall Carbon Nanotube Composite. Materials Science Forum 695 (2011): 336-339.
4. In-situ electrochemical synthesis of novel sensitive layer of polyaniline/multiwall carbon nanotube/tin oxide hybrid materials for ethylene gas detection, manuscript in preparation

Local Presentation

1. Pattanauwat P, Aht-Ong D., (2009). Electro-deposition of sensitive layer of polyaniline: effect of acid dopants on ethylene gas sensing and characteristics of acid doped polyaniline. Proceedings of The Research Symposium on Petroleum, Petrochemicals, and Advanced Materials and The 16 th PPC Symposium on Petroleum, Petrochemicals, and Polymers